TRANSCRIPTION AND CHROMATIN DYNAMICS IN THE NOTCH SIGNALLING RESPONSE

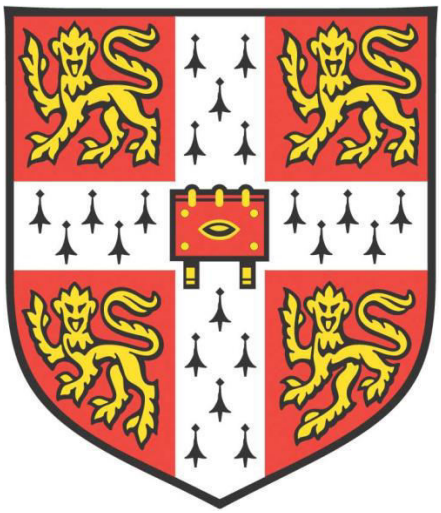

Zoe Pillidge

Churchill College

Department of Physiology, Development and Neuroscience

University of Cambridge

This dissertation is submitted for the degree of Doctor of Philosophy

September 2018

TRANSCRIPTION AND CHROMATIN DYNAMICS IN THE NOTCH SIGNALLING RESPONSE

During normal development, different genes are expressed in different cell types, often directed by cell signalling pathways and the pre-existing chromatin environment. The highly-conserved Notch signalling pathway is involved in many cell fate decisions during development, activating different target genes in different contexts. Upon ligand binding, the Notch receptor itself is cleaved, allowing the intracellular domain to travel to the nucleus and activate gene expression with the transcription factor known as Suppressor of Hairless (Su(H)) in *Drosophila melanogaster*. It is remarkable how, with such simplicity, the pathway can have such diverse outcomes while retaining precision, speed and robustness in the transcriptional response. The primary goal of this PhD has been to gain a better understanding of this process of rapid transcriptional activation in the context of the chromatin environment.

To learn about the dynamics of the Notch transcriptional response, a live imaging approach was used in *Drosophila* Kc167 cells to visualise the transcription of a Notch-responsive gene in real time. With this technique, it was found that Notch receptor cleavage and trafficking can take place within 15 minutes to activate target gene expression, but that a ligand-receptor interaction between neighbouring cells may take longer. These experiments provide new data about the dynamics of the Notch response which could not be obtained with static time-point experiments.

The chromatin accessibility and nucleosome dynamics at Notch-responsive enhancers were also studied using a variety of molecular techniques. These experiments showed that enhancers occupied by Su(H) were highly accessible with a high level of nucleosome turnover, and that Notch signalling promoted a further increase in accessibility. The BRM complex, a SWI/SNF chromatin remodeller implicated in many cancers, was identified as essential for the high chromatin accessibility at these regions and the Notch response. This new insight into the link between a simple signalling pathway and chromatin remodelling could have implications for understanding the complicated process of development and what goes wrong in diseases like cancer.

ACKNOWLEDGEMENTS

Firstly, my greatest thanks go to my supervisor, Professor Sarah Bray, without whom this PhD would not have been possible. I am incredibly grateful for her taking me on as a rotation student at short notice and quickly making arrangements for me to learn the experimental techniques in which I was the most interested. Joining the Bray laboratory was one of the best decisions of my life. Sarah has been a fantastic supervisor, providing just the right amount of guidance at all stages of my PhD, and I have learnt a lot from her. I would also like to thank my adviser Rob White, who has been an ongoing source of academic guidance, and a very friendly and supportive person to work alongside.

Next, I would like to thank the members of the Bray laboratory who have aided my research immensely over the years. I would like to thank Maria Gomez-Lamarca and Jin Li, particularly for their support when I first joined the Bray laboratory. Jin continued to send advice by email after leaving the country, and Maria has continued to support me throughout the entire PhD, both experimentally and emotionally. I am also deeply grateful for the hard work of our laboratory manager Kat Millen and assistant Agnes Asselin. Together, they have made sure that everything runs smoothly in the Bray laboratory, looking after both the shared space and the people within it. Other member of the Bray laboratory who have either been great friends, offered experimental advice or, in most cases, both include: Matthew Jones, Eva Zacharioudaki, Julia Falo-Sanjuan, Hadi Boukhatmi, Stella Lempidaki, Gustavo Cerda-Moya, Stephen Chan, Silvie Fexova, Torcato Martins, Jonty Townson and Sara Morais-da-Silva.

For their contributions to particular experiments, I would like to specifically mention the following people. Fellow PhD student Julia Falo-Sanjuan was heavily involved in setting up the MS2 system in the Bray laboratory, writing the MATLAB code for the analysis. On top of this, I am grateful for her intelligent insights and encouraging discussions, which pushed the project forward. Damiano Porcelli, a former member of the White laboratory, was a great help with setting up the ATAC experiments, sharing his protocol and even some reagents. I deeply appreciate having him as both a laboratory and office

neighbour for most of my PhD, as he almost always (when he wasn't drumming too loudly on the desk) brightened my day. The locus tag, as we call it, has been an invaluable tool for studying the live Notch response *in vivo*, and I am therefore thankful for the hard work by Matthew Jones to implement this system. I would also like to thank Peter Verrijzer for providing antibodies against some BRM complex subunits, Kami Ahmad for sending me flies which express GFP-tagged histone proteins, Neus Visa for sending me plasmids containing the *brm* sequence, and Dirk Schübeler for sending me plasmids containing V5-tagged histone sequences.

I would also briefly like to mention several people who have shaped my life choices over the years, without whom I would not have successfully undertaken a PhD. I am thankful to Rita Monson for pushing me through my undergraduate studies, being the best person at giving pep talks I've ever met, and giving me the opportunity to teach after graduating. Without the kindness of Bill Wisden (Imperial College London), I would not have had the amazing opportunity to experience academic research and become an author on a very high impact publication. I am grateful to Hans Hoppe for allowing me to do my PIPS (professional internship) with him and being a generally inspirational character.

I am thankful to my friends and family for being a part of my life outside of the PhD. In particular, I deeply appreciate my boyfriend of seven years, Ian Orton, being there for me through it all.

I am grateful to the Biotechnology and Biological Sciences Research Council (BBSRC) for selecting me for a PhD and providing my funding. Thank you to Kayla Friedman and Malcolm Morgan (Centre for Sustainable Development, University of Cambridge) for producing the Microsoft Word thesis template used to produce this document.

CONTENTS

1 INTRODUCTION 1

1.1 Transcription and its regulation..... 2

1.1.1 Regulation by enhancers.....2

1.1.2 Transcription factor binding to enhancers 5

1.1.3 Transcription activation.....8

1.2 Chromatin structure and its regulation 12

1.2.1 Chromatin structure 12

1.2.2 Regulation by chromatin modifiers.....17

1.2.3 Transcription factor interaction with the chromatin.....21

1.3 Notch signalling 23

1.3.1 Notch as a cell signalling pathway 23

1.3.2 Role of Notch signalling in development and disease 24

1.3.3 Activation mechanism 25

1.3.4 Nuclear complexes 27

1.3.5 The switch from repression to activation.....28

1.3.6 Achieving cell type specificity 29

1.4 Aims and outline of the thesis.....31

2 MATERIALS AND METHODS..... 33

2.1 Key reagents and methods 33

2.1.1 Molecular cloning.....33

2.1.2 Cell culture conditions 33

2.1.3 Transfection reagents.....34

2.1.4 Antibiotics and inhibitors.....34

2.1.5 Antibodies.....34

2.2 Generation of mβ MS2 cell line 35

2.2.1 Cloning of constructs 35

2.2.2 Generation of MCP-GFP-expressing cells.....38

2.2.3 CRISPR transfection 39

2.2.4 Removal of the blasticidin resistance cassette 39

2.2.5 Genotyping 40

2.3 Cell culture for MS2 experiments 40
2.3.1 MS2 imaging and EGTA-induced Notch activation 40
2.3.2 Drug treatments 41
2.3.3 Co-culture with S2 cells 42
2.3.4 Immunofluorescence staining of cultured cells 42
2.3.5 Plasma membrane stain 43
2.4 MS2 computational analysis 43
2.4.1 Cell tracking 43
2.4.2 Data processing 45
2.4.3 Analyses 46
2.5 Salivary gland experiments 47
2.5.1 Fly stocks 47
2.5.2 Live imaging 49
2.5.3 Immunofluorescence staining of salivary glands 50
2.6 Cell culture for molecular biology experiments 50
2.6.1 Generation of stable cell lines 50
2.6.2 Notch activation 51
2.6.3 Copper induction of pMT constructs 51
2.6.4 RNAi in Kc167 cells 52
2.7 Molecular biology techniques 53
2.7.1 RNA extraction and reverse transcription 53
2.7.2 Su(H) co-immunoprecipitation 53
2.7.3 Western blots 53
2.7.4 Assay for transposase accessible chromatin 54
2.7.5 Chromatin immunoprecipitation 54
2.7.6 CATCH-IT 55
2.7.7 qPCR 56

3 TRANSCRIPTION DYNAMICS IN THE NOTCH RESPONSE 59

3.1 Introduction 59

3.2 Results 61

3.2.1 Implementing the MS2 system in Kc167 cells 61

3.2.2 Characterising the MS2 response to Notch 63

3.2.3 Effects of MG132 on the dynamics of the Notch response 73

3.2.4 The dynamic response to ligand-induced Notch activation 77

3.3 Discussion 80

4 CHROMATIN DYNAMICS IN THE NOTCH RESPONSE 87

4.1 Introduction 87

4.2 Results 88

4.2.1 Ectopic Notch signalling causes largescale changes in chromatin structure 88

4.2.2 The BRM chromatin remodelling complex promotes high chromatin accessibility at Notch-regulated enhancers 93

4.2.3 The BRM complex is also required at Notch-regulated targets in Kc167 cells 100

4.2.4 Nucleosome turnover increases in response to Notch signalling and is BRM complex-dependent 102

4.3 Discussion 109

4.3.1 Model 112

5 CONCLUSIONS AND OUTLOOK 115

5.1 Most significant findings.....115

5.2 Main unanswered questions.....116

5.3 Future outlook 119

6 REFERENCES.....121

7 APPENDICES..... 165

LIST OF FIGURES

Figure 1.1. Transcription and its regulation. 3

Figure 1.2. Chromatin structure and its regulation. 13

Figure 1.3. Overview of Notch signalling pathway. 26

Figure 2.1. Generation of mβ MS2 cell line. 36

Figure 2.2. Cell tracking and data processing for MS2 analysis. 44

Figure 3.1. Implementing the MS2 system in Kc167 cells. 62

Figure 3.2. Live imaging of Notch-responsive transcription. 65

Figure 3.3. Observed foci are EGTA-dependent and represent transcription. ... 67

Figure 3.4. The timing of the Notch transcriptional response is reproducible. 69

Figure 3.5. Removal of the blasticidin resistance cassette did not alter the speed of the detected transcriptional response. 72

Figure 3.6. Active NICD levels decrease slowly over time. 74

Figure 3.7. MG132 treatment disrupts transcription dynamics. 75

Figure 3.8. Ligand-induced Notch activation takes longer and can signal via cell projections. 78

Figure 4.1. The *E(spl)-C* changes structure in Notch-ON nuclei. 90

Figure 4.2. Histone H3.3 levels increase at the *E(spl)-C* in Notch-ON nuclei. ... 92

Figure 4.3. Chromatin remodelling factors required for Su(H) recruitment. 94

Figure 4.4. Core components of the BRM complex are required for Su(H) recruitment 95

Figure 4.5. Chromatin accessibility of the *E(spl)-C* is regulated by Notch signalling and dependent on the BRM complex. 98

Figure 4.6. The BRM complex is required for Su(H) recruitment and Notch-dependent transcription in Kc167 cells. 101

Figure 4.7. Nucleosome turnover at Su(H)-bound enhancers is increased in Notch-ON cells and is dependent on the BRM complex. 103

Figure 4.8. Notch activation or BRM complex depletion does not affect the overall distribution of histones H3 and H3.3.....106

Figure 4.9. Histone H3.3 is incorporated rapidly at Notch-responsive enhancers in a BRM complex-dependent manner. 108

Figure 4.10. Model of BRM complex action in the Notch response. 113

LIST OF TABLES

Table 1. List of drugs used for selection of stable cell lines and cell treatments. 34

Table 2. List of antibodies used. 34

Table 3. Primers used in cloning the MS2 constructs. 38

Table 4. Primers used for genotyping. 40

Table 5. Number of cells per category in each MS2 experiment shown in chapter 3. 47

Table 6. *Drosophila* RNAi stocks used. 48

Table 7. Primers used in BrmK804R mutagenesis and histone-V5 cloning into the pMT vector. 51

Table 8. T7 primers used to make double-stranded RNA for RNAi in Kc167 cells. 52

Table 9. Primer pairs targeting *E(spl)mβ-HLH* MS2 construct. 56

Table 10. Primer pairs targeting the *E(spl)-C*. 57

Table 11. Primer pairs targeting control regions for ATAC. 57

Table 12. Primer pairs targeting control regions for CATCH-IT. 58

LIST OF VIDEOS

Video 1. Live imaging of Notch-dependent transcription. 166

Video 2. Transcription foci do not appear under control conditions. 166

Video 3. Removal of the blasticidin cassette did not dramatically alter the Notch-dependent transcriptional response. 166

Video 4. MG132 perturbs the transcriptional response to EGTA. 166

Video 5. The transcriptional response to ligand-induced Notch activation. 166

LIST OF APPENDICES

Appendix 1: Video information 166

Appendix 2: MATLAB scripts for cell tracking 167

Appendix 3: R scripts for MS2 data processing 170

List of Abbreviations and Acronyms

Gene and protein names are marked by *H.s.* if the human name is provided and *D.m.* if the *Drosophila* name is provided.

ATAC
: Assay for Transposase Accessible Chromatin

ATPase
: Enzyme that releases energy by decomposing adenosine triphosphate (ATP)

BAF complex
: BRG1-Associated Factor complex

Baf60c
: Synonym for SMARCD3 (SWI/SNF related, matrix associated, actin dependent regulator of chromatin, subfamily d, member 3) *H.s.*

BAP complex
: Brahma Associated Proteins complex

BAP170
: Brahma associated protein 170kD *D.m.*

BMP
: Bone Morphogenetic Protein family of growth factors

BRD4
: Bromodomain containing 4 *H.s.*

Brg1
: Synonym for SMARCA4 (SWI/SNF related, matrix associated, actin dependent regulator of chromatin, subfamily a, member 4) *H.s.*

BRM complex
: Brahma complexes including BAP and PBAP

Brm
: Brahma (the ATPase subunit of the BRM complex) *D.m.*

BrmK804R
: Dominant-negative Brahma protein

BrmWT
: Recombinant Brahma protein with wild-type sequence

BSA
: Bovine serum albumin

CAF-1
: Chromatin Assembly Factor-1 complex

Cas9
: CRISPR Associated Protein 9

CATCH-IT
: Covalent Attachment of Tagged Histones to Capture and Identify Turnover

CBF1
: Synonym for RBPJ *H.s.*

CBP/p300
: Family of co-activators including CREBBP (CREB Binding Protein; synonym CBP) and EP300 (E1A binding protein p300; synonym p300) *H.s.*

cDNA
: Complementary DNA reverse transcribed from RNA

c-Fos
: Synonym for FOS (Fos proto-oncogene, AP-1 transcription factor subunit) *H.s.*

CHD
: Chromodomain Helicase DNA-binding family of chromatin remodellers

ChIP
: Chromatin immunoprecipitation

ChIP-seq
: ChIP combined with high throughput sequencing

c-Myc
: synonym for MYC (myelocytomatosis oncogene) *H.s.*

CRISPR
: Clustered Regularly Interspaced Short Palindromic Repeat

CSL
: CBF1, Su(H), LAG-1; collective name for the Notch transcription factor

CtBP
: C-terminal Binding Protein *D.m.*

DAXX
: Death domain associated protein *H.s.*

DEK
: DEK proto-oncogene *H.s.*

DMSO
: Dimethyl sulfoxide

DNA
: Deoxyribonucleic acid

Pax2
: Synonym for shaven *D.m.*

Dpp
: Decapentaplegic *D.m.*

Drosophila
: *Drosophila melanogaster*

DSIF
: DRB-Sensitivity Inducing Factor

dTCF
: Synonym for pangolin *D.m.*

E(spl)-C
: Enhancer of split complex *D.m.*

E(spl)mβ-HLH, E(spl)m3-HLH, E(spl)m8-HLH
: Enhancer of split mβ, m3, m8, helix-loop-helix *D.m.*

EGF
: Epidermal growth factor

EGFR
: Epidermal growth factor receptor *H.s., D.m.*

EGTA
: Ethylene glycol-bis(β-aminoethyl ether)-*N,N,N′,N′*-tetraacetic acid

EPHB2
: EPH receptor B2 *H.s.*

ERK
: Synonym for EPHB2 *H.s.*

eve
: even skipped *D.m.*

FBS
: Fetal bovine serum

FoxA
: Family of Forkhead box transcription factors

FRT sites
: Flippase recombination target sites

GATA
: Family of zinc finger domain-containing transcription factors

GFP
: Green fluorescent protein

GR
: Glucocorticoid receptor; synonym for NR3C1 (nuclear receptor subfamily 3 group C member 1) *H.s.*

gRNA
: Guide RNA for CRISPR

H2A, H2A.Z, H2B, H3, H3.3, H4
: Histone proteins

H3K4, H3K9, H3K27, H3K36, H3K56
: Specific lysine residues in histone H3

H3K27me3
: Tri-methylation mark on lysine 27 in histone H3

H3.3K4
: Lysine 4 in histone H3.3

H3.3K27M
: Mutation of lysine 27 to methionine in histone H3.3

HDAC
: Histone deacetylase

Hes1
: Hes family bHLH transcription factor 1 *H.s.*

Hey1
: Hairy/enhancer-of-split related with YRPW motif 1 *H.s.*

Hic-5
: Synonym for TGFB1I1 (transforming growth factor beta 1 induced transcript 1) *H.s.*

HIRA
: Histone cell cycle regulator *H.s.*

HR
: Homologous recombination

Hsp70
: Synonym for Hsp70Aa (Heat-shock-protein-70Aa) *D.m.*

Hsp83
: Heat shock protein 83 *D.m.*

INO80
: Inositol-requiring protein 80 family of chromatin remodellers

INT
: DNA sequence containing *ParS* binding sites for the ParB proteins

ISWI
: Imitation Switch family of chromatin remodellers

Kc cells
: Kc167 cells

KDM5A
: Lysine demethylase 5A *H.s.*

KMT2D
: Lysine methyltransferase 2D *H.s.*

LacZ
: β-galactosidase

LDB1
: LIM domain binding 1 *H.s.*

LEF1
: Lymphoid enhancer binding factor 1 *H.s.*

Lig4
: Synonym for DNAlig4 (DNA ligase 4) *D.m.*

LSD1
: Synonym for KDM1A (lysine demethylase 1A) in human *H.s.* and Su(var)3-3 in *Drosophila* *D.m.*

Mam
: Mastermind *D.m.*

MAML1-3
: Mastermind like transcriptional coactivators 1-3 *H.s.*

mβ, m3
: *E(spl)mβ-HLH, E(spl)m3-HLH*

MCP
: MS2 bacteriophage coat protein

Med12, Med13, MED14, Med25
: Mediator complex subunits 12, 13 (known as Kohtalo and Skuld respectively in *Drosophila* *D.m.*), 14, 25 *H.s.*

MLL4
: Synonym for KMT2D *H.s.*

MMTV
: Mouse mammary tumour virus

MS2
: Refers to a live RNA labelling technique, often used to detect nascent transcription, derived from the MS2 bacteriophage

MyoD
: Synonym for *MYOD1* (myogenic differentiation 1) *H.s.*

$N^{\Delta ECD}$
: Constitutively active Notch protein

NELF
: Negative Elongation Factor complex

NF-κB
: Nuclear factor kappa-light-chain-enhancer of activated B cells family of dimeric transcription factors

NHEJ
: Non-homologous end-joining

NICD
: Notch intracellular domain

Notch-OFF
: Refers to the state where NICD is absent from the nucleus and CSL may partner with co-repressors

Notch-ON
: Refers to the state where NICD is present and CSL can form the ternary activating complex

NuRD
: Nucleosome Remodelling and Deacetylase complex

Oct-3, OCT4
: Synonyms for POU5F1 (POU domain, class 5, transcription factor 1) *H.s.*

p300
: Synonym for EP300 (see CBP/p300) *H.s.*

p53
: Synonym for TP53 (tumor protein 53) *H.s.*

ParB
: Family of bacterial partition proteins which bind to *ParS* binding sites in the INT DNA sequence

PBAF complex
: Polybromo-associated BAF complex

PBAP complex
: Polybromo-containing BAP complex

PBS
: Phosphate-buffered saline

PCNA
: Proliferating cell nuclear antigen *H.s.*

PCR
: Polymerase chain reaction

p-ERK
: Phosphorylated ERK *H.s.*

PIC
: Pre-initiation complex

pMT
: Vector containing the metallothionein promoter

PMT detector
: Photomultiplier tube

Pol II
: RNA polymerase II

PPARγ
: Peroxisome proliferative activated receptor gamma *H.s.*

PRC2
: Polycomb Repressive Complex 2

P-TEFb
: Positive Transcription Elongation Factor-b

PTM
: Post-translational modification

qPCR
: Quantitative PCR (also known as real-time PCR)

RBPJ
: Recombination signal binding protein for immunoglobulin kappa J region *H.s.*

REL
: Homology domain found in a family of transcription factors including NF-κB and Dorsal

RNA
: Ribonucleic acid

RNAi
: RNA interference

RNA-seq
: RNA sequencing

RpL32
: Ribosomal protein L32 *D.m.*

RUNX
: Family of runt-related transcription factors

S2 cells
: S2-Mt-Dl cells

SDS-PAGE
: Sodium dodecyl sulfate-polyacrylamide gel electrophoresis

SEM
: Standard error of the mean

SHARP
: SMRT and HDAC Associated Repressor Protein, synonym for SPEN (spen family transcription factor) *H.s.*

Shh
: Sonic hedgehog *H.s.*

Smad
: Family of transcription factors that transduce TGFβ signalling

SMRT
: Synonym for NCOR2 (nuclear receptor corepressor 2) *H.s.*

Snr1
: Snf5-related 1 *D.m.*

Sox-2, Sox9
: SRY-box 2, 9 *H.s.*

Su(H)
: Suppressor of Hairless *D.m.*

SWI/SNF
: Switching-defective/Sucrose Non-Fermenting family of chromatin remodellers

SWR-C
: Yeast Swr1 chromatin remodelling complex

T2A
: 2A-like self-cleaving peptide sequence from *Thosea asigna*

TBS
: Tris-buffered saline

TCF7L2
: Transcription factor 7 like 2 *H.s.*

TGF-β
: Transforming Growth Factor-beta family of cytokines

TNFα
: Tumor necrosis factor alpha *H.s.*

Trr
: Trithorax-related *D.m.*

UAS
: Upstream activating sequence

UTR
: Untranslated region

V5
: Epitope tag derived from simian virus 5

ZRS
: Zone of polarising activity Regulatory Sequence

1 INTRODUCTION

The discovery that specialised adult cells can be reprogrammed, giving them the potential to become any cell of an organism, was ground-breaking (Gurdon 1962; Takahashi and Yamanaka 2006). This can occur because almost every cell in an organism contains the same genetic material, an initially surprising finding considering the large variation that exists in cell morphology and function. These apparent differences between cells arise as a result of different genes being utilised or expressed. Therefore, to understand how different cell types arise during the development of an animal, it is necessary to understand how gene expression is controlled on a cellular level.

Gene expression involves the processes of transcription and translation, whereby DNA is converted into RNA and RNA into protein, respectively. It can therefore be regulated by controlling any stage of this pipeline. However, perhaps the most major axis of regulation is at the stage of transcription, which confers tissue-specific gene expression that is fundamental to development (Levine and Tjian 2003). Considering that the human genome contains three billion base-pairs of information, the structural packaging of this DNA into chromatin has a great impact on the accessibility of the DNA. The dynamic regulation of chromatin structure is therefore a key aspect of transcriptional control (ENCODE Project Consortium 2012).

During development, different patterns of gene expression are triggered in response to cell-cell signalling pathways (Basson 2012). The mechanisms

regulating gene expression in response to the Notch signalling pathway are the subject of this thesis. Therefore, in this introductory chapter, general principles of gene expression will first be discussed in terms of transcription and chromatin, followed by a summary of the current state of knowledge about Notch signalling.

1.1 Transcription and its regulation

1.1.1 Regulation by enhancers

To allow for the different gene expression profiles found across cells in complex organisms, gene transcription is tightly controlled. Regulation depends primarily on the binding of nuclear proteins, called transcription factors, to the DNA at enhancer sequences. Enhancers are genomic regions that modulate the transcription of genes, despite sometimes being very long distances from the regulated gene in the linear genome (Levine et al. 2014). The functional role of enhancers and the way they activate transcription is therefore of fundamental importance to development.

It is thought that enhancers contact promoters by looping of the DNA (Figure 1.1A), a concept for which there is now considerable evidence. For example, DNA loops have been observed by electron microscopy between the SV40 enhancer and promoter (Su et al. 1991). Also, tethering a protein (LDB1) usually bound at a distal enhancer (the locus control region) to the beta-globin promoter rescued transcription under conditions where looping would otherwise not occur, suggesting that physical contact is sufficient for enhancer activity (Deng et al. 2012). Long-range interactions are prevalent across genomes, with many appearing stable in different cell types through development, suggesting that enhancer-promoter contact may be formed before gene activation (Dixon et al. 2012; Ghavi-Helm et al. 2014). It is less clear whether looping is required for short-range enhancer-promoter interactions, partly because the biochemical methods used for detecting DNA contacts give high background at close distances, and microscopy-based techniques lack the sufficient resolution, making these interactions difficult to detect (Shlyueva et al. 2014).

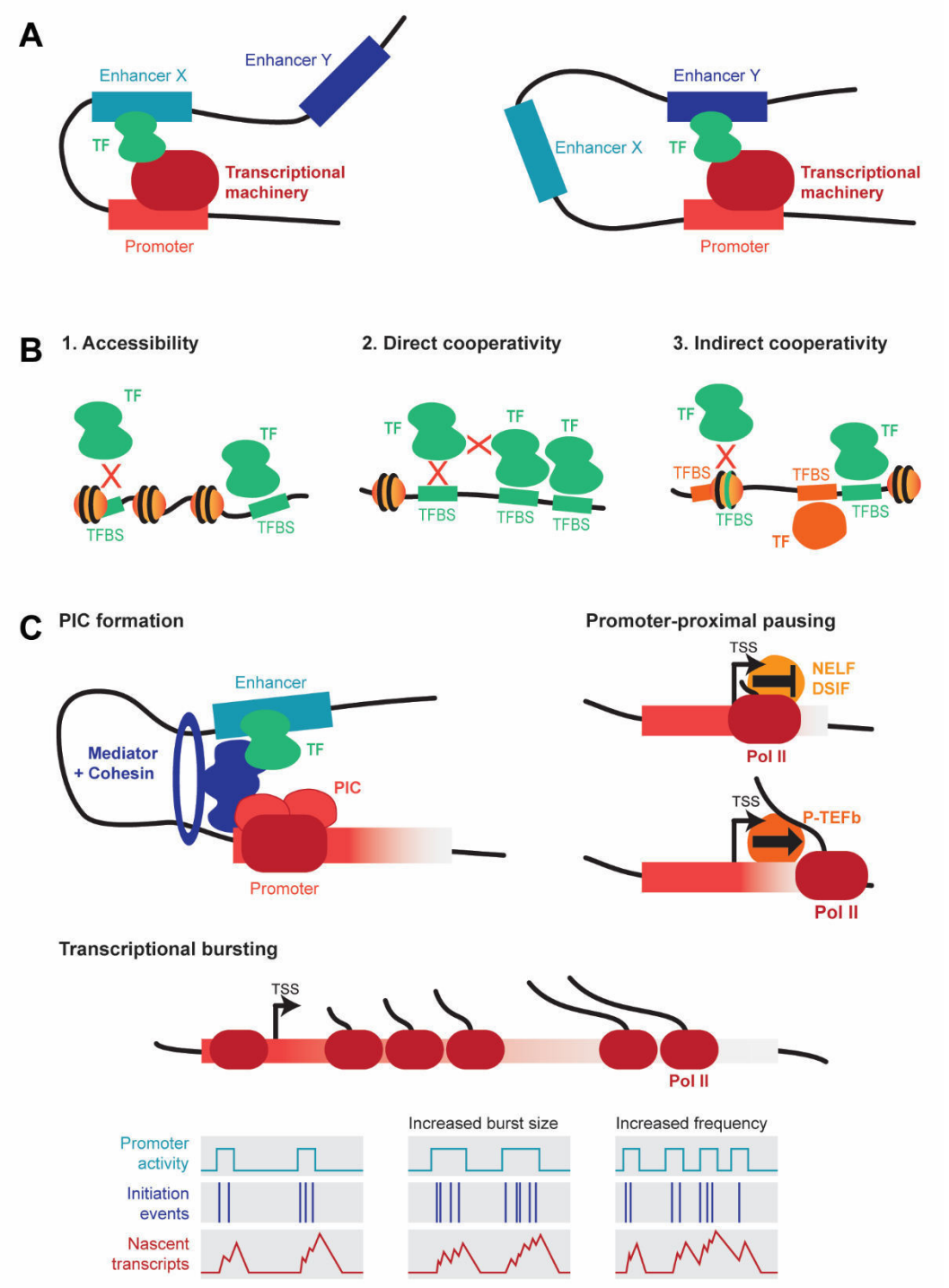

Figure 1.1. Transcription and its regulation. (A) Control of transcription by enhancer-promoter interactions. DNA looping allows physical contact between enhancers and promoters via DNA binding proteins. Different enhancers can be utilised in different cells. (B) Factors influencing transcription factor binding. 1. Transcription factors usually bind to accessible DNA. 2. Direct cooperativity occurs when direct protein-protein interactions result in improved binding affinity. This can occur between different transcription factors or multiple molecules of the same factor, and usually relies on the correct spacing of binding sites along the DNA. *Continued on next page.*

Developmental genes are commonly regulated by multiple enhancers (Zeitlinger et al. 2007b), allowing different enhancers to be active in different cell types or developmental time periods (Figure 1.1A). For example, the expression pattern of the *Drosophila melanogaster* pair-rule gene even skipped (*eve*) is regulated by several different enhancers, with the best-characterised enhancer (*eve* stripe 2) regulating only one of the seven stripes (Small et al. 1992). Another well-known example is the regulation of sonic hedgehog (*Shh*) by the ZRS enhancer in the developing limb, where the enhancer specifically regulates *Shh*, and furthermore only co-localises with the *Shh* coding region, in the *Shh*-expressing cells of the limb bud (Williamson et al. 2016). In some cases, several enhancers function redundantly by regulating similar spatiotemporal gene expression patterns and can be deleted with no obvious phenotype. These have been named shadow enhancers and a comprehensive study in *Drosophila* has found them to be prevalent (Cannavò et al. 2016). It is suggested that these enhancers ensure robustness in developmental progression, but further studies of how they

Figure 1.1 continued (B, continued) 3. Indirect cooperativity occurs when one factor influences the binding of another without a direct protein-protein interaction between them. This can occur via several different mechanisms, but often involves changes to the chromatin structure or displacement of nucleosomes. In the example shown, the presence of the orange transcription factor displaces the nucleosome to allow the green transcription factor to bind to its site. (C) Regulation of transcriptional output. Cofactors such as Mediator can promote enhancer-promoter interactions and PIC formation for transcription initiation. Promoter-proximal pausing poises genes for rapid activation. Bursting is thought to occur due to the release of several polymerases in quick succession during an active period. Bursting may be modulated by a change in burst size or frequency. Note that bursts at high frequency may appear as a single larger burst when measuring RNA transcript levels (graphs inspired by Wang et al. 2018). Abbreviations not defined elsewhere in the text are: “TF” = transcription factor, “TFBS” = transcription factor binding site and “TSS” = transcription start site (Spitz and Furlong 2012; Haberle and Stark 2018).

interact with different genes under different conditions are needed to understand their role in development. Indeed, despite some instances where enhancer function has been intensively studied, a global understanding of how specific enhancer-promoter interactions are chosen in a particular cell type at a particular time is lacking.

1.1.2 Transcription factor binding to enhancers

Enhancers can contain multiple binding sites for transcription factors and can therefore integrate different signals. For example, the *sparkling* enhancer of the *Pax2* gene in *Drosophila* is regulated by both Notch and Epidermal Growth Factor Receptor (EGFR) signalling, and at least 12 transcription factor binding sites have been mapped to this 400-base-pair region (Swanson et al. 2010). This example illustrates how the overlapping patterns of transcription factor binding across the genome present a combinatorial code, increasing the complexity of gene expression control by a finite set of transcription factors.

The specific DNA sequences bound by transcription factors are known as motifs, which are typically six to ten base-pairs long and degenerate, meaning that they allow different nucleotides at some positions (Shlyueva et al. 2014). Although motifs are highly prevalent, transcription factors usually do not occupy all of their potential binding sites and binding does not correlate directly with DNA affinity (Carr and Biggin 1999). Furthermore, transcription factors occupy different sites in different cell types (Kaplan et al. 2011). Thus, an important question is what determines transcription factor binding.

One key factor is chromatin structure, specifically the accessibility of enhancers, which can greatly affect transcription factor occupancy. The packaging of DNA into nucleosomes can occlude or change the structure of DNA motifs, thus regulating their accessibility to transcription factors (Figure 1.1B). Transcription factor binding has been found to correlate well with DNaseI sensitivity, a measure of chromatin accessibility (Li et al. 2011; Degner et al. 2012), and when combined with DNA sequence data, chromatin accessibility can be predictive for transcription factor binding (Pique-Regi et al. 2011). Chromatin accessibility can be regulated by chromatin remodelling complexes, which will be discussed in

detail in section 1.2.2. The complex interaction between transcription factors and chromatin remodellers is also discussed in section 1.2.3.

Since transcription factors often bind in close proximity at enhancers, it is also possible for one transcription factor to influence the binding of another (Figure 1.1B). Cooperative binding has been illustrated in many contexts and may depend on sequence motifs being appropriately arranged in the DNA (Kazemian et al. 2013). For example, REL and GATA binding sites are positioned in the same orientation near many fat-specific immunity genes (Senger et al. 2004). The correct positioning of binding motifs is also required at the interferon-β enhancer where several transcription factors bind cooperatively (Thanos and Maniatis 1995; Panne et al. 2007). Cooperative binding of transcription factors can result in binary ("on-off" switch-like) effects on transcription, a concept illustrated by the translation of morphogen gradients into sharp transcriptional responses, such as in the control of patterning in the *Drosophila* embryo by Bicoid, where cooperative DNA binding is required for sharp patterning of the target gene *hunchback* (Lebrecht et al. 2005). The converse is true for NF-κB in human cells, where a lack of cooperativity is thought to give a graded transcriptional response (Giorgetti et al. 2010).

Cooperativity can also occur indirectly, due to the involvement of other factors (Figure 1.1B). For example, the co-activator p300 mediates the synergistic effects of Sox-2 and Oct-3 at the distal *FGF-4* enhancer (Nowling et al. 2003). The use of common co-activators by many different transcription factors makes this a widespread phenomenon and can explain the presence of transcription factor hotspots in the genome (Moorman et al. 2006; Chen et al. 2008; Siersbæk et al. 2014). As well as the recruitment of transcription factors by protein-protein interactions, many examples of cooperativity rely on changes to the chromatin structure. For example, the competition of the glucocorticoid receptor (GR) for DNA binding with another receptor that had identical binding specificity unexpectedly led to increased levels of binding due to increased accessibility of the chromatin (Voss et al. 2011).

The concept that transcription factors compete with histones for DNA binding was first discussed around the early 1990s (Felsenfeld 1992) following

experiments on the yeast *PHO5* promoter and GAL4 system. It was shown that the trans-acting proteins PHO2 and PHO4 are required to generate the active chromatin state at the *PHO5* promoter (Fascher et al. 1990). And it became apparent that different transcription factors have different requirements for DNA binding when it was shown that GAL4 could bind to nucleosomal DNA alone and binding improved when multiple sites were present, whereas heat shock factor (HSF) could only bind to nucleosomal DNA in the presence of TFIID (Taylor et al. 1991). The diversity in the ways that transcription factors access the DNA in different systems means that there remains no universal model for transcription factor binding to chromatin. Recent studies have shown that different transcription factors have different positional biases in relation to nucleosomes (Zhu et al. 2018) and nucleosome-depleted regions (Grossman et al. 2018). And while most transcription factors facilitate nucleosome dissociation, others can stabilise nucleosome binding (Zhu et al. 2018). Thus, it is important that the requirements for transcription factor binding to the DNA continue to be studied in different systems *in vivo* to understand the full regulation of gene expression.

Transcription factor binding events at enhancers can be integrated in an additive, synergistic or antagonistic manner (Grossman et al. 2017). For example, in the *Drosophila* mesoderm, the response to Dpp signalling requires the synergistic binding of both Smad and Tinman (Xu et al. 1998). However, Wingless signalling antagonises this response in visceral mesoderm induction at the *bagpipe* enhancer (Lee et al. 2005). Antagonistic interactions sometimes result from transcription factors competing for overlapping binding sites, as is the case in the epithelial to mesenchymal transition in colorectal cancer, where SNAIL1 silences EPHB2 expression via the displacement of TCF7L2 by LEF1 at its enhancer (Schnappauf et al. 2016). Alternatively, indirect mechanisms can mediate the outcomes from transcription factor interactions. For example, the coregulator Hic-5 antagonises the binding of GR to enhancers by interfering with the mechanisms regulating chromatin accessibility (Lee and Stallcup 2017).

Recent evidence from single molecule tracking experiments has argued that many transcription factors interact with the DNA transiently, with residence

times at specific binding sites recorded in the order of seconds or tens of seconds (Chen et al. 2014; De Angelis et al. 2015; Zhang et al. 2016). These data have shifted the paradigm that the stable binding of transcription factors is necessary for enhancer activity, believed partly due to early kinetic dissociation studies performed *in vitro* where dissociation constants corresponded to a residence time in the order of hours (Perlmann et al. 1990; Lieberman and Nordeen 1997). New studies have led to more dynamic models where transcription factors continually search for binding sites via many short-lived, non-specific interactions with the DNA (Cartailler and Reingruber 2015; Dror et al. 2016). The dynamics of transcription factor binding have been shown to affect gene expression in a study where a longer residence time of transcription factor binding was correlated with higher transcriptional output (Lickwar et al. 2012). It is therefore likely that local concentrations of transcription factors are also important for enhancer activity, and future studies of enhancer function will need to address both the dynamics of transcription factor binding and the architecture of the nucleus.

1.1.3 Transcription activation

Enhancer activity ultimately controls gene expression via transcription. Of the three RNA polymerase enzymes in eukaryotes, RNA polymerase II (Pol II) is responsible for the transcription of protein-coding genes (Carter and Drouin 2009). To initiate transcription, Pol II interacts with a set of initiation factors and the DNA sequence at the promoter. This involves the sequential binding of these initiation factors (known as formation of the pre-initiation complex; PIC), DNA melting to separate the double helix, and promoter escape, whereby Pol II is released from the core promoter and begins transcribing the gene in the elongation phase (Haberle and Stark 2018). Mechanisms that perturb or promote these steps can therefore control whether a gene is transcribed.

Enhancer activity is linked to transcriptional activation by co-activators such as Mediator or CBP/p300, which facilitate transcription via a wide range of mechanisms due to their ability to interact with other proteins or add post-translational modifications (PTMs). For example, Mediator recruits Cohesin, a protein which can connect two DNA segments, to promote enhancer-promoter

interactions (Kagey et al. 2010), and can interact with initiation factors to aid formation of the PIC (Figure 1.1C; Esnault et al. 2008; Eychenne et al. 2016). p300 can also promote PIC formation by phosphorylating the C-terminal domain of Pol II (Imhof et al. 1997; Schröder et al. 2013).

Co-activators may also modify transcription factors themselves, as occurs with p53, where acetylation is required for p53-mediated transcription activation (Tang et al. 2008). Since histone PTMs are thought to affect the structure of the chromatin (Hansen et al. 1998), the acetylation or methylation of histones by co-activators also has the potential to affect transcription factor binding and thus transcription. For example, methylation of histone H3K4 by MLL4 is required for enhancer activation in adipogenesis and myogenesis (Lee et al. 2013). By regulating the interplay of transcription factors, chromatin structure and enhancer-promoter interactions, co-activators are able to coordinate the necessary steps for robust transcription activation.

Many developmental processes rely on co-activator proteins or complexes. For example, Mediator is required for PPARγ-stimulated adipogenesis of mouse embryonic fibroblasts, most likely recruited via the MED14 subunit (Grøntved et al. 2010). In *Drosophila*, the Med12 and Med13 subunits of Mediator interact with Pygopus, an effector of Wingless signalling, and are required for Wingless target gene transcription (Carrera et al. 2008a). And the regulation of chondrogenesis by Sox9 in vertebrates depends on CBP/p300 and the Med25 subunit of Mediator (Tsuda et al. 2003; Nakamura et al. 2011). However, it is not known whether Mediator and CBP/p300 are required for all enhancer-promoter interactions and transcriptional activation.

At many developmental genes, a phenomenon called promoter-proximal pausing occurs, whereby Pol II stops transcribing after only 30 to 50 nucleotides (Figure 1.1C; Muse et al. 2007; Zeitlinger et al. 2007a). Pol II can be detected at this promoter-proximal site, for example at the heat-shock-responsive *Hsp70* gene in *Drosophila* (Gilmour and Lis 1986; Rougvie and Lis 1988). It is thought that the presence of Pol II pausing poises genes for activation such that when induced by a developmental signal, transcription can proceed more rapidly and synchronously (Lagha et al. 2013). Some argue that Pol II binding at the pause

site is relatively stable with a high residence time (Buckley et al. 2014). However, another hypothesis is that Pol II pausing is due to premature termination of transcription, and a recent study using high resolution footprinting supports this (Krebs et al. 2017). Which of these models is correct has implications for transcriptional regulation, since the premature termination model implies that transcription initiation rate may not change upon gene induction, while the initiation rate must vary in the case of stable Pol II binding. Another recent study found that paused Pol II inhibited transcription initiation, implying that pausing must be released before new initiation can occur (Shao and Zeitlinger 2017). Resolving these discrepancies will lead to a clearer understanding of which are the key regulated steps in transcription.

Although the exact behaviour of Pol II in promoter-proximal pausing is controversial, several proteins involved in its regulation are well established. The Negative Elongation Factor complex (NELF) and DRB-Sensitivity Inducing Factor (DSIF) both inhibit transcription elongation (Yamaguchi et al. 2013), while release from pausing involves Positive Transcription Elongation Factor-b (P-TEFb; Figure 1.1C). P-TEFb allows elongation to proceed by phosphorylating the C-terminal domain of Pol II as well as other factors (Peterlin and Price 2006), for example in response to heat shock at heat-shock-responsive genes (Lis et al. 2000). Thus by interacting with P-TEFb, transcription factors can promote pause release, as has been shown for the cofactor BRD4 in human cells (Jang et al. 2005; Yang et al. 2005), and the transcription factor c-Myc in embryonic stem cells (Rahl et al. 2010).

Pausing is widespread in *Drosophila* embryogenesis and is important for regulating developmental genes involved in both anterior-posterior and dorsal-ventral patterning (Saunders et al. 2013). However, pausing was not found to be the rate-limiting step for the transcription of all genes, since some Zelda-activated genes are regulated at the stage of Pol II recruitment (Saunders et al. 2013). Although developmental genes were not found to have significant levels of paused Pol II in embryonic stem cells (Min et al. 2011), the involvement of pausing in somatic cell reprogramming (Liu et al. 2014) and cancer (Lee et al. 2001; Mitra et al. 2012; Galbraith et al. 2013) suggests that it may play a role in the conversion of cell fates in mammalian systems. Further studies on different

cell types will be required to address which developmental processes are regulated at the stage of transcription pause release.

Transcription has been found to occur in discrete pulses, a phenomenon known as transcriptional bursting and conserved between prokaryotes and eukaryotes (Golding et al. 2005; Chubb et al. 2006; Raj et al. 2006; Paré et al. 2009). Each burst is thought to involve a number of closely-spaced polymerases producing several transcripts during an active period (Figure 1.1C; Tantale et al. 2016). Mediator was found to control the number of polymerases per burst in this study. Thus, it is speculated that transcription can re-initiate repeatedly once a gene is in an active conformation, and that this is followed by a refractory period with no transcription. Mathematical models support these hypotheses (Fukaya et al. 2016; Wang et al. 2018); however, more experimental evidence is required to confirm what controls this switching of states and to fully understand why bursting occurs.

The implications of bursting are that transcriptional output can be altered by changing either the size (amplitude or duration) or the frequency of bursts. Some transcription factors have been found to affect these bursting dynamics. For example, the bursting of the connective tissue growth factor (*CTGF*) gene responds to TGF-β1 stimulation (Molina et al. 2013), and the nuclear translocation of p-ERK modulates the bursting of *c-Fos* transcription (Senecal et al. 2014). Studying the bursting dynamics of genes opens up a new avenue for exploring transcription regulation, since it is possible to gain insight into transcription initiation and elongation rates (Larson et al. 2011; Muramoto et al. 2012; Garcia et al. 2013; Fukaya et al. 2017), which may lead to novel findings about how genes are controlled through development.

In summary, the developmental control of gene expression involves the integration of information at enhancers via transcription factor binding events, which is translated into transcriptional output by enhancer-promoter interactions. How different enhancers are used at different developmental time points is not fully understood, nor is what determines the exact patterns of transcription factor binding in different cell types. Enhancer-promoter interactions make heavy use of the co-activators Mediator and CBP/p300 to link

transcription factor occupancy to polymerase activity. Yet further studies are needed to understand how transient interactions of transcription factors with the DNA and other proteins can lead to robust levels of transcription. Gaining a further understanding of transcription dynamics in terms of elongation rates and bursting frequency could help to determine how developmental signals bring about developmental outcomes.

1.2 Chromatin structure and its regulation

1.2.1 Chromatin structure

Since transcription involves reading the DNA code, the way the DNA is packaged into chromatin is highly important. Furthermore, transcription factor binding at enhancers relies on the recognition of binding motifs, which may or may not be accessible to the transcription factor depending on the chromatin structure. Therefore, it is important to determine which aspects of the chromatin structure have a significant influence on gene expression.

The basic unit of chromatin is the nucleosome, consisting of 146 base-pairs of DNA wound around a histone octamer made up of the histone proteins H2A, H2B, H3 and H4 (Figure 1.2A; Kornberg 1974). Beyond this, the chromatin may also have a higher-order structure regulating its folding in the nucleus (Li and Reinberg 2011). Therefore, the chromatin can have a more open or closed conformation depending on how tightly packed the nucleosomes are. Additionally, chromatin structure can be influenced by localised histone marks or variants, adding complexity to the nuclear landscape in which gene expression takes place.

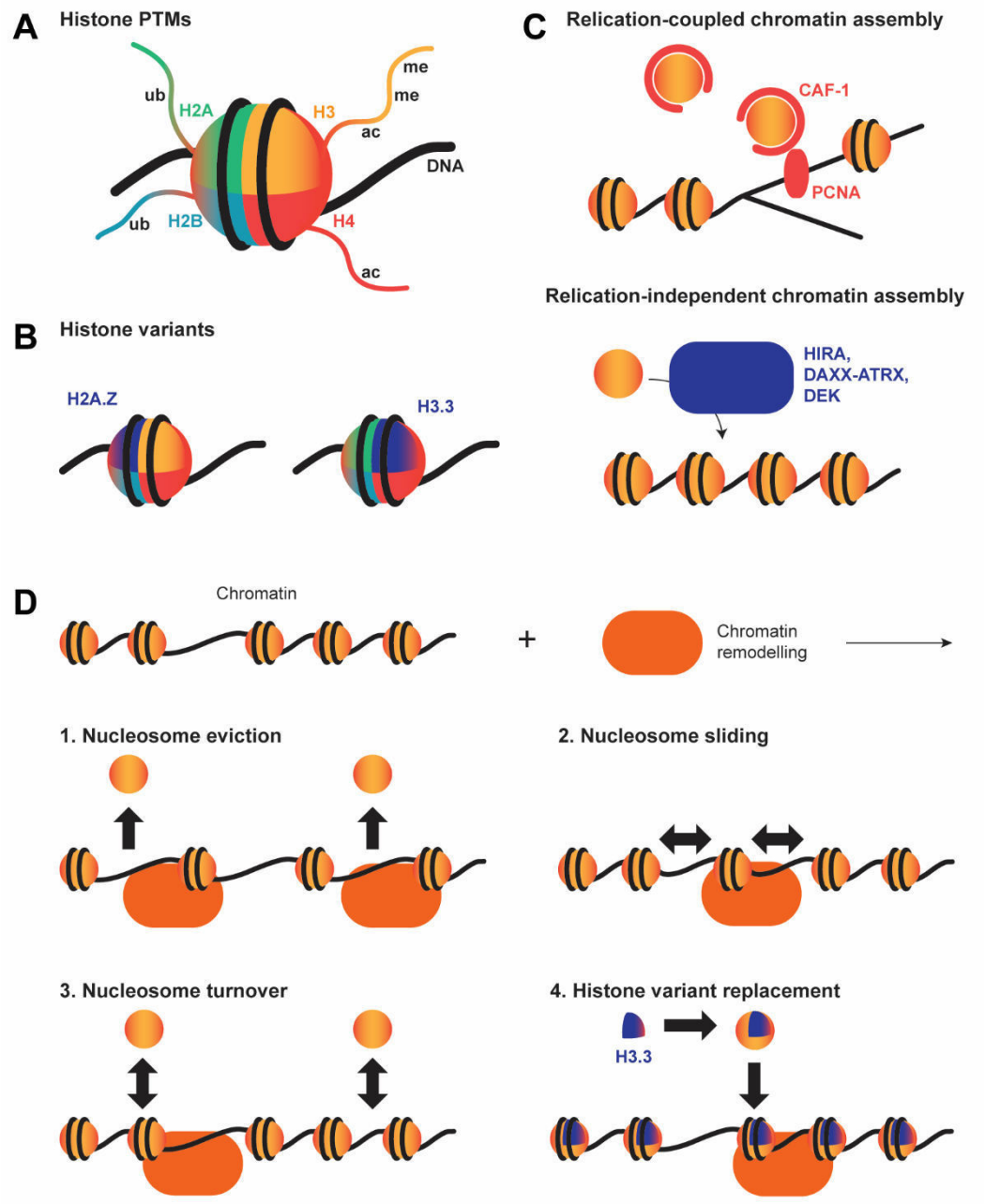

Figure 1.2. Chromatin structure and its regulation. (A) The nucleosome consists of 146 base-pairs of DNA wound around a histone octamer. The histones, particularly the N-terminal tails, can be post-translationally modified. (B) Chromatin structure can be altered by the presence of histone variants such as histones H2A.Z and H3.3. (C) Histones are incorporated into the DNA in either a replication-dependent or independent manner, involving different chaperone proteins. (D) Chromatin remodelling can alter the chromatin structure in several ways as shown, which may change the DNA accessibility and thus transcription factor binding (Burgess and Zhang 2013; Venkatesh and Workman 2015; Clapier et al. 2017).

The discovery that the N-terminal tails of histone proteins can be modified, for example by acetylation or methylation (Figure 1.2A), led to the "histone code" hypothesis that histone PTMs may direct chromatin structure and gene expression by altering the physical properties of the nucleosomes (Hansen et al. 1998) or by recruiting proteins which recognise specific PTMs (Strahl and Allis 2000). Indeed, there is a lot of evidence showing that different histone PTMs mark specific chromatin regions; for example, H3K27 acetylation is frequently a marker of active enhancer chromatin (Creyghton et al. 2010). Indeed, different chromatin states have been established from the patterns of PTMs (Mikkelsen et al. 2007; Kharchenko et al. 2011; Ho et al. 2014). Furthermore, correlative studies have found relationships between the pattern of PTMs, chromatin accessibility and transcription factor binding (Robertson et al. 2008; Shu et al. 2011), suggesting that PTMs are intimately linked to the activity of genomic regions in a given cell type.

It is well established that many proteins are able to "read" histone PTMs (Patel and Wang 2013). For example, proteins with bromodomains recognise acetylated lysine residues (Sanchez and Zhou 2009). Interestingly, many chromatin modifiers responsible for depositing histone PTMs also contain reader domains, such that the presence of PTMs can influence further PTM deposition. For example, CBP/p300 contains both a bromodomain and acetyltransferase activity, suggesting that a positive feedback loop may be important at CBP/p300-regulated enhancers to promote robust levels of acetylated histones (Chen et al. 2010). Additionally, it has been found in some cases that the enzymatic activity of chromatin modifiers can be influenced by PTM recognition. For example, the demethylase activity of KDM5A is enhanced when the PHD1 domain binds to the unmodified H3K4 residue (Torres et al. 2015). These types of feedback loop provide a mechanism for how chromatin marks can spread through the genome, leading to distinct genomic domains. However, it is still unclear how the boundaries of these domains are set and how activating and repressive histone PTMs are balanced.

Since many studies on histone PTMs are correlative, it has been difficult to elucidate how much of a functional role they play in transcription regulation. Many of the histone methyltransferases and acetyltransferases have non-histone

substrates, making it difficult to attribute phenotypic effects from disrupting these enzymes to perturbed PTM levels (Henikoff and Shilatifard 2011). Mutations of specific residues in yeast have been used to show that PTMs are important for normal gene expression levels, although often phenotypes only arise when several residues are mutated, and mutations of the N-terminal tails are rarely lethal (Ling et al. 1996; Martin et al. 2004; Dai et al. 2008; Jin et al. 2009). In order to probe metazoan histones in the same way, the entire histone gene complex in *Drosophila* was deleted such that it can be replaced with mutant histones (Günesdogan et al. 2010). With this approach, it was found that H3K36 as well as residues on the globular domain, such as H3K56, were required for viability (McKay et al. 2015; Graves et al. 2016). H3K27me3 was shown to remain heritably associated at a repressed gene through multiple rounds of replication and is essential for Polycomb-mediated gene silencing (Pengelly et al. 2013; McKay et al. 2015; Coleman and Struhl 2017). Together these results indicate that in some cases histone PTMs have a clear function in development. However, further studies are required to fully understand the combinatorial action of histone PTMs with their interacting proteins, and to distinguish their role in the recruitment of reader proteins from their effects on chromatin structure.

Histone variants present another way for the chromatin structure to be altered (Figure 1.2B), and similarly to histone PTMs, specific variants have been associated with particular genomic regions. For example, histone H2A.Z is enriched at promoter regions (Subramanian et al. 2015) and reduces the stability of the nucleosome (Luger et al. 2000), while histone H3.3 is found at enhancers and active genes bodies and is associated with histone exchange (Mito et al. 2005; Wirbelauer et al. 2005; Kraushaar et al. 2013; Deaton et al. 2016). The presence of these variants at key regulatory regions allows them to influence transcription. For example, it is thought that the presence of histone H2A.Z at the +1 (first) nucleosome reduces the barrier to Pol II at the start of transcription (Weber et al. 2014). Indeed it was found that promoter-proximal pausing negatively correlated with histone H2A.Z presence at the +1 nucleosome, and that histone H2A.Z levels were low at strong circadian promoters, suggesting that genes regulated by Pol II pausing benefit from a lack of histone H2A.Z to aid stalling of the polymerase (Westermark 2016).

Histone H3.3 appears to have several different roles. For example, it is enriched at telomeres where the H3K9 residue is trimethylated (Lewis et al. 2010; Udugama et al. 2015), and here it undergoes slow turnover (Kraushaar et al. 2013). However, its deposition at enhancers and gene bodies has a higher turnover rate and is associated with gene activity (Kraushaar et al. 2013; Ha et al. 2014). For example, histone H3.3 turnover rates changed at enhancer regions after the differentiation of embryonic stem cells into neural stem cells (Deaton et al. 2016). And in the mammalian brain, histone H3.3 levels have been found to accumulate at active genes with age (Maze et al. 2015; McNally et al. 2016). This accumulation of histone H3.3 has been proposed to affect learning and memory, and *Drosophila* mutants for the orthologue of the intellectual disability gene *BRWD3* have increased histone H3.3 levels and disrupted gene expression (Chen et al. 2015). Although these studies would imply an important role for histone H3.3 at genomic regulatory regions, this is called into question by studies in *Drosophila* with mutations in histone H3.3. While there are some transcriptional defects, null mutant animals are still viable, with histone H3.3 only essential for male fertility (Sakai et al. 2009; Hödl and Basler 2009). Thus, in the same manner as with histone PTMs, it has been difficult to define a clear mechanistic function for histone H3.3.

In addition to the ability of histone H3.3 to undergo replication-independent nucleosome assembly (Ahmad and Henikoff 2002), some of its effects may be linked to the presence of PTMs, since specific PTMs have been found to be enriched on histone H3.3 (McKittrick et al. 2004). For example, histone H3.3 is required for establishing PRC2-dependent H3K27me3 at developmentally-regulated promoters in embryonic stem cells (Banaszynski et al. 2013), and the H3.3K27M mutation is associated with reduced H3K27me3 levels in paediatric glioma (Chan et al. 2013). Furthermore, H3.3K4 was required for epigenetic memory at the *MyoD* promoter in nuclear transplant embryos (Ng and Gurdon 2008). Despite these examples relating histone H3.3 PTMs to specific functions, no PTMs were found to be present on histone H3.3 exclusively (McKittrick et al. 2004). It is therefore possible that PTMs on canonical histone H3 variants perform similar functions to those on histone H3.3 in most cases, perhaps with reduced efficiency, which may explain the lack of lethality from histone H3.3 mutants. The effects of histone H3.3 on transcription most likely result from a

combination of both the local histone dynamics and PTMs acting synergistically. This highlights the need to study the chromatin structure from several angles in order to understand its complex regulation.

The physical chromatin structure is also affected by nucleosome occupancy, positioning or dynamics. Nucleosomes have intrinsic sequence preferences, so the positioning of nucleosomes in the genome is determined to some extent by DNA sequence (Segal et al. 2006; Kaplan et al. 2009). However, the positioning of most nucleosomes in the genome is not rigid, and can be influenced by chromatin remodellers or other proteins (Struhl and Segal 2013). For example, there is evidence to suggest that the transcriptional machinery itself positions the +1 nucleosome (Zhang et al. 2009; Rhee and Pugh 2012). Furthermore, transcription factor binding at regulatory regions can affect nucleosome occupancy (Barozzi et al. 2014; Ramachandran and Henikoff 2016b), and thus occupancy changes at enhancers with cell differentiation and reprogramming (West et al. 2014). In order for these changes to occur, the chromatin structure must be dynamic, with nucleosomes continually being replaced and moved. It has become apparent from studies of histone exchange that nucleosome turnover is not uniform across the genome, with the highest rates of turnover at active genes and regulatory elements (Deal et al. 2010; Ray-Gallet et al. 2011; Kraushaar et al. 2013; Yildirim et al. 2014). Therefore, the dynamic exchange of nucleosomes is likely to play a key role in the regulation of gene expression.

1.2.2 Regulation by chromatin modifiers

Regulation of the chromatin structure depends on histone chaperones, proteins which bind to histones and regulate their assembly into the chromatin (Burgess and Zhang 2013). A large part of nucleosome assembly occurs during DNA replication, where CAF-1 interacts with the replication machinery via PCNA to deposit histones onto the DNA (Shibahara and Stillman 1999; Burgess and Zhang 2013). However, replication-independent nucleosome assembly is thought to involve histone H3.3 (Ahmad and Henikoff 2002) and therefore involves different histone chaperones (Figure 1.2C). The deposition of histone H3.3 at telomeres involves DAXX and ATRX, while HIRA regulates H3.3 enrichment at active genes (Ray-Gallet et al. 2002; Goldberg et al. 2010). It is

thought that HIRA-dependent histone H3.3 incorporation occurs at naked DNA to fill nucleosome-depleted gaps (Ray-Gallet et al. 2011; Schneiderman et al. 2012). However, another chaperone DEK has been proposed to control the pattern of histone H3.3 deposition in embryonic stem cells (Ivanauskiene et al. 2014).

In *Drosophila*, mutants for histone H3.3 are viable, with histone H3.3 only being essential for male fertility, and it was found that an upregulation of canonical histone H3 can compensate for a loss of histone H3.3 to some extent (Sakai et al. 2009). Similarly, HIRA is only required for the assembly of paternal chromatin in the gametes and histone H3.3 deposition is not affected in HIRA mutant embryos or adults (Bonnefoy et al. 2007), suggesting that other chaperones are able to deposit histone H3.3 in place of HIRA. A candidate may be XNP, since double mutants for XNP and HIRA are lethal in *Drosophila* and both were shown to bind to nucleosome-depleted chromatin (Schneiderman et al. 2012).

A variety of studies have identified different mechanisms of histone H3.3 deposition in different contexts. For example, dBRWD3 was shown to negatively regulate HIRA-mediated histone H3.3 deposition important for normal gene expression levels in neurons (Chen et al. 2015). At chromatin boundaries, HIRA was found to interact with the DNA-binding protein GAGA factor, the chromatin factor FACT and the PBAP chromatin remodelling complex (Nakayama et al. 2007, 2012). And DEK was shown to be involved in ecdysone-induced puff formation in the *Drosophila* salivary gland (Sawatsubashi et al. 2010). Despite these studies, a comprehensive comparison of histone chaperones in different contexts has not been performed, and thus it remains unknown which mechanisms are context-specific versus widely applicable. Furthermore, the mechanisms of histone H3.3 deposition have not been described in great detail, so it is likely that more proteins will be implicated in coming years.

By affecting chromatin structure, histone chaperones can have an impact on transcription and cell fate. For example, HIRA-mediated incorporation of histone H3.3 at an enhancer element is required for the expression of RUNX1

that generates haematopoietic stem cells (Majumder et al. 2015). DEK was found to bind to transcription start sites and its depletion caused changes in expression level of the regulated genes (Sandén et al. 2014). And suppression of CAF-1 complex subunits was found to affect transcription factor-mediated reprogramming of mouse fibroblasts by increasing the accessibility of enhancer elements (Cheloufi et al. 2015). While it is clear that histone chaperones play a role in regulating chromatin structure and are intimately linked to specific histone variants, further work is required to fully understand their different functions. For example, it is unclear how different histone H3.3 chaperones target different genomic regions and whether there is any redundancy between different chaperones or pathways.

Chromatin structure is further regulated by chromatin remodellers, proteins or complexes which can alter nucleosome positioning and dynamics using energy from ATP. They fall into four main classes based on the presence of well-defined protein domains: SWI/SNF, ISWI, CHD and INO80 (Längst and Manelyte 2015), and their function in development and disease is well documented (Hota and Bruneau 2016). For example, a mammalian SWI/SNF catalytic subunit Brg1 is required during peri-implantation development for the proper development of the inner cell mass and trophectoderm (Bultman et al. 2000). Furthermore, chromatin remodellers are very frequently mutated in cancers (Nair and Kumar 2012; Hodges et al. 2016). Therefore, an understanding of how chromatin remodellers function is beneficial for research on human diseases.

All four classes contain the ATPase-translocase domain, and thus it has been argued that all chromatin remodelling may involve the same translocation mechanism (Clapier et al. 2017). Since there are many histone-DNA contacts within a nucleosome, it is energetically more favourable to break only a few of these contacts at a time, resulting in a wave of DNA that propagates around the nucleosome. Indeed, DNA loops have been detected with single molecule approaches as evidence of this (Lia et al. 2006; Zhang et al. 2006). The “loop-recapture” model predicted that this DNA loop is introduced at the nucleosome entry site (Strohner et al. 2005). However, others have found that the translocase binds to a particular site near the nucleosome dyad and remains at a fixed position during translocation, where it pulls DNA in from one side and

transfers it to the other (Saha et al. 2005; Zofall et al. 2006). This has been named the "wave-ratchet-wave" model, and some have found it to involve a small step size of only a few base-pairs (Sirinakis et al. 2011; Deindl et al. 2013).

Despite the current belief by some that there is a conserved mechanism of translocation among the four classes of chromatin remodellers, the effects of this translocation appear to differ (Figure 1.2D). In some circumstances, mainly involving SWI/SNF complexes, chromatin remodelling is thought to induce nucleosome eviction. Evidence for this comes from studies of the yeast *PHO5* promoter, where gene induction involves the complete disassembly of nucleosomes (Almer et al. 1986; Boeger et al. 2003, 2004, 2008). Models of this system suggest that nucleosome disassembly occurs continually with nucleosome reassembly (Boeger et al. 2008; Brown et al. 2011), suggesting that chromatin remodelling can promote nucleosome turnover instead of simply reducing nucleosome occupancy. Additional *in vitro* studies suggest that eviction may involve the stepwise loss of H2A/H2B dimers before the rest of the histone octamer (Lorch et al. 2006; Rowe and Narlikar 2010; Dechassa et al. 2010), but it remains to be tested how this fits with the model of translocation.

In other systems, ISWI, CHD and INO80 chromatin remodellers are thought to promote nucleosome sliding, due to their ability to affect the spacing or positioning of nucleosomes on DNA (Stockdale et al. 2006; Yang et al. 2006; Udugama et al. 2011; McKnight et al. 2011). Some evidence argues that SWI/SNF chromatin remodelling also involves sliding, since a barrier in the DNA blocked nucleosome displacement (Whitehouse et al. 1999) and adjacent nucleosomes were required for nucleosome disassembly (Dechassa et al. 2010), suggesting that the sliding of one nucleosome displaces its neighbour. In fact, it has been argued that both nucleosome eviction and sliding occur via the same mechanism, with differential translocation efficiency regulating whether the result is sliding or eviction, mediated by the binding of actin-related proteins (Clapier et al. 2016).

Chromatin remodellers, namely of the INO80 class, have also been implicated in histone variant replacement. It has been shown that SWR-C replaces H2A/H2B dimers with H2A.Z/H2B dimers and the INO80 complex does the

opposite, together resulting in the proper localisation of histone H2A.Z at promoters (Mizuguchi et al. 2004; Papamichos-Chronakis et al. 2011). Structural studies of SWR-C and INO80 complexes have identified the domains responsible for nucleosome binding and remodelling activity (Watanabe et al. 2015). Less is known about how chromatin remodellers interact with the histone H3.3 variant, but a link has been made between the *Drosophila* PBAP SWI/SNF complex and histone H3.3 replacement at chromatin boundaries (Nakayama et al. 2012). Therefore, it is possible that SWI/SNF remodelling is responsible for promoting nucleosome turnover involving histone H3.3.

The vast majority of studies revealing mechanistic details of chromatin remodelling have been performed *in vitro*. However, a number of studies have gained mechanistic insight *in vivo*. For example, a yeast ISWI chromatin remodeller was shown to catalyse the sliding of nucleosomes towards target gene promoters, since sliding intermediates were detected (Fazzio and Tsukiyama 2003). Evidence of partially unwrapped nucleosomes was found to correlate with binding of the yeast RSC SWI/SNF remodeller *in vivo* (Ramachandran and Henikoff 2016a). And while few studies have made mechanistic comparisons between the different classes of chromatin remodellers, a comprehensive study in a *Drosophila* cell line showed that the depletion of different classes of chromatin remodellers led to different effects on nucleosome occupancy at target sites (Moshkin et al. 2012). Further studies like these are needed to bridge the gap between the mechanistic knowledge gained *in vitro* and the functional roles of chromatin remodellers *in vivo*.

1.2.3 Transcription factor interaction with the chromatin

By mobilising nucleosomes, chromatin remodellers have the ability to regulate DNA accessibility, either positively or negatively, which can impact transcription factor binding. Most transcription factors bind to accessible DNA (Li et al. 2011; Degner et al. 2012), and therefore mechanisms resulting in the exposure of motifs will promote transcription factor binding. However, this may not be the case for all transcription factors, since the progesterone receptor was found to require nucleosomes for optimal binding (Ballaré et al. 2013a, 2013b).

The term “pioneer factor” has been used to describe transcription factors such as FoxA, which have the ability to bind to nucleosomal DNA and subsequently cause changes in chromatin structure (Zaret and Carroll 2011). Thus, they can access their motifs even when present within nucleosomes, enabling the opening of relatively inaccessible regions of chromatin. Despite this, pioneer factors still do not occupy all of their binding sites in the genome and do exhibit cell-type-specific binding, most likely due to their inability to bind to highly compacted heterochromatin (Zaret and Mango 2016). The line between pioneer factors and other transcription factors is blurred by examples of indirect cooperativity, where transcription factors compete with nucleosomes for dynamic binding to the DNA and lead to “passive” nucleosome eviction (Mirny 2010). Thus, it is not always clear whether high chromatin accessibility at enhancers is the cause or effect of transcription factor binding. To distinguish between these possibilities, a mathematical modelling approach was used, since the chromatin accessibility at pioneer factor binding motifs is expected to correlate with the expression of the relevant pioneer factor (Lamparter et al. 2017). Using large datasets for chromatin accessibility and gene expression, this approach was able to predict pioneer function for six out of eight pioneer subfamilies.

Regardless of whether they are pioneers, transcription factors can access the DNA and change the chromatin structure by interacting with chromatin remodellers, a process becoming known as “assisted loading” (Voss et al. 2011; Madsen et al. 2014; Swinstead et al. 2016). For example, INO80 is recruited by OCT4 at pluripotency genes in ES cells to maintain their accessibility (Wang et al. 2014b), and GR recruits SWI/SNF remodellers which subsequently inhibit GR binding at the MMTV promoter (Fryer and Archer 1998; Nagaich et al. 2004). Although in most cases, the effect of chromatin remodelling on transcription factor binding has been studied, it is also possible for transcription factor binding to affect chromatin remodelling. It has been shown *in vitro* that transcription factor binding can present a barrier to ISWI but not SWI/SNF remodelling (Li et al. 2015). Thus, the dynamic order of events is likely to be key for the correct regulation of gene expression.

In summary, the chromatin represents a highly dynamic and complex structure with which transcription factors and the transcription machinery interact. A range of features including histone PTMs, histone variants, nucleosome occupancy and positioning can all affect chromatin structure. These features are interdependent and it is likely that the cooperation of histone marks with the physical properties of the chromatin is important for precise developmental control of transcription. The chromatin structure is controlled by chromatin modifying proteins such as histone chaperones and chromatin remodellers. By re-structuring the chromatin, chromatin modifiers can affect transcription factor binding and thus represent crucial elements for the control of transcription. However, there remain many unanswered questions about how these different factors operate together to control whether a gene is expressed.

1.3 Notch signalling

1.3.1 Notch as a cell signalling pathway

Since every cell of an animal exists in the context of others, cell-cell communication is essential for the correct cell types and tissues to develop in the right place at the right time. Signalling pathways exist as mechanisms to transduce external signals into transcriptional outcomes (Basson 2012). Many signalling molecules are secreted and diffusible, allowing concentration gradients to be produced across tissues, with different concentrations resulting in different cellular outcomes. For example, graded BMP and Chordin signalling in the *Xenopus laevis* embryo pattern the dorsoventral axis, such that transplantation of the dorsal mesoderm to a ventral location results in a duplication of the body axis (Bier and De Robertis 2015). Later in development, a spatial and temporal gradient of SHH patterns the vertebrate neural tube to give the different neuronal subtypes dorsoventrally (Ribes and Briscoe 2009).

Notch signalling differs from these pathways for two main reasons. Firstly, Notch itself is a transmembrane receptor activated in most cases by transmembrane ligands, so signalling usually occurs between neighbouring cells. Soluble forms of Notch ligands have been used experimentally (Klose et al. 2015), and truncations of the ligand JAGGED1 which occur in human disease

also result in a soluble ligand (Ponio et al. 2007). Interestingly however, soluble ligands usually antagonise Notch signalling by competing with membrane-bound ligands (D'Souza et al. 2010) and were shown to activate signalling only when immobilised (Varnum-Finney et al. 2000). Exceptions to this are found in *Caenorhabditis elegans,* where a number of soluble ligands are able to activate Notch signalling (Chen and Greenwald 2004; Komatsu et al. 2008). It is thus possible that these secreted ligands can act as morphogens, and indeed a gradient of Notch-dependent transcription was found to occur in the germline stem cells of *C. elegans* (Lee et al. 2016). However, since most ligands studied are membrane-bound, Notch signalling has mostly been implicated in cell fate decisions involving individual cells or triggered by proximal events.

A second way in which Notch signalling differs from other signalling pathways is its signalling cascade. Ligand binding triggers cleavage of the receptor such that part of the receptor itself, the Notch intracellular domain (NICD), travels directly to the nucleus to activate transcription (Bray 2016). Without any protein intermediates, there is no opportunity for amplification, so the level of the response is directly determined by the level of signalling. With such simplicity, the Notch pathway presents an opportunity to study the basic mechanisms involved in regulated gene expression, whilst being integral for many stages of normal development.

1.3.2 Role of Notch signalling in development and disease

Notch signalling is involved in many cell fate decisions during development and is conserved through eukaryotic evolution. It is well known for its role in lateral inhibition, a process where inhibitory signalling between cells prevents neighbouring cells from adopting the same fate. This occurs during vertebrate neural development where neurons express Notch ligands to inhibit neurogenesis in surrounding cells (Pierfelice et al. 2011). Notch can also play a role in boundary formation between cell compartments, such as at the dorsoventral compartment boundary in the *Drosophila* wing disc (Major and Irvine 2005), or the boundary between the organ of Corti and Kölliker's organ in the mouse cochlea (Basch et al. 2016). Many cell fate decisions controlled by Notch are concerned with balancing proliferation with differentiation. In the

mammalian intestine, high levels of Notch signalling maintain the proliferation of intestinal stem cells in the crypt base, but promote enterocyte differentiation in the transit amplifying cells (Sancho et al. 2015).

Notch signalling is implicated in many diseases. Mutations in Notch receptors or ligands themselves cause a range of genetic disorders such as Alagille and Hajdu-Cheney syndromes, Cerebral Autosomal Dominant Arteriopathy with Subcortical Infarcts and Leukoencephalopathy (CADASIL) and spondylocostal dysostosis (Penton et al. 2012). Notch signalling also plays a key role in cancer, acting as an oncogene in some cases and a tumour suppressor in others (Lobry et al. 2011). It is best known for its role in T-cell acute lymphoblastic leukaemia where activating mutations in Notch1 are prevalent, but it is also crucial for some solid tumours such as breast and glioblastoma (Ranganathan et al. 2011). Notch signalling research therefore has implications for finding potential therapeutics for such diseases.

Studies of Notch signalling over the last few decades have led to a good understanding of the basic activation mechanism and the main components involved, particularly since it is a relatively simple pathway (Bray 2016). However, some features of Notch signalling are less well understood and remain controversial. For instance, the Notch-specific transcription factor can act as either a repressor or activator, and it is unclear exactly how it switches function. And the genes upregulated by Notch signalling differ between cell types. This is clearly critical to the role of Notch signalling during development, but how it is regulated is not fully known. These features are all discussed below.

1.3.3 Activation mechanism

In mammals there are four Notch receptors, paralogues of the single *Drosophila* Notch receptor, created by genome duplications through evolution. The Notch extracellular domain contains Epidermal Growth Factor (EGF)-like repeats and a negative regulatory region, while the intracellular domain contains an RBPJ Association Module (RAM) domain, an ankyrin repeat domain, a Transactivation Domain (TAD) and several nuclear localisation signals. The two ligands in *Drosophila* are called Delta and Serrate while the five mammalian

ligands fall into two synonymous classes, Delta-like and Jagged. Binding of these to the Notch receptor triggers the S2 cleavage within the negative regulatory region by ADAM metalloproteases, followed by the S3 and S4 cleavages within the transmembrane domain by γ-secretase, releasing NICD (Figure 1.3A; Kopan and Ilagan 2009). In the absence of ligand-induced activation, the negative regulatory region occludes the S2 site, preventing cleavage (Gordon et al. 2007). Ligand binding exerts a force which exposes this site to the metalloprotease and allows the subsequent cleavages to also occur (Gordon et al. 2015). Since the negative regulatory region structurally relies on calcium ions, removal of calcium by chelation causes cleavage of the receptor and Notch activation, a feature utilised in many studies on Notch signalling (Rand et al. 2000; Housden et al. 2013; Skalska et al. 2015).

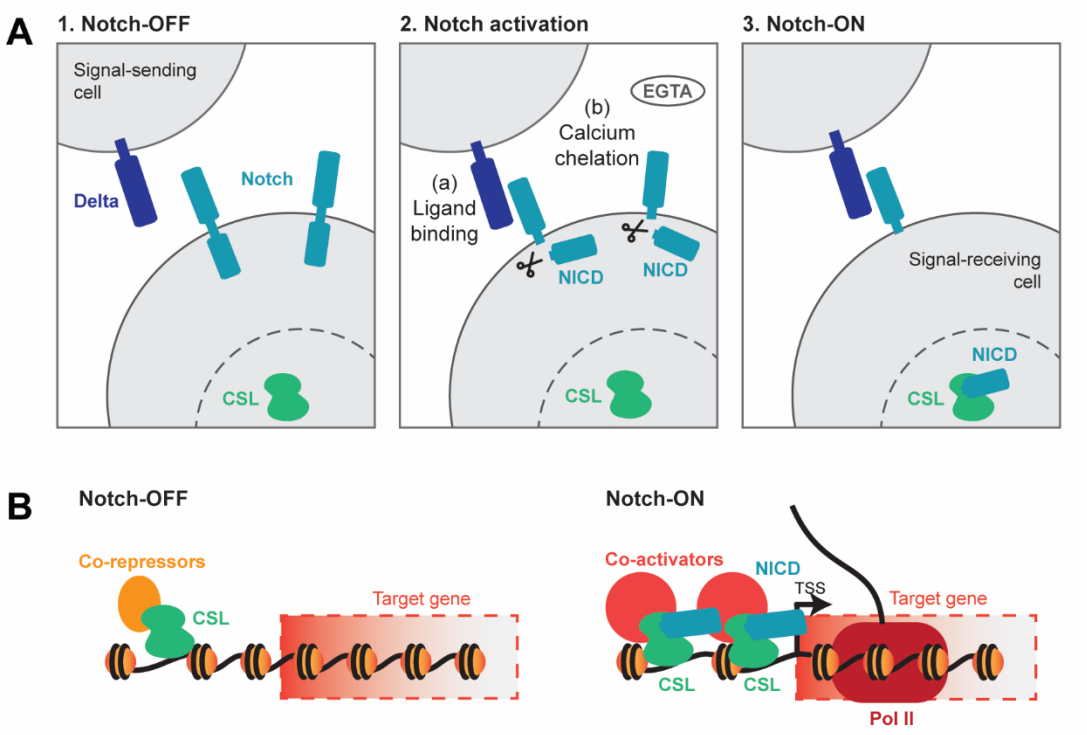

Figure 1.3. Overview of Notch signalling pathway. (A) The Notch transmembrane receptor is activated by transmembrane ligands on neighbouring cells, which triggers cleavage of the receptor, releasing NICD. Alternatively, cleavage can be chemically induced by calcium chelators such as EGTA. NICD travels to the nucleus where it activates target genes with the transcription factor CSL. (B) In the absence of signalling, CSL can act with co-repressors to repress certain genes. Upon signalling, CSL forms an activating complex and occupancy increases at target sites to activate transcription (Bray 2016; Bray and Gomez-Lamarca 2018).

1.3.4 Nuclear complexes

In the nucleus, NICD binds to the transcription factor known by several names (CBF1 or RBPJ in mammals, Su(H) in *Drosophila*, LAG-1 in *C. elegans*) or CSL collectively. This allows the subsequent binding of the co-activator Mastermind (Mam in *Drosophila*, MAML1-3 in mammals) to form the ternary activating complex (Figure 1.3B, Notch-ON; Nam et al. 2006; Wilson and Kovall 2006). Mam is then thought to recruit the acetyltransferase CBP/p300 and the Mediator complex to target genes to promote transcription (Fryer et al. 2002; Wallberg et al. 2002; Fryer et al. 2004). However, the precise mechanism of action has not been well characterised and NICD itself may also have an important role.

In the absence of Notch activation, CSL can form complexes with co-repressors which inhibit the transcription of target genes (Figure 1.3B, Notch-OFF). While other components of the Notch pathway are well conserved between vertebrates and invertebrates, surprisingly the co-repressors differ somewhat. In *Drosophila*, the key co-repressor Hairless binds to Suppressor of Hairless (Su(H)) directly (Kurth et al. 2011) and has the potential to recruit C-terminal Binding Protein (CtBP) and Groucho (Barolo et al. 2002). Removal of any of these factors can lead to upregulation of Notch target genes (Nagel et al. 2005). In mammals, CSL has been shown to physically interact with a range of different factors (Kao et al. 1998; Hsieh et al. 1999; Collins et al. 2014) including the SMRT and HDAC Associated Repressor Protein (SHARP, also known as Msx2-Interacting-Nuclear Target protein, MINT; VanderWielen et al. 2011). Despite Hairless only being conserved in insects (Maier et al. 2008), there are some similarities in the co-repressive mechanisms between *Drosophila* and mammals. For example, SHARP can recruit CtBP (Oswald et al. 2005) and the SMRT homologue, SMRT-related and Ecdysone Receptor interacting factor (SMRTER) has been linked to Notch signalling in *Drosophila* (Heck et al. 2012). However, the functionally different roles that the mammalian co-repressors play and how CSL swaps between these different partners is not well understood.

1.3.5 The switch from repression to activation

It is clear in some cases that the genes suppressed by the repressive CSL complex are the same genes which are Notch-responsive upon signalling, with repression functioning to keep the genes switched off in the absence of a Notch signal (Castro et al. 2005). It was therefore initially thought that Notch activation triggered gene expression by the displacement of the co-repressors with the co-activators, making the assumption that CSL remains bound to the DNA (Kao et al. 1998). However this is not always the case, as some genes which are not under Hairless-mediated repression are able to respond to ectopic Notch signalling in the *Drosophila* wing disc (Chan et al. 2017). Additionally, some sites bound by CSL do not respond to Notch signalling (Castel et al. 2013). The original exchange model was further challenged by the key finding that CSL occupancy increases at Notch-responsive enhancers in response to Notch signalling (Krejci and Bray 2007; Castel et al. 2013; Wang et al. 2014a), since this implies that Notch-dependent transcription does not rely solely on CSL which was already present before signalling. A simple exchange of the co-repressors for NICD is also less likely based on the affinities of the co-repressors and NICD for CSL, as the repressors were found to have a higher affinity (VanderWielen et al. 2011; Collins et al. 2014; Yuan et al. 2016).

Recent work studying the dynamics of CSL showed that it binds transiently to the DNA in the absence of Notch signalling (Gomez-Lamarca et al. 2018). Furthermore, the residence time of CSL binding increased locally at target genes in response to Notch signalling, and in a manner that was dependent on MAM, suggesting that the interaction of CSL with the DNA is altered upon formation of the ternary activating complex. Surprisingly, Hairless recruitment was increased by Notch signalling at Notch-responsive targets, suggesting that there may be ongoing competition between the activating and repressing complexes, even under conditions of Notch activation. These findings also suggested a possible change in chromatin structure and accessibility with Notch signalling, which is discussed in detail and tested experimentally in chapter 4.

In mammals, a different model has recently been proposed involving a “permissive” state between repression and activation, where SHARP interacts

with the activating histone methyltransferase KMT2D (Oswald et al. 2016). Interestingly, the KMT2D homologue in *Drosophila*, Trr, has also been found to be essential for the Notch response (Gomez-Lamarca et al. 2018). However, since the co-repressors are not well conserved between *Drosophila* and mammals, further work is required to elucidate whether the mechanisms controlling the Notch response are the same in the two cases.

One parallel can be drawn between the new models of Notch-regulated transcription, since in both there is a focus on changes to the chromatin environment as well as the changes to the protein complexes themselves. However, it is still unclear how these changes to the chromatin structure are brought about, and how this impacts on CSL residence time and transcriptional output.

1.3.6 Achieving cell type specificity

It is remarkable how a single, very simple pathway can lead to such diverse outcomes. Notch does this by activating different sets of target genes under different conditions and in different cell types (Krejcí et al. 2009; Wang et al. 2011; Jin et al. 2013; Terriente-Felix et al. 2013). Although not completely understood how this is achieved in all cases, there are some indications of mechanisms that influence the choice of target genes.

A key aspect is likely to be the presence of tissue-specific transcription factors which cause changes in chromatin structure and thus affect CSL binding to enhancers. For example, RUNX transcription factors cooperate with Notch in several contexts, with some target genes only responding to Notch when RUNX is present (Terriente-Felix et al. 2013; Wang et al. 2014a; Hass et al. 2015). Furthermore, RUNX expression in *Drosophila* cells led to changes in histone PTMs and *de novo* recruitment of CSL to enhancers (Skalska et al. 2015). This is likely to involve other chromatin modifiers, since RUNX is known to interact with many different proteins (Chuang et al. 2013). For example, a SWI/SNF complex interacts with RUNX in human cells to control haematopoietic genes (Bakshi et al. 2010). This, along with the fact that no direct interaction between

CSL and RUNX has been detected, suggests that the recruitment of CSL by RUNX is likely to act via a mechanism of indirect recruitment.

Several Notch-responsive enhancers have been characterised which contain binding sites for multiple transcription factors. By converging at specific enhancers, Notch signalling can interact with other signalling pathways. For example, Notch and Wingless signalling both control the *vestigial* gene in the *Drosophila* wing disc via Su(H) and dTCF binding sites in the enhancer (Klein and Arias 1999). Notch also cooperates with EGFR signalling to control *Pax2* expression in cone cells of the *Drosophila* eye disc (Flores et al. 2000). This is mediated by the *sparkling* enhancer where many transcription factor binding sites must be properly arranged for transcriptional activity and cell type specificity (Swanson et al. 2010). It is therefore possible that direct protein-protein interactions between CSL and other transcription factors may be important for enhancer activity in some cases. Indeed, in another example, Notch interacts with Transforming Growth Factor-β (TGF-β) signalling by direct recruitment of the transcription factor Smad3 to Notch targets (Blokzijl et al. 2003).

Since it is becoming apparent that the dynamics of transcription factor binding are important for transcriptional output (Lickwar et al. 2012; Gomez-Lamarca et al. 2018), the target genes which are activated by Notch signalling may be influenced in some way by the levels or temporal dynamics of Notch activation. Indeed, a recent study suggested that the two ligands Delta-like1 and Delta-like4 activate different Notch targets by altering Notch dynamics (Nandagopal et al. 2018). It remains to be seen how this kind of regulation could interact with the chromatin structure mechanistically to coordinate the response. Gaining a deeper understanding of the mechanisms controlling Notch-responsive transcription temporally could help to define how these different factors bring about different cellular responses.

1.4 Aims and outline of the thesis

The simplicity of the Notch pathway makes it a useful system in which to study the regulation of inducible gene expression. The basic mechanism of Notch signalling activation provides little opportunity for modulation, yet the transcriptional and phenotypic outcomes which result are diverse. Understanding how this is achieved would be of benefit to our understanding of both normal development and disease. While some factors are known to influence the Notch response in certain contexts, a holistic model of how Notch target genes are selected does not exist. During this PhD, the aim has been to gain a deeper understanding of the mechanisms involved in bringing about the Notch response, to take us closer to understanding the complex processes of gene expression, relevant for cell fates controlled by Notch and for cell signalling responses more widely.

One question is what the temporal dynamics of transcription are in response to Notch activation. In chapter 3, a live imaging technique is used to measure the transcription of a Notch target gene in cultured *Drosophila* cells, on a single-cell basis and in real time. This gives insight into which aspects of the Notch transcriptional response are homogenous or heterogeneous between cells, and how reliable, rapid and robust the transcriptional response is.

A second question is what role changes in chromatin accessibility play in the Notch response, and what factors are required to implement these. In chapter 4, the regulation of the Notch response by the chromatin structure is investigated using molecular biology techniques and *in vivo* imaging. Through these experiments, a SWI/SNF chromatin remodelling complex was shown to have a crucial role in the Notch response.

2 MATERIALS AND METHODS

2.1 Key reagents and methods

To avoid recurring information, details of some key reagents and methods used throughout this chapter are given here.

2.1.1 Molecular cloning

Unless otherwise specified, all polymerase chain reactions (PCR) used either Phusion or Q5 High-Fidelity DNA polymerase (NEB #M0491 or #M0530 respectively), restriction endonuclease enzymes were obtained from New England BioLabs (NEB), and ligations used T4 DNA Ligase (Promega #M1794).

2.1.2 Cell culture conditions

Unless otherwise specified, Kc167 cells (Drosophila Genomics Resource Center stock#1) were cultured in Schneider's *Drosophila* medium (Gibco #21720024) supplemented with 5% fetal bovine serum (FBS; Sigma #F9665) and 1x Antibiotic-Antimycotic (Gibco #15240062) at 25°C.

2.1.3 Transfection reagents

Transfections and RNAi in Kc167 cells made use of Opti-MEM (Gibco #31985070) and FuGENE HD Transfection Reagent (FuGENE; Promega #E2311) at the volumes specified.

2.1.4 Antibiotics and inhibitors

Table 1. List of drugs used for selection of stable cell lines and cell treatments.

Drug	Source
G418 (Geneticin™)	ThermoFisher #11811031
Blasticidin	ThermoFisher #R21001
Puromycin	Sigma #P9620
Triptolide	Sigma #T3652
Flavopiridol	Cayman Chemical #10009197
MG132	Sigma #C2211

2.1.5 Antibodies

Table 2. List of antibodies used.

Antibody	Source
Mouse anti-GFP	Developmental Studies Hybridoma Bank #GFP-12A6
Mouse anti-NICD	Developmental Studies Hybridoma Bank #C17.9C6
Mouse anti-Delta	Developmental Studies Hybridoma Bank #C594.9B
Mouse anti-OSA	Gift from Peter Verrijzer (Moshkin et al. 2007)
Guinea-pig anti-BAP170	Gift from Peter Verrijzer (Moshkin et al. 2007)
Goat anti-Su(H)	Santa Cruz Biotechnology, no longer available
Rabbit anti-Su(H)	Santa Cruz Biotechnology, no longer available
Rabbit anti-H3	Abcam #ab1791
Mouse anti-V5	Invitrogen #R960-25

2.2 Generation of mβ MS2 cell line

The MS2 system was implemented to visualise the transcription of *E(spl)mβ-HLH* in Kc167 cells. Making the mβ MS2 cell line first involved making an MCP-GFP-expressing cell line, followed by CRISPR gene editing to alter the *E(spl)mβ-HLH* gene. This required several DNA constructs described below. Diagrams illustrating the constructs and the steps of the CRISPR gene editing are shown in Figure 2.1. The method used for CRISPR was inspired by publications and protocols from Klaus Förstemann's laboratory (Böttcher et al. 2014; Kunzelmann et al. 2016).

2.2.1 Cloning of constructs

To make a plasmid for stable MCP-GFP expression, MCP-GFP was cloned from the pMS2-GFP plasmid (a gift from Robert Singer; Addgene #27121) into the Ac5-STABLE2-neo plasmid (a gift from Rosa Barrio and James Sutherland; Addgene #32426). The sequence for MCP-GFP was amplified by PCR (primers listed in Table 3), digested and ligated into Ac5-STABLE2-neo at the XbaI and HindIII sites.

To make the CRISPR gRNA, oligonucleotides specific for *E(spl)mβ-HLH* were incorporated into a vector containing the U6:3 promoter. Oligonucleotides were annealed and phosphorylated in a reaction containing 100 picomoles of each oligonucleotide, 1x T4 DNA Ligase Reaction Buffer (NEB #B0202) and 5 units of T4 Polynucleotide Kinase enzyme (NEB #M0201). The reaction was incubated at 37°C for 30 minutes, then heated to 95°C and cooled slowly. The pCFD3-dU6:3gRNA plasmid (a gift from Simon Bullock; Addgene #49410) was digested with BbsI and ligated with the annealed oligonucleotides using T4 DNA Ligase (NEB #M0202). To reduce the chance of stable incorporation of the gRNA plasmid, a double-stranded DNA PCR product was made for transfection. The gRNA-expression cassette was amplified by PCR from the U6:3 promoter to the RNA polymerase III termination signal.

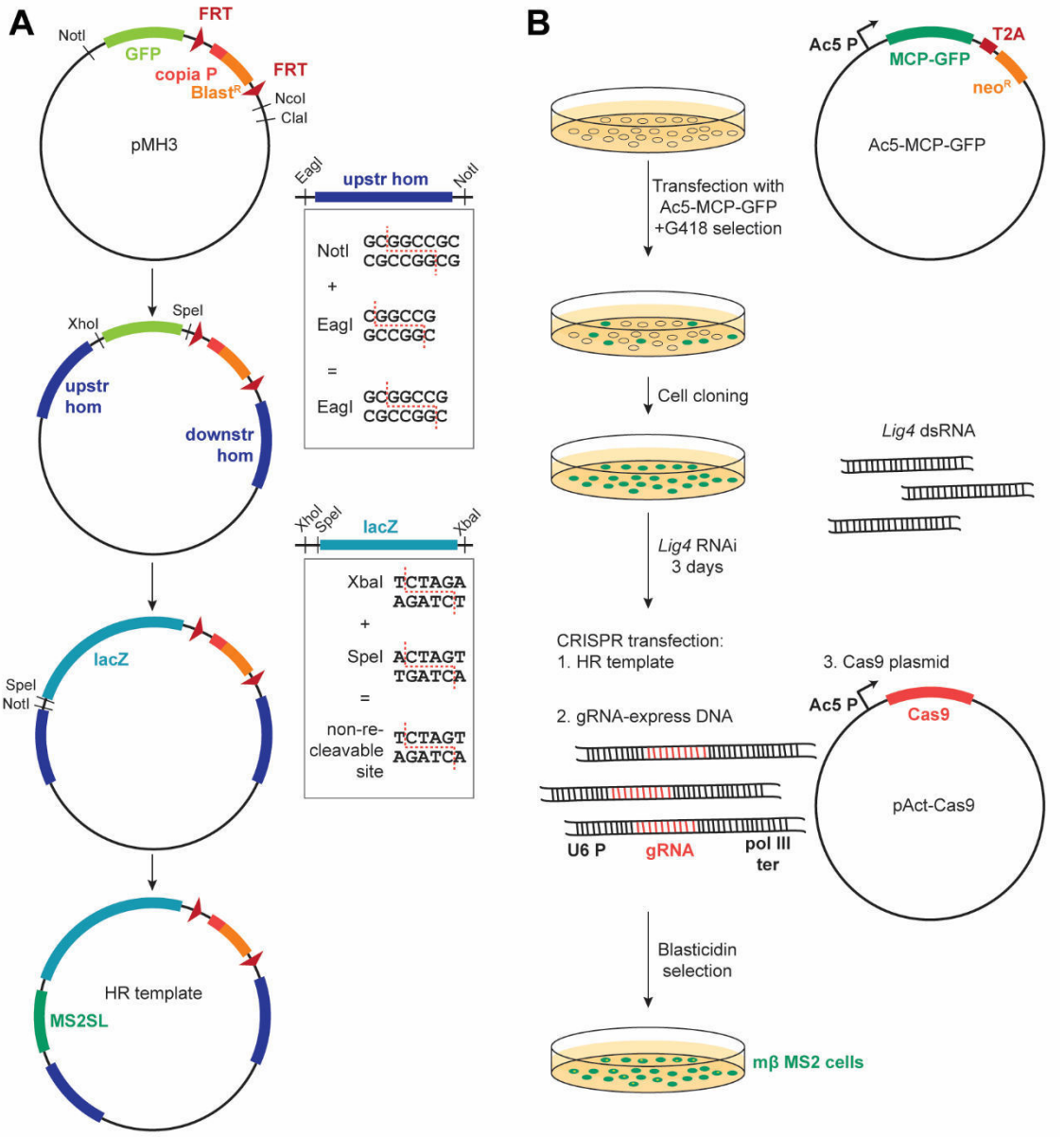

Figure 2.1. Generation of mβ MS2 cell line. (A) Cloning of the HR template as described in the text. The original pMH3 plasmid contains the blasticidin resistance gene ("Blast^R") expressed from the *copia* promoter ("copia P") between two FRT sites. Upstream and downstream homology regions ("upstr hom" and "downstr hom" respectively), followed by the DNA sequences for *lacZ* and the *MS2 stem-loops* ("MS2SL"), were added by traditional cloning methods. The restriction endonuclease sites used are shown on the plasmids. Two steps involved ligating compatible cohesive ends produced by distinct enzymes, as illustrated. This allowed NotI and SpeI to be re-used without re-cleaving all original cut sites. *Continued on next page.*

Construction of the homologous recombination (HR) template involved several steps to add the following to the pMH3 plasmid (a gift from Klaus Förstemann; Addgene #52528): 800-base-pair upstream and downstream homology regions, the sequence coding for the *MS2 stem-loops* and a 3-kilobase section of the *lacZ* gene (Figure 2.1A). Firstly, the downstream homology region was amplified by PCR, digested and ligated into pMH3 at the NcoI and ClaI sites. Secondly, the upstream homology region was amplified by PCR, digested with EagI (compatible cohesive ends with NotI) and ligated into the vector digested with NotI. Thirdly, a 3-kilobase region of the *lacZ* gene was amplified by PCR from the pBlueRabbit plasmid (Housden et al. 2012), digested with XhoI and XbaI (compatible cohesive ends with SpeI) and ligated into the vector digested with XhoI and SpeI. Finally, the sequence for the *MS2 stem-loops* was digested from the pCR4-24XMS2SL-stable plasmid (a gift from Robert Singer; Addgene #31865) and ligated into the vector using NotI and SpeI sites.

Figure 2.1 continued (B) Steps used to generate the mβ MS2 cells as described in the text. Diagrams represent Kc167 cells growing in culture and the constructs used in transfections. The Ac5-MCP-GFP plasmid expresses MCP-GFP from the *Actin5C* promoter ("Ac5 P") in a single transcript with the neomycin resistance gene ("neo^R", confers resistance to G418), separated by a T2A self-cleaving peptide (González et al. 2011). The gRNA was provided as a DNA template expressing the gRNA from the U6:3 promoter ("U6 P") up to the RNA polymerase III termination signal ("pol III ter").

Table 3. Primers used in cloning the MS2 constructs.

Primer name	Sequence
XbaI_MCP-GFP_for	TATCTCTAGAGCCACCATGGCTTCTAACTTTACTCAGT
HindIII_MCP-GFP_rev	CCTCAAGCTTGTACAGCTCGTCCATGCCG
BbsI_gRNA_sense	GTCGGGACGCCACATGGGGCCAG
BbsI_gRNA_anti	AAACCTGGCCCCATGTGGCGTCC
U6-promoter_for	GCTCACCTGTGATTGCTCCTAC
Pol-III-ter_rev	GCTTATTCTCAAAAAAGCACCGACTCGGTGCCACT
NcoI_downstr-hom_for	GACTCCATGGTGCCCCATGTGGCGTCCCTGGTGA
ClaI_downstr-hom_rev	GGCTATCGATGGTCAAGCGCAGTTAAAGCTGT
EagI_upstr-hom_for	GACTCGGCCGGCGCACGAGGCAAAATGAGTGT
NotI_upstr-hom_rev	TATTCTCGAGGCGGCCGCTGGAGCTGGCCTCGCTGGGCG
XhoI_LacZ_for	GACTCTCGAGACTAGTATGCCTGCTATTGGAATCGAT
XbaI_LacZ_rev	GACTTCTAGATTAGTCGACGGATCCCCGACACC

2.2.2 Generation of MCP-GFP-expressing cells

Kc167 cells were transfected with the MCP-GFP-expressing plasmid as follows. 18 μg of the plasmid was mixed with 925 μL Opti-MEM and 54 μL FuGENE HD at room temperature for 30 minutes before adding dropwise to cells in 10 cm plates. After 24 hours, the media was replaced to contain 1 mg/mL G418. Cells were grown in G418-containing media for approximately one month to undergo selection.

To homogenise the GFP expression levels, cell cloning was performed in a 96-well plate. 25,000 cells were added to the top-left well and 2-fold serial dilutions performed down the first column and along the rows, leading to some wells containing single cells. Conditioned media, prepared by filtering media from a plate of Kc167 cells, was used for this. After several weeks, colonies had formed from the single cells which were picked and grown up in new plates. Colonies

were stained for GFP and compared to identify a colony with a high level of MCP-GFP expression.

2.2.3 CRISPR transfection

CRISPR induces double-stranded DNA breaks at sites directed by the gRNA (Doudna and Charpentier 2014). The double-stranded breaks can either be repaired via the Non-Homologous End-Joining (NHEJ) pathway, which is error-prone and can therefore cause small mutations, or the HR pathway to insert new sequences (Kakarougkas and Jeggo 2014). Therefore, Lig4, a component of the NHEJ pathway, was knocked down by RNAi in 5 million cells distributed in a 6-well plate (see section 2.6.4 for details of method), in order to encourage HR to occur.

After 3 days, cells were approximately 50% confluent, the culture media was replaced and the CRISPR transfection was performed. 1 μg each of the gRNA-expression PCR product, the HR template plasmid and the pAct-Cas9 plasmid (a gift from Simon Bullock; Addgene #62209) were mixed with 200 μL Opti-MEM and 9 μL FuGENE at room temperature for 30 minutes before adding dropwise to cells in one well. A control was performed using 1.5 μg each of the HR template plasmid and the pAct-Cas9 plasmid (excluding the gRNA). After 48 hours, 1 mg/mL G418 and 10 μg/mL blasticidin (increased to 50 μg/mL 3 days later) were added to the media.

2.2.4 Removal of the blasticidin resistance cassette

To remove the blasticidin resistance cassette by flippase-induced recombination, the mβ MS2 cells were transfected with the pMH5 plasmid (a gift from Klaus Förstemann; Addgene #52531) which expressed flippase recombinase from a ubiquitous promoter. Transfections were performed in several wells of a 96-well plate with 40,000 cells per well. 150 ng of pMH5 was mixed with 20 μL Opti-MEM and 1 μL FuGENE at room temperature for 30 minutes before adding to cells (volumes given per well). Cells were maintained in media containing G418 but no blasticidin.

After initial genotyping to confirm that flippase-induced recombination had occurred in some cells, cell cloning was set up as above (see section 2.2.2) to isolate cell clones where no copies of the blasticidin cassette remained.

2.2.5 Genotyping

DNA was extracted from samples of cells using the DNeasy Blood and Tissue Kit (Qiagen #69504), and selected regions were amplified by PCR with the primers listed in Table 4. PCR products were run on 2% agarose by gel electrophoresis.

Table 4. Primers used for genotyping.

Primer name	Sequencing reaction	Sequence
Gtype_upstr_for	rxn 1 & 2	ATAGCCCACGAGCCATAACA
Gtype_MS2SL_rev	rxn 1	GGATCCAAGGGCGAATTCGCGG
Gtype_LacZ_rev	rxn 2	TGCAAGGCGATTAAGTTGGG
Gtype_LacZ_for	rxn 3 & 4	ATATGGGGATTGGTGGCGAC
Gtype_downstr_rev	rxn 3	CGCGGGCTTAATTTGCAATG
Gtype_BlastR_rev	rxn 4	CCCAGGATGCAGATCGAGAA

2.3 Cell culture for MS2 experiments

2.3.1 MS2 imaging and EGTA-induced Notch activation

2 million mβ MS2 cells were plated in a 35 mm FluorDish Cell Culture Dish (World Precision Instruments #FD35-100) 24 hours before imaging. Imaging was performed using a Leica TCS SP8 confocal microscope with a 40x/1.30 NA oil objective lens. GFP fluorescence was captured using a PMT detector with a laser at 488 nm. Z-stacks were acquired with 15 slices 1 μm apart, at 512x512 resolution with a 12-bit depth and scanning speed of 400Hz. Scanning was continuous such that a Z-stack was acquired every 9.816 seconds.

To activate Notch with EGTA, imaging was first set up with the plate of cells in normal culture media. With the plate on the microscope stage, imaging was

paused and media was replaced with 4 mM EGTA in phosphate-buffered saline (PBS), before imaging re-commenced. This was always performed quickly such that the start of imaging represented 1 to 2 minutes after EGTA addition. This small time delay was ignored in analysis such that time is given as time from the start of imaging. The PBS control experiment was performed in exactly the same way, excluding EGTA.

2.3.2 Drug treatments

Triptolide and flavopiridol experiments were performed as follows. For the reverse transcription-qPCR experiment, mβ MS2 cells were plated in a 6-well plate the day before. Cell culture media was replaced with media containing 10 μM triptolide, 10 μM flavopiridol or DMSO (same volume added as a carrier control), for 10 minutes. Media was then replaced with 4 mM EGTA in PBS also containing DMSO or the drugs for 30 minutes before RNA extraction and reverse transcription-qPCR (details given in section 2.7.1). For MS2 imaging experiments with transcription inhibitors, cells were imaged as described above (section 2.3.1) 24 hours after plating. With the plate on the microscope stage, cell culture media was replaced with media containing 10 μM triptolide or flavopiridol and imaged for 10 minutes. Subsequently, media was replaced with 4 mM EGTA in PBS also containing the drug at 10 μM and imaging continued.

For MG132 experiments, cell culture media was replaced with media containing 5 μg/mL MG132 (approximately 10 μM) for 5 hours before imaging. Imaging was performed as above and media was replaced with 4 mM EGTA in PBS also containing MG132 at the same concentration. For the Su(H) co-immunoprecipitation experiment, cells were treated with 5 hours of 5 μg/mL MG132 or DMSO (same volume added as a carrier control) in media followed by 4 mM EGTA treatment in PBS also containing MG132 or DMSO for 30 minutes. Controls without EGTA treatment were staggered such that cells were all harvested at the same time for protein extraction and co-immunoprecipitation (details given in section 2.7.2).

MS2 imaging was also performed with a 5 hour DMSO treatment in cell culture media followed by EGTA treatment containing DMSO, to serve as a control for MG132, triptolide and flavopiridol imaging experiments.

2.3.3 Co-culture with S2 cells

S2-Mt-Dl cells (which express Delta from the metallothionein promoter; Drosophila Genomics Resource Center stock #152) were maintained in Schneider's *Drosophila* medium supplemented with 10% FBS, 1x Antibiotic-Antimycotic and 200 nM methotrexate (Sigma #A6770) at 25°C. For co-culture imaging experiments, a 35 mm FluorDish Cell Culture Dish (World Precision Instruments #FD35-100) was treated with 0.01% poly-L-lysine (Sigma #P4707) for 1 hour and then left to dry before plating 2 million S2-Mt-Dl cells. After cells had settled to the bottom of the plate, media was replaced with media containing 5 mM copper sulfate to induce Delta expression 24 hours before imaging. Imaging was set up, and with the plate on the microscope stage, the media was replaced to contain 1 million mβ MS2 cells. Imaging proceeded while the mβ MS2 cells settled to the bottom of the plate to contact the S2 cells. The transmitted light was captured alongside the GFP fluorescence to allow the S2 cells to be visible and distinguished from the GFP-containing mβ MS2 cells.

The same method was used to induce and plate the cells for the immunofluorescence stain, where the cells were fixed 30 minutes after addition of the mβ MS2 cells.

2.3.4 Immunofluorescence staining of cultured cells

For staining, cells were plated on coverslips treated with 0.01% poly-L-lysine. Cells were fixed with 4% formaldehyde for 10 minutes, then treated with 50 mM ammonium chloride and 0.1% triton X-100, and blocked with 5% bovine serum albumin (BSA; Sigma). Cells were incubated with primary antibodies diluted in 2.5% BSA at 4°C overnight, washed with PBS, and incubated with secondary antibodies in 2.5% BSA for 1 hour at room temperature. The primary antibodies used were: mouse anti-GFP diluted at 1:100, mouse anti-NICD diluted at 1:20 and mouse anti-Delta diluted at 1:20. Coverslips were mounted in Vectashield

Mounting Medium with DAPI (Vector Laboratories #H-1200) and imaged using either the Leica TCS SP8 or Nikon D-Eclipse C1 confocal microscopes.

2.3.5 Plasma membrane stain

To observe cell projections in co-culture, 1x CellMask Deep Red Plasma membrane stain (Invitrogen #C10046) was added to the S2 cells before imaging, and co-culture imaging was set up as above (section 2.3.3). S2 cells were washed once with fresh media and then mβ MS2 cells were added.

2.4 MS2 computational analysis

2.4.1 Cell tracking

For the analysis of MS2 videos, first, a maximum projection was made using the Fiji software (Schindelin et al. 2012). A MATLAB script (MATLAB Release 2016b, The Mathworks, Inc.) was used to segment and track the cells (written by Julia Falo-Sanjuan, Bray laboratory; tracking shown in Figure 2.2A; for code see Appendix 2). Briefly, cells were segmented from the MCP-GFP signal using a combination of median filtering and identification of circular shapes using the "imfindcircles" function (Atherton and Kerbyson 1999). Cells were then tracked over time by finding the closest neighbour in a 15 pixel radius and allowing search in the previous 5 frames. Tracked cells were overlaid with the MCP-GFP signal to obtain the maximum intensity pixel for each nucleus and time point, which is used as a proxy for the MCP focus intensity. The outputs from this were the maximum fluorescence values for each tracked cell over time.

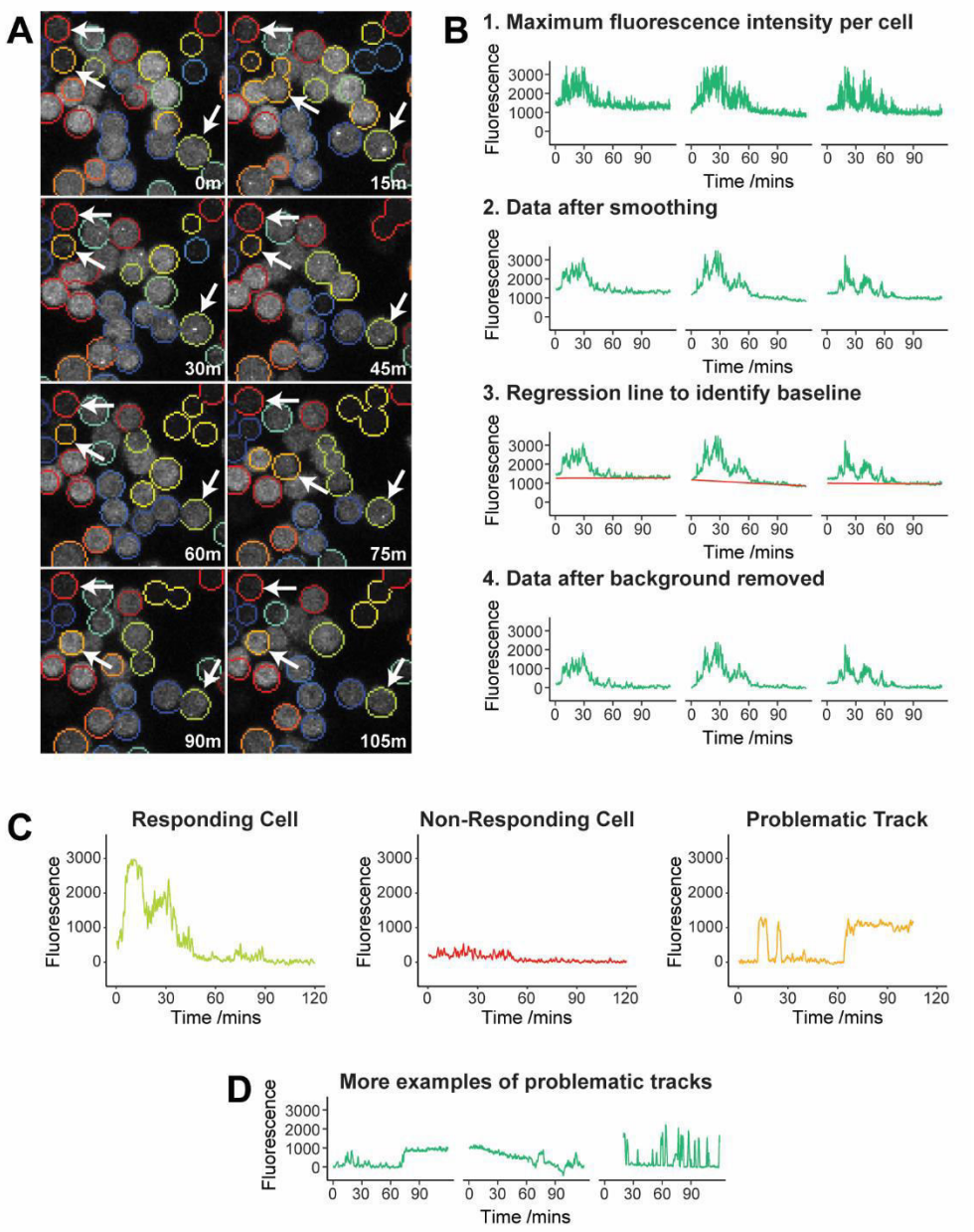

Figure 2.2. Cell tracking and data processing for MS2 analysis. (A) Cell tracking shown as coloured circles overlaid upon maximum projection fluorescence images, at the time points indicated in minutes after EGTA treatment. Note that while some cells are correctly tracked from start to finish, other tracks are lost over time or jump between cells. (B) Data processing performed in R. 1. Cell tracking yielded maximum fluorescence values for each cell over time. 2. Data was smoothed to remove noise by calculating a moving average. 3. Linear regression based on the lower quartile of values for each cell was used to predict the background level of fluorescence (shown as a red line). 4. The background level was removed from all values of maximum fluorescence such that the baseline level fell roughly around zero for each cell. *Continued on next page.*

2.4.2 Data processing

The fluorescence data was processed using an R script (R, R Core Team, R Foundation for Statistical Computing). See Appendix 3 for full code with explanations. Briefly, tracks were removed from analysis if they contained fewer than 360 frames (approximately 1 hour). Some noise was removed from the data by calculating a moving average using 5 consecutive frames. Since all cells had different general levels of GFP fluorescence, background was removed using a regression line calculated using the lower quartile of values for each cell (illustrated in Figure 2.2B).

The data for co-culture videos was processed in much the same way. However, since the mβ MS2 cells contacted the plate at different times, the start times were adjusted for the tracks from responding cells. The frame when each cell contacted the plate was found manually and subtracted from the data such that time zero reflected the time of first contact for each cell.

All tracks were plotted, and upon examination, it became apparent that there was a recurring pattern in many of the tracks, while others appeared erratic. A numbering system generated by the MATLAB script allowed tracks to be correlated with individual cells in the video, as illustrated by the colour-coded plots in Figure 2.2C. This confirmed that the tracks showing peaks within the first 60 minutes corresponded to cells exhibiting clear transcription foci observed by eye (for example, the green cell in Figure 2.2A and C). It also showed that tracks with large jumps in fluorescence or a baseline that was not

---

Figure 2.2 continued (C) Example tracks corresponding to cells highlighted by white arrows in A. Tracks are colour-coded: green track appears to show a transcriptional response, red track has no clear response, and orange track clearly jumps between cells in the video. (D) Further examples of tracks that were categorised as problematic and therefore discarded.

flat corresponded to cells which were moving or tracked poorly (for example, the orange cell in Figure 2.2A and C). And finally, tracks with very flat profiles indeed corresponded to cells where no clear transcription foci was visible by eye (for example, the red cell in Figure 2.2A and C).

Therefore, the tracks were used to manually categorise the cells as responding, non-responding or problematic, and the problematic tracks were removed from further analysis. This occurred with varying frequency between experiments, but always a minority of tracks were discarded. The exact numbers of tracks in each category and the percentage discarded are shown in Table 5. Using this chosen method of analysis, there is the possibility that some real transcriptional responses were discarded. However, the lack of consistency between the shapes of the problematic tracks (see more examples in Figure 2.2D) suggested that any potential ignored response was unusual and occurred with a low frequency. Thus, further analysis focused on tracks showing a clear response (responding cells) or lack of response (non-responding cells) that matched the patterns observed by eye. All percentages given in chapter 3 do not take problematic tracks into account.

2.4.3 Analyses

The mean maximum fluorescence values with standard deviations were found for all responding and non-responding cells and plotted.

To investigate whether focus intensity depended on the general level of MCP-GFP fluorescence, a measure of baseline fluorescence was found for each cell by taking the mean of the regression line calculated to remove background. This was compared with the maximum fluorescence value for each cell (see results in Figure 3.2G).

To analyse the timing of transcription, cells were considered to switch on transcription when at least 15 consecutive frames (approximately 2.5 minutes) had a value above 250, and to switch off transcription when at least 15 consecutive frames had a value below 250. These values were chosen by trial

and error to give transcription periods that matched what was observed in the graphs by eye.

Table 5. Number of cells per category in each MS2 experiment shown in chapter 3.

Experiment	Responding	Non-responding	Problematic	Percentage discarded
EGTA induction rep 1	147	228	105	21.9%
EGTA induction rep 2	119	218	154	31.3%
PBS control	0	379	184	32.7%
Triptolide	0	378	124	24.7%
Flavopiridol	0	339	96	22.1%
Clone cells (no blasticidin cassette)	125	208	174	34.4%
DMSO control	110	219	154	31.9%
MG132	30 (unusual cells)	299	203	38.2%
Ligand induction	16	64	13	14.0%

2.5 Salivary gland experiments

2.5.1 Fly stocks

For expression of all UAS constructs in the *Drosophila* salivary gland, *1151-Gal4* was used (L S Shashidhara, Centre for Cellular and Molecular Biology, Hyderabad, India; Roy and VijayRaghavan 1997). Notch signalling was activated by UAS-$N^{\Delta ECD}$ (Fortini et al. 1993; Rebay et al. 1993). The *E(spl)-C* was imaged using the ParB-INT DNA tagging system where UAS-ParB1-mCherry or UAS-ParB2-GFP was expressed in the presence of the INT sequence inserted

either between *E(spl)mδ-HLH* and *E(spl)mγ-HLH* or between *E(spl)m7-HLH* and *E(spl)m8-HLH* (*E(spl)-C* INT insertions made by Matthew Jones, Bray laboratory; Saad et al. 2014; Gomez-Lamarca et al. 2018). Histone-GFP imaging made use of UAS-H3-GFP, UAS-H3.3-GFP and UAS-H3.3^{core}-GFP constructs (flies kindly provided by Kami Ahmad; Henikoff et al. 2000; Ahmad and Henikoff 2002). Su(H) recruitment was monitored using Su(H)-GFP (Gomez-Lamarca et al. 2018). Dominant negative Brm was expressed from UAS-BrmK804R (Elfring et al. 1998). RNAi lines used are listed in Table 6.

Table 6. *Drosophila* RNAi stocks used.

RNAi	**Source** [1]	**RNAi**	**Source** [1]
w	BL-35573	*Dek*	BL-28696
Iswi	BL-32845	*yem*	V-26808
Chrac-16	BL-51155	*His3.3B*	BL-34940
MTA1-like	BL-33745	*BRWD3*	V-40208
Moira	BL-34919	*zeste*	BL-31615
Ino80	BL-33708	*Snr1*	BL-32372
Tip60	BL-28563	*osa* (1)	BL-31266
Chd1	BL-34665	*osa* (2)	V-7810
Chd3	V-13636	*Bap170* (1)	BL-26308
Caf1-55	V-26455	*Bap170* (2)	V-34581
Caf1-180	BL-32478	*polybromo*	BL-32840

[1] Bloomington *Drosophila* Stock Center is abbreviated BL, and Vienna *Drosophila* RNAi Center is abbreviated V.

For MS2 imaging in the salivary gland, MCP-GFP was expressed ubiquitously from the *Hsp83* promoter (Bloomington *Drosophila* Stock Center #7280) and localisation was observed due to the presence of *MS2 stem-loops* in the *E(spl)mβ-HLH* transcript. To achieve this, the *E(spl)mβ-HLH* gene was CRISPR-edited by injection of the HR template and gRNA-containing plasmids described in section 2.2.1, at a molar ratio of 3:1 respectively, and at a final

concentration of approximately 1 μg/μL, using a fly stock expressing Cas9 in the germline (injections performed by Kat Millen, Bray laboratory; Port et al. 2014).

2.5.2 Live imaging

Salivary glands were dissected and mounted as described previously (Gomez-Lamarca et al. 2018), using Shields and Sang M3 Insect Medium (Sigma #S3652) supplemented with 5% FBS and 1x Antibiotic-Antimycotic for dissection and the same medium with the addition of 2.5% methyl-cellulose (Sigma) for mounting. For live DNA stains, salivary glands were incubated in dissecting media containing 200 μg/mL Hoechst 33342 (ThermoFisher #H1399) for 10 minutes at room temperature before washing with PBS and mounting.

Image acquisition was performed with a Nikon D-Eclipse C1 confocal microscope using lasers at 405, 488 and 543 nm. Images captured of nuclei used the 60x oil objective with a 4.5x zoom level. To monitor Su(H)-GFP recruitment, nuclei were scanned slowly through the Z-stack using a 2x zoom level while looking for accumulations of fluorescence. 10 glands and 5 nuclei per gland were analysed and scored per condition, with the five nuclei closest to the coverslip chosen each time.

For quantifications of histone-GFP, representative images where the *E(spl)-C* could be clearly observed were used with the Fiji software (Schindelin et al. 2012) as follows. The images were rotated such that the *E(spl)-C* was vertical and a rectangle 1.29 μm by 2.58 μm was placed over it, centered on the peak fluorescence of the ParB-mCherry marker. The “plot profile” function was used to obtain mean fluorescence intensity across the rectangle in each channel. Arbitrary fluorescence values were adjusted such that the highest value obtained was set to one and the lowest to zero, and the mean values were taken from several nuclei (n numbers given in figure legend).

2.5.3 Immunofluorescence staining of salivary glands

Staining of salivary glands was performed as described (Gomez-Lamarca et al. 2018) except for the following changes. Glands were permeabilised with 1% Triton X-100 for 30 minutes. Antibodies against OSA and BAP170 were used at dilutions of 1:200 and 1:100 respectively.

2.6 Cell culture for molecular biology experiments

2.6.1 Generation of stable cell lines

Stable Kc167 cell lines were generated by transfection followed by antibiotic selection. In all cases, 18 μg of the relevant plasmid was mixed with 925 μL Opti-MEM and 54 μL FuGENE HD Transfection Reagent at room temperature for 30 minutes before adding dropwise to cells in 10 cm plates. After 24 to 48 hours media was replaced to contain antibiotic selection. Cells were grown in the presence of antibiotic and experiments were performed after significant cell death and recovery had taken place to indicate selection (usually after approximately 3 weeks). The cell lines used were as follows:

CATCH-IT was performed in the pMT-NICD cell line generated previously (Skalska et al. 2015), where cells were maintained with 2 μg/mL puromycin.

Cell lines expressing BrmWT and BrmK804R were generated using plasmids kindly provided by Neus Visa (Yu et al. 2014). BrmK804R was re-made by mutagenesis to ensure homogeneity between the two constructs using Pfu DNA Polymerase (Promega #M7741) with the primers listed in Table 7. The BrmWT and BrmK804R sequences were then cloned into the pMT-puro vector (a gift from David Sabatini; Addgene #17923) by digestion and ligation at SpeI and PmeI sites. After transfection of pMT-BrmWT and pMT-BrmK804R, cells were selected then maintained with 5 μg/mL and 2 μg/mL puromycin respectively.

Constitutive expression of histone-V5 proteins made use of pIB-H3-V5 and pIB-H3.3-V5 plasmids kindly provided by Dirk Schübeler and used as described (Wirbelauer et al. 2005). Cells were selected then maintained with 50 μg/mL and 20 μg/mL blasticidin respectively. For Notch activation in these cells, they

were further transfected with pMT-NICD, and selected then maintained with 5 μg/mL and 2 μg/mL puromycin respectively.

For inducible expression of histone-V5 proteins, H3 and H3.3 sequences were cloned from pIB-H3-V5 and pIB-H3.3-V5 into the pMT-puro vector using SpeI and XhoI sites with the primers listed in Table 7. After transfection of pMT-H3-V5 and pMT-H3.3-V5, cells were selected then maintained with 5 μg/mL and 2 μg/mL puromycin respectively.

Table 7. Primers used in BrmK804R mutagenesis and histone-V5 cloning into the pMT vector.

Primer name	Sequence
BrmK804R_for	CCGATGAAATGGGTTTGGGTCGAACCATTCAAACCATTTCGC
BrmK804R_rev	GCGAAATGGTTTGAATGGTTCGACCCAAACCCATTTCATCGG
SpeI_histone_for	CCTACTAGTCATGGCTCGTACCAAGCAAACTGC
XhoI_histone_rev	CACCTCGAGGCGGCCGCCACTGTGCTGGATA

2.6.2 Notch activation

Notch was activated in Kc167 cells either by NICD expression from the pMT vector (cell lines described above in section 2.6.1) or by EGTA treatment where media was replaced with 4 mM EGTA in PBS for 30 minutes (or the length of time specified).

2.6.3 Copper induction of pMT constructs

To induce expression from all pMT constructs in Kc167 cells, cell culture media was replaced to contain 5 mM copper sulfate. Induction was performed for 24 hours in experiments to express pMT-BrmWT and pMT-BrmK804R, for 6 hours in experiments to express pMT-NICD in cells with constitutive histone-V5 expression, and for the lengths of time specified in experiments to induce pMT-histone-V5 expression. See CATCH-IT method (section 2.7.6) for details of copper induction in this experiment.

2.6.4 RNAi in Kc167 cells

300 to 800 base-pair regions of *lig4*, *brm* and *Snr1* DNA were amplified from Kc167 cell genomic DNA, and *GFP* and *lacZ* sequences were amplified from plasmids as controls, by PCR with overhanging primers containing the T7 promoter sequence listed in Table 8. *In vitro* transcription was performed using the MEGAscript T7 Transcription Kit (Invitrogen #AM1334). RNA was purified by phenol-chloroform extraction and then annealed to form double-stranded RNA by heating to 75°C and cooling slowly. 100 µg double-stranded RNA was mixed with 3.5 mL Opti-MEM and added to approximately 10 million cells in a 10 cm plate for 30 minutes before topping up to 10 mL with normal culture medium. Volumes were scaled down for some smaller experiments. Experiments were performed 3 days later.

Table 8. T7 primers used to make double-stranded RNA for RNAi in Kc167 cells.

Primer name	Sequence
T7_Lig4_for	CCGAATTAATACGACTCACTATAGGGCCCAATGATCCAAAGTGTTTTTGCA
T7_Lig4_rev	CCGAATTAATACGACTCACTATAGGGAAGTAGGATGCCTTCGCGA
T7_GFP_for	TAGTAATACGACTCACTATAGGGAAAGGGCAGATTGTGTGGAC
T7_GFP_rev	TAGTAATACGACTCACTATAGGGTCAAGGACGACGGGAACTAC
T7_lacZ_for	CCGAATTAATACGACTCACTATAGGGCCGCTGGATAACGACATTGG
T7_lacZ_rev	CCGAATTAATACGACTCACTATAGGGGACTGTAGCGGCTGATGTTG
T7_brm_for	TAGTAATACGACTCACTATAGGGCGATCATAAACCCAAGGTGG
T7_brm_rev	TAGTAATACGACTCACTATAGGGCAGTGATGGTTCTTCATGCG
T7_Snr1_for	TAGTAATACGACTCACTATAGGGCTGGACATGGAGCTAGAGGG
T7_Snr1_rev	TAGTAATACGACTCACTATAGGGCGTCGGTAAGCGTCTCTAGG

2.7 Molecular biology techniques

2.7.1 RNA extraction and reverse transcription

To extract RNA from Kc167 cells, TRI reagent solution (Invitrogen #AM6738) was used, followed by phenol chloroform extraction and isopropanol precipitation at -20°C overnight. For reverse transcription, RNA was resuspended in water and first DNase-treated with the DNA-free DNA Removal Kit (Invitrogen #AM1906), before reverse transcribing with M-MLV Reverse Transcriptase (Promega #M1705) using $Oligo(dT)_{15}$ Primers (Promega #C1101). cDNA was diluted 5-fold before analysis with qPCR.

The same protocol was used to extract RNA from salivary glands, exactly as described previously (Gomez-Lamarca et al. 2018).

2.7.2 Su(H) co-immunoprecipitation

Co-immunoprecipitation was performed similarly to described previously (Housden et al. 2013). Approximately 20 million mβ MS2 cells were lysed in 500 µL lysis buffer (50 mM Tris-HCl, pH 8.0, 150 mM NaCl, 10% glycerol, 0.5% triton X-100) on ice for 30 minutes before debris was removed by centrifugation at 13,000xg, 4°C for 30 minutes. Cell lysate was incubated with 2 µg of goat anti-Su(H) antibody at 4°C overnight, followed by addition of protein G agarose beads (Roche # 11719416001) for 2 hours. The beads were washed 4 times before resuspending in loading buffer (10 mM Tris-HCl, pH 6.8, 20% glycerol, 4% SDS, 0.025% bromophenol blue, 2% mercaptoethanol) and boiling.

2.7.3 Western blots

To extract protein from cells expressing histone-V5 proteins, approximately 20 million cells were lysed in 100 µL lysis buffer (as above, section 2.7.2). Samples were then combined with loading buffer (as above, section 2.7.2) and boiled. Samples from CATCH-IT experiments were taken at different stages of the streptavidin capture and boiled with loading buffer.

Proteins were resolved using standard protocols with 7% SDS-PAGE for all Su(H) co-immunoprecipitation experiments, or 15% SDS-PAGE for histone-V5 and CATCH-IT experiments, and transferred to nitrocellulose. All blots were blocked with milk (3% milk powder, 0.05% tween-20 in Tris-buffered saline, TBS), except for CATCH-IT experiments when blots were blocked with BSA (5% BSA, 0.05% tween-20 in TBS). The primary antibodies used were: mouse anti-NICD diluted at 1:100, rabbit anti-Su(H) diluted at 1:400, rabbit anti-H3 diluted at 1:1000 and mouse anti-V5 diluted at 1:4000. Horseradish peroxidase-conjugated secondary antibodies were used and detected with the ECL system (GE Life Sciences). Streptavidin-peroxidase (Roche #11089153001) was used to detect biotinylated proteins in CATCH-IT samples.

2.7.4 Assay for transposase accessible chromatin

ATAC using salivary glands was performed exactly as described previously with no changes (Gomez-Lamarca et al. 2018). ATAC was performed with Kc167 cells in a similar manner with the following changes. After a 30-minute EGTA treatment in 10 cm culture plates containing approximately 40 million cells, cells were immediately harvested taking a quarter of the cells for the experiment (roughly 10 million). Cells were pelleted at 500xg, 4°C for 5 minutes, washed in 10 mL of cold PBS and pelleted again. The cells were then lysed by resuspending in 50 µL lysis buffer (10 mM Tris-HCl, pH 7.4, 10 mM NaCl, 3 mM $MgCl_2$, 0.3% NP-40), vortexing for 10 seconds, keeping on ice for 3 minutes, and vortexing again. Nuclei were pelleted at 400xg, 4°C for 5 minutes and resuspended in 30 µL TD buffer (Illumina #FC-121-1030). 25 µL was used for the tagmentation reaction and the rest of the protocol performed exactly as described previously for salivary glands (Gomez-Lamarca et al. 2018).

2.7.5 Chromatin immunoprecipitation

Su(H) and V5 ChIP were performed largely as described previously (Krejci and Bray 2007; Skalska et al. 2015), using 2.5 µg goat anti-Su(H) antibody and 1-2 µg mouse anti-V5 antibody. Briefly, cells were cross-linked with 1% formaldehyde (Sigma #F8775) in PBS for 10 minutes at 25°C. After lysis, chromatin was diluted 2-fold for sonication and then a further 5-fold for pre-

clearing with goat or mouse IgG and 40 µL protein G or protein A/G PLUS-Agarose (Santa Cruz Biotechnology #sc-2002 and #sc-2003 respectively) for Su(H) and V5 ChIP respectively. Immunoprecipitation was performed with 40 µL of the same beads at 4°C overnight, followed by washes, elution by vortexing, de-crosslinking with 0.3 M NaCl, 0.1 mg/mL RNase A and 0.1 mg/mL proteinase K treatment. DNA was purified with the QIAquick PCR purification kit (Qiagen #28106) and eluted in 100 µL water for analysis with qPCR.

2.7.6 CATCH-IT

Schneider's Drosophila medium without methionine (PAN Biotech #P04-90599), supplemented with 5% FBS and 1x Antibiotic-Antimycotic was added to cells for 1 hour, followed by adding either 4 mM azidohomoalanine (AnaSpec #AS-63669), or 4 mM methionine (Sigma #M9625) as a control, for 4 hours. To activate Notch, pMT-NICD cells were induced with 5 mM copper sulfate for 1 hour before the medium was substituted for methionine-free medium, also containing 5 mM copper sulfate, so that cells were incubated with copper sulfate for a total of 6 hours.

CATCH-IT was performed as previously described (Teves et al. 2012), except where stated otherwise. Briefly, cells were harvested and nuclei were extracted with 30 µL of 10% NP-40. Nuclei were resuspended in 180 µL of HB125 buffer, and the following were added: 5 µL of 2 nM biotin-alkyne (Invitrogen #B10185), 10 µL of 100 mM THPTA (Sigma #762342) premixed with 2 µL of 100 mM copper sulfate (Jena Bioscience #CLK-M1004), and 6 µL of freshly-prepared 500 mM sodium ascorbate (Jena Bioscience #CLK-M1005). Cycloaddition reaction was performed for 30 minutes at room temperature on a rotor. Reaction with MNase (Sigma #N3755) was performed at 37°C for 3 minutes. After capture with Dynabeads M-280 Streptavidin (Invitrogen #11205) as described, captured chromatin and input chromatin samples were treated with 0.25 mg/mL RNase A and 0.25 mg/mL proteinase K. DNA was purified with the QIAquick PCR purification kit (Qiagen #28106) and analysed by qPCR.

2.7.7 qPCR

All qPCR was performed using a LightCycler 480 Instrument II (Roche) with the SYBR Green I Mastermix (Roche #04707516001) as described previously (Gomez-Lamarca et al. 2018). For all experiments, two technical replicate qPCR reactions were performed per sample and the mean taken for analysis. Replicate numbers given in figure legends do not count these technical replicates and instead refer only to repeats of the full experimental protocol from start to finish with different cells or animals (biological replicates). For ATAC experiments, tagmented samples were normalised to genomic DNA and the closed chromatin control region (as described in Gomez-Lamarca et al. 2018). For reverse transcription experiments, relative amounts of the genes of interest were normalised to the control gene *RpL32*. For ChIP, immunoprecipitated samples were normalised to input samples. For CATCH-IT, pulldown samples were normalised to input samples and then to the Sec15 transcribed region as an internal control. Primers used for qPCR are shown in Tables 9-12.

Table 9. Primer pairs targeting *E(spl)mβ-HLH* MS2 construct.

Primer name	Forward sequence	Reverse sequence
mβ_5'	AGGTAGTTGAGACGATGGCC	GCTGCCAATGAAGTGTCCAA
LacZ	GATCCCAGCGGTCAAAACAG	TAGCAGAGCGGGTAAACTGG
BlastR	AGCTGGCAACCTGACTTGTA	CCCAGGATGCAGATCGAGAA
mβ_3'	AGAAGTGAGCAGCAGCCATC	GCTGGACTTGAAACCGCACC

Table 10. Primer pairs targeting the *E(spl)-C*.

Primer name	Forward sequence	Reverse sequence
mγ-mβ_igr	GGAGTTGAGGAGTTGGTCG	ATAAGTGTGGTTGGGTGCCT
mβ_tr	AGAAGTGAGCAGCAGCCATC	GCTGGACTTGAAACCGCACC
mβ_enh	AGAGGTCTGTGCGACTTGG	GGATGGAAGGCATGTGCT
mβ-mα_igr	AAGCCAGTGGACTCTGCTCT	TGATCTCCAAGCGGAGTATG
mα_tr	GCAGGAGGACGAGGAGGATG	GATCCTGGAATTGCATGGAG
m2-m3_igr	GCGCGTATTTCCCAAATAAA	GATTGTACGTGCATGGGAAA
m3_enh	ACACACACAAACACCCATCC	CGAGGCAGTAGCCTATGTGA
m3_tr	CGTCTGCAGCTCAATTAGTC	AGCCCACCCACCTCAACCAG
m8_tr	CAATTCCACGAAGCACAGTC	GAGGAGCAGTCCATCGAGTT

Table 11. Primer pairs targeting control regions for ATAC.

Primer name	Forward sequence	Reverse sequence
Rab11_tr	ACTGAAAATGGGCCGTTTCG	AGGAGTGGTAATCGACGGTC
Eip78C_enh	AGAAGTAGGGGCCGTCAAGT	GTGTAAGACCCGTCGCATTT
Closed_ctrl	GCATTTTTGTGGCAGAGGCA	CTCTTTCGGTGTCGCCTTCT
Mst87F_tr	ATCCTTTGCCTCTTCAGTCC	AATAATGATACAAAATCTGGT TACGC
CTPsyn_tr	TCGATTGTTGTTGGCTGAGC	TTCCTTCGCTCTTCCTGTCC
fru_tr	CTCTTTCGCACACTTGGCAT	CCGTTCGTTGCCCATCTAAG
kay_tr	CTCTCTCATTGGCTCTCCCC	TGAAGCGGAGACCACACAAT
vri_tr	TGTGTGTTTGTGTCTGCGAG	TCACTCACCCTCACCATGAC

Table 12. Primer pairs targeting control regions for CATCH-IT.

Primer name	Forward sequence	Reverse sequence
p53_tr	TTATAGCAATGCACCGACGC	GACGAACGCCAGCTCAATAG
CG17119_enh	TACATGGGCTTTGTCGGTCG	CACGGCCCTCGCCATATAAA
sav_tr	GAGTAGGTGTTCCGACTGGTG	ATCAGCGGGCCAAGAAGAAAT
PPO1_enh	AAGTCCCAACCGCAAAACTG	GCTATCGACTAAACCACAACGT
Him-Her_enh	CGAACCGAGTTGTGGGAAAT	CCCTTGGAGTGACAATTAGCTG
Rab11_tr1	GTAAAGTGTGTGAGCCGACG	AATCCAATAATCCCTGCGCG
Rab11_tr2	ACTGAAAATGGGCCGTTTCG	AGGAGTGGTAATCGACGGTC
Sec15_tr	GGTAGCGGTTCTCTTGCTTG	GTAACCGTCAGCTGTTGGAC

3 TRANSCRIPTION DYNAMICS IN THE NOTCH RESPONSE

3.1 Introduction

Notch signalling is ultimately a means to activate genes. In order for development to proceed reliably and successfully, gene activation must be reliable and occur with the correct timing. Very few studies have examined the dynamics of the Notch response on a temporal or single cell level. It therefore remains unclear how the different factors controlling Notch signalling are translated into a transcriptional output. For example, it is not known whether there is any stochasticity in the transcriptional output leading to heterogeneous cell populations within the same developmental context. Nor is it known how rapidly transcription is initiated when the receptor is activated. To answer these questions, a live imaging method was used to investigate the dynamics of the Notch response in single cells.

The MS2 system makes it possible to quantitatively measure active transcription in real time (Larson et al. 2013; Bothma et al. 2014; Corrigan et al. 2016). This system relies on the interaction between the MS2 bacteriophage coat protein (MCP) and the *MS2* RNA *stem-loops*, such that if fluorescently labelled with GFP, MCP-GFP can be visualised accumulating on nascent transcripts containing *MS2 stem-loops* (Bertrand et al. 1998). Due to the high temporal resolution of this technique, it has been used to examine transcriptional

bursting dynamics, and to study whether transcriptional output is controlled by burst size or frequency. While some have found evidence for the modulation of burst size (Skupsky et al. 2010; Dar et al. 2012; Molina et al. 2013), others believe that bursting frequency underpins all differences in gene expression and have used mathematical modelling to demonstrate this (Fukaya et al. 2016; Wang et al. 2018). Several studies have observed changes in burst frequency in response to signalling and transcription factor concentration (Larson et al. 2013; Senecal et al. 2014; Bartman et al. 2016). Most experimental methods that have been used to detect bursting are unable to distinguish a series of closely timed bursts from one larger burst (refer to Figure 1.1C for illustrations of this), and thus it is currently unproven which is true. Furthermore, since only a limited number of systems have been studied, it remains plausible that different mechanisms regulate different genes to give differing bursting profiles.

The MS2 system has been used in *Drosophila* embryos to study the transcription of early patterning genes (Garcia et al. 2013; Lucas et al. 2013; Bothma et al. 2014, 2015; Fukaya et al. 2016). This has allowed the dynamic regulation of these genes to be uncovered with fine temporal resolution, and led to the finding that a single enhancer can drive transcriptional bursts from multiple promoters simultaneously (Fukaya et al. 2016). So far, these experiments in *Drosophila* have used reporter constructs. However, the Clustered Regularly Interspaced Short Palindromic Repeat (CRISPR)/CRISPR Associated protein 9 (Cas9) system now allows genes to be tagged endogenously with ease (Roberts et al. 2017) and has been used extensively for genome editing in recent years (Zhang et al. 2014). This is based on the ability of Cas9 to cause double-stranded DNA breaks at specific sites in the genome, directed by a guide RNA (gRNA) species (Doudna and Charpentier 2014), making CRISPR a highly specific and flexible system for genome editing.

In this chapter, CRISPR is used to set up the MS2 system for monitoring the transcription of the endogenous Notch target gene *E(spl)mβ-HLH* in a *Drosophila* cell line. This aims to answer questions about the dynamics of Notch signalling and to discover how quickly transcription is initiated after Notch receptor activation.

3.2 Results

3.2.1 Implementing the MS2 system in Kc167 cells

In order to study the precise dynamics of the Notch transcriptional response, the MS2 system was implemented in *Drosophila* Kc167 cells, where Notch signalling can be activated in several ways. If NICD is expressed from a plasmid, it travels directly to the nucleus to activate transcription, a method which will be used in chapter 4. Alternatively, the endogenous Notch receptor can be activated by exposing it to a ligand, which may be immobilised (Varnum-Finney et al. 2000) or expressed on a co-cultured cell line, as will be demonstrated later in this chapter. And perhaps the simplest method, which also provides the most rapid activation, is to add a calcium chelator such as EGTA to the cells. This destabilises the negative regulatory region of the Notch receptor, causing its rapid cleavage and the activation of target genes (Rand et al. 2000; Housden et al. 2013; Skalska et al. 2015).

To set up the MS2 system in this cell type, first, a cell line was created which expressed MCP-GFP constitutively (Figure 3.1B). To ensure cells within the population had similar levels of MCP-GFP expression, a clone was grown up from a single transfected cell. Then, the DNA sequence coding for the *MS2* RNA *stem-loops* was inserted, by CRISPR gene editing, into the *E(spl)mβ-HLH* gene, a reliable Notch target in Kc167 cells. This yielded a cell line in which nascent *E(spl)mβ-HLH* transcripts would be bound by MCP-GFP, producing a focus of accumulated fluorescence at the transcription site (schematic shown in Figure 3.1A). Also inserted into the gene were a blasticidin resistance cassette between two FRT sites, to enable selection of the engineered cells, and a three-kilobase section of the *lacZ* gene (Figure 3.1C) to increase the length of the transcript and improve detection of transcription foci (Garcia et al. 2013; Bothma et al. 2014).

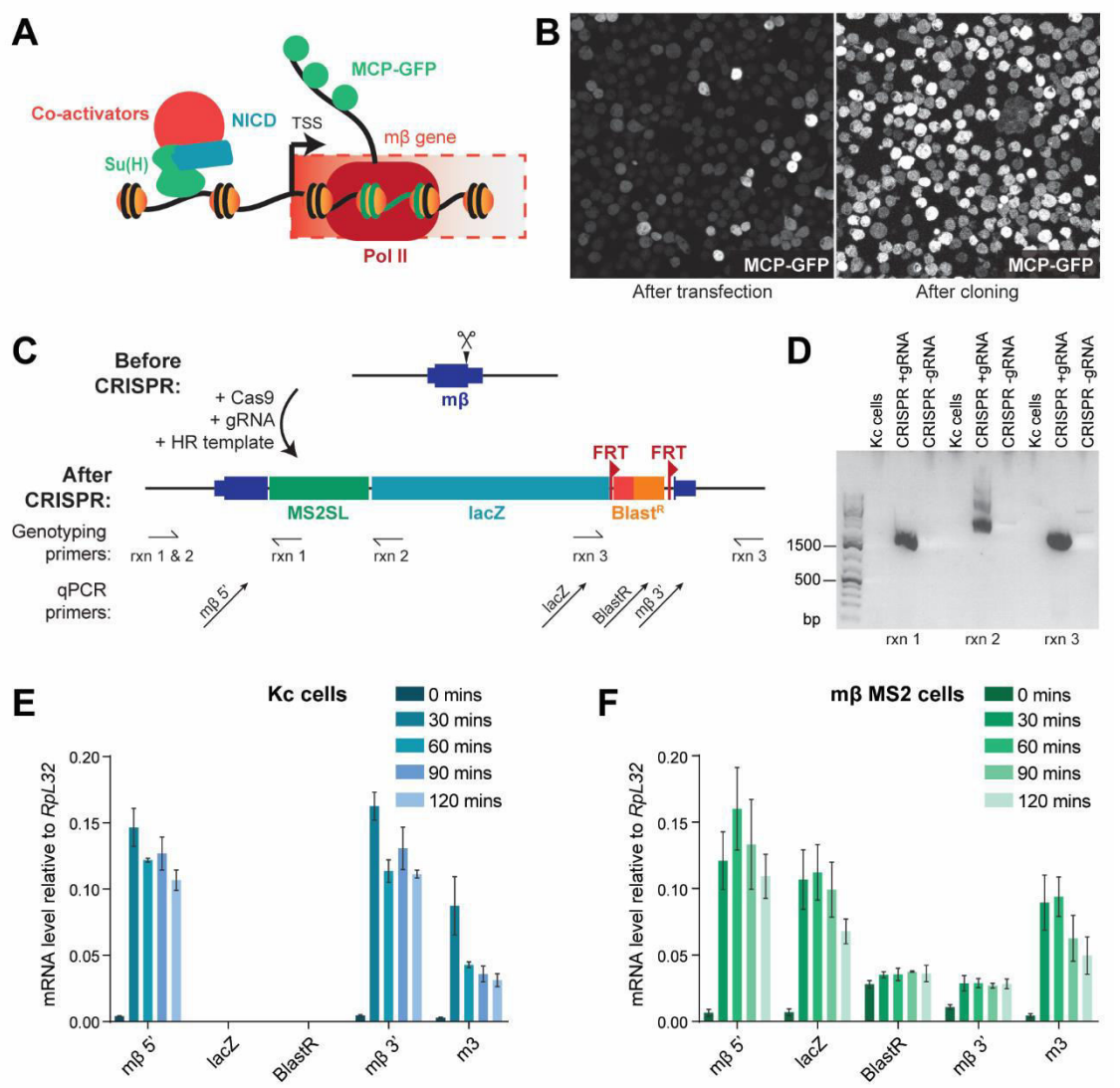

Figure 3.1. Implementing the MS2 system in Kc167 cells. (A) Schematic illustrating the MS2 system. Transcripts of the Notch target gene *E(spl)mβ-HLH* contain *MS2 stem-loops* which are bound by MCP-GFP, leading to an accumulation of fluorescence detectable by live imaging. (B) MCP-GFP-expressing cell line shown both after initial transfection and after cell cloning to produce more homogenous GFP levels. Images show immunofluorescence staining of GFP. (C) Schematic illustrating *E(spl)mβ-HLH* gene editing with CRISPR. New gene includes the DNA sequence coding for *MS2 stem-loops* ("MS2SL"), part of the *lacZ* gene and a blasticidin resistance cassette ("Blast^R") between FRT sites. (D) Successful gene editing demonstrated by genotyping PCR reactions. Positions of primers used are shown by half arrows in C. PCR products are formed from reactions 1 to 3 ("rxn 1, 2 and 3") only when CRISPR transfection included guide RNA ("CRISPR +gRNA") and not in control conditions (without guide RNA, "CRISPR -gRNA", and un-transfected "Kc cells"). *Continued on next page.*

Genotyping confirmed successful CRISPR gene editing (Figure 3.1D), and reverse transcription-qPCR confirmed that the engineered cell line responded to Notch signalling normally, with transcript levels of two Notch target genes increasing rapidly within the first 30 minutes of EGTA treatment at comparable levels to un-transfected Kc167 cells (Figure 3.1E and F). This included the CRISPR-targeted *E(spl)mβ-HLH* gene, as well as the additional, unmodified *E(spl)m3-HLH* gene. Probes targeted to different regions of the engineered construct showed that although transcription terminated before the 3' end of the gene (most likely due to the presence of the blasticidin resistance cassette), the tagged *E(spl)mβ-HLH* gene was still strongly Notch-responsive. These engineered cells, referred to here as mβ MS2 cells, can therefore be used to monitor the real-time response of *E(spl)mβ-HLH* to Notch activation.

3.2.2 Characterising the MS2 response to Notch

Live imaging revealed the full dynamic transcriptional response to Notch when activated by EGTA treatment. In order to perform this experiment, cells were first imaged continuously in culture medium to observe their pattern of fluorescence in the absence of Notch signalling. Imaging was then paused for a short time (around two minutes) while the culture medium was removed and replaced with a solution containing EGTA, with the cells still on the microscope stage. Imaging recommenced and cells were observed continuously for around

Figure 3.1 continued (E and F) Engineered mβ MS2 cells and the edited *E(spl)mβ-HLH* gene are Notch-responsive, shown by reverse transcription-qPCR at the lengths of time indicated after Notch activation by EGTA. Positions of primers used are indicated by black arrows in C. Expression of the *lacZ* transcript responds to Notch, and is detected in mβ MS2 cells (F) and not in un-transfected Kc cells (E). Expression of the 3' end of the gene is reduced in mβ MS2 cells. Relative levels of *lacZ* and 3' expression indicate that a large proportion of *E(spl)mβ-HLH* copies are successfully edited. *E(spl)m3-HLH* ("m3") is shown as another Notch-responsive gene. Mean ± SEM; n = 3.

two hours. With this experimental set-up, transcription foci were observed in many of the mβ MS2 cells only 15 minutes after EGTA addition and remained present for a period of time before disappearing (Video 1; Figure 3.2F).

To obtain precise single cell data from the video, cells were segmented and tracked computationally, and the maximum fluorescence values for each cell were used as a measure of the intensity of the fluorescent foci (see Materials and methods for full details). When maximum fluorescence intensities for individual cells were plotted over time, patterns emerged which reflected what was observed in the video by eye. In many tracks, the maximum fluorescence level increased after EGTA addition and peaked after 15 to 30 minutes before dropping back to baseline (Figure 3.2A and B), while other tracks had very flat profiles (Figure 3.2D). The peaks in fluorescence were confirmed to represent the transcription foci observed. In addition to these common profiles, some tracks were erratic and corresponded to poorly segmented and tracked cells; these data were therefore discarded from further analysis (see Materials and methods for further explanation of this and the number of tracks discarded for each experiment).

It was found that 35 to 40% of the well-tracked cells showed a transcriptional response (Figure 3.2A and B) and the majority of transcriptional activity occurred in the first 60 minutes after EGTA addition, as illustrated by the mean maximum fluorescence from these cells (Figure 3.2C). The remaining cells had no detectable transcription foci (Figure 3.2D and E), but it is unclear whether this is because the signal was below the level of detection or because these cells did not respond.

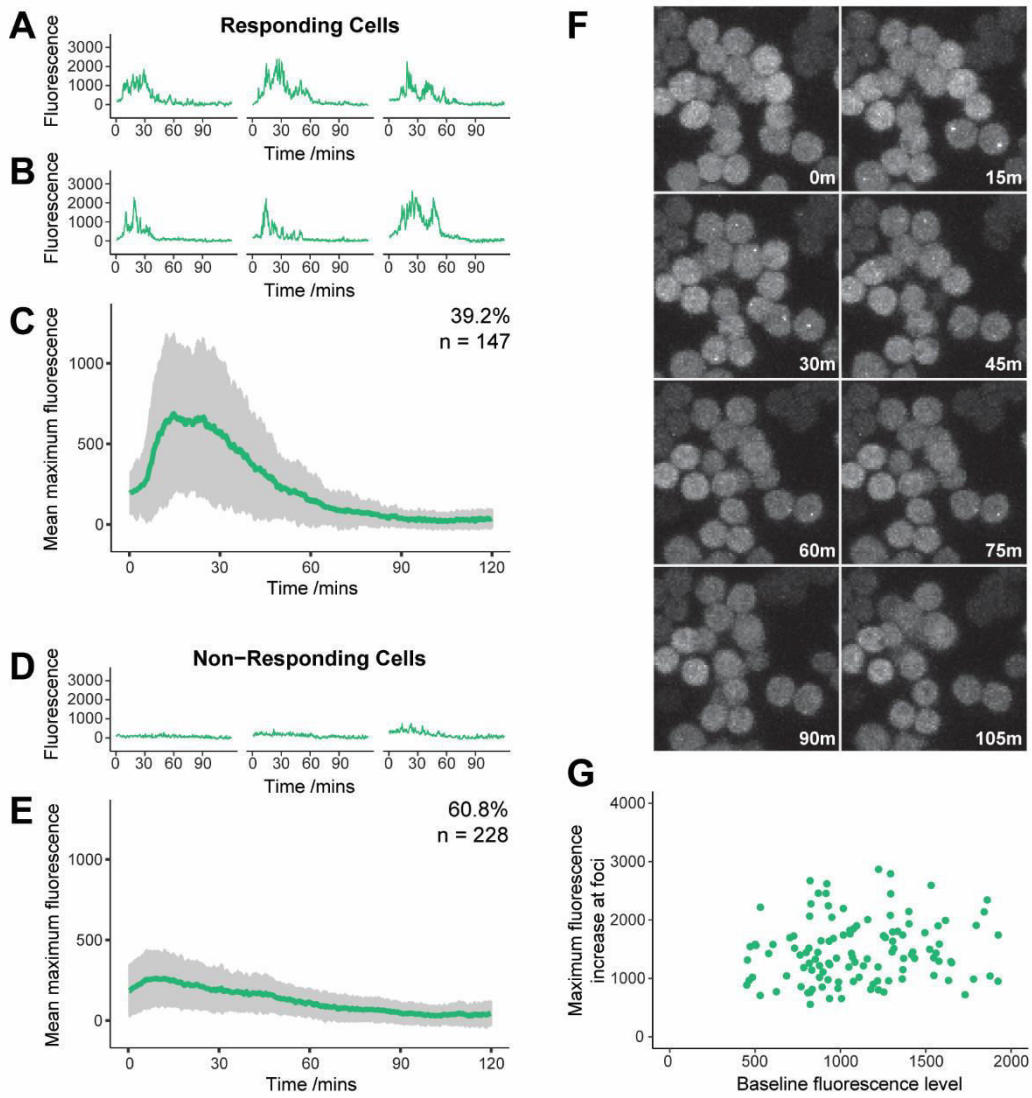

Figure 3.2. Live imaging of Notch-responsive transcription. (A-C) Many cells respond to EGTA-induced Notch activation and are labelled "Responding Cells". They upregulate and subsequently down-regulate transcription over a period of approximately 60 minutes after Notch activation. (D-E) Some cells show no response and are labelled "Non-Responding Cells". Graphs are example tracks illustrating maximum fluorescence intensity from individual cells (A, B and D, where A and B show graphs from two independent experiments; see Materials and methods for details of data processing), and mean maximum fluorescence with standard deviation for all responding (C) or non-responding (E) cells. Time zero represents initiation of EGTA treatment to activate Notch. Percentages and n numbers (top right) indicate the number of cells in each category. (F) Images of mβ MS2 cells at the time points indicated in minutes after EGTA treatment, showing transcription foci within 15 minutes of Notch activation. (G) Maximum increase in fluorescence at foci plotted for individual cells against baseline fluorescence level (see Materials and methods for calculation of this). There is no significant correlation, indicating that MCP-GFP concentration does not strongly influence focus formation. Pearson product moment correlation coefficient: $r = 0.078$, $p = 0.40$.

The intensities of the transcription foci varied greatly from cell to cell. Since focus formation depends on the cooperative binding of MCP-GFP to the *MS2 stem-loops* (Bos et al. 2016), it is possible that the concentration of MCP-GFP in the cell could have affected the formation of foci. Therefore, it was investigated whether the intensity of fluorescent foci was influenced by the general level of MCP-GFP expression in the cell. To this end, the maximum increase in fluorescence measured at transcription foci during the response was plotted against the baseline MCP-GFP level for each responding cell (Figure 3.2G). Since there was no significant correlation, it appears that the level of MCP-GFP expression did not influence fluorescent focus formation and thus the profiles obtained are likely to represent the levels of real transcription.

These initial results suggest that varying *E(spl)mβ-HLH* transcription levels were detectable with the MS2 system in these cells, and that the transcriptional response was temporary.

No transcription foci were observed in control videos without EGTA, showing that the response is EGTA-dependent (Video 2; Figure 3.3A and B). To further confirm that the fluorescent foci represented sites of active transcription, two different transcription inhibitors were added to the cultures. Triptolide inhibits the ATPase activity of the transcription initiation factor TFIIH to prevent transcription initiation (Titov et al. 2011; Vispe et al. 2009; Henriques et al. 2013), while flavopiridol prevents the release from Pol II pausing by inhibiting P-TEFb (Chao et al. 2000; Henriques et al. 2013). Both of these transcription inhibitors were highly effective at inhibiting transcription, based on the levels of mRNA produced. Even the low levels of transcription detected in the Notch-OFF state were abolished (Figure 3.3C). Importantly, when either of these inhibitors were added only 10 minutes prior to EGTA treatment, transcription foci were no longer detected (Figure 3.3D-G). Together these results show that the fluorescent foci represent sites of active transcription and are dependent on conditions that activate Notch.

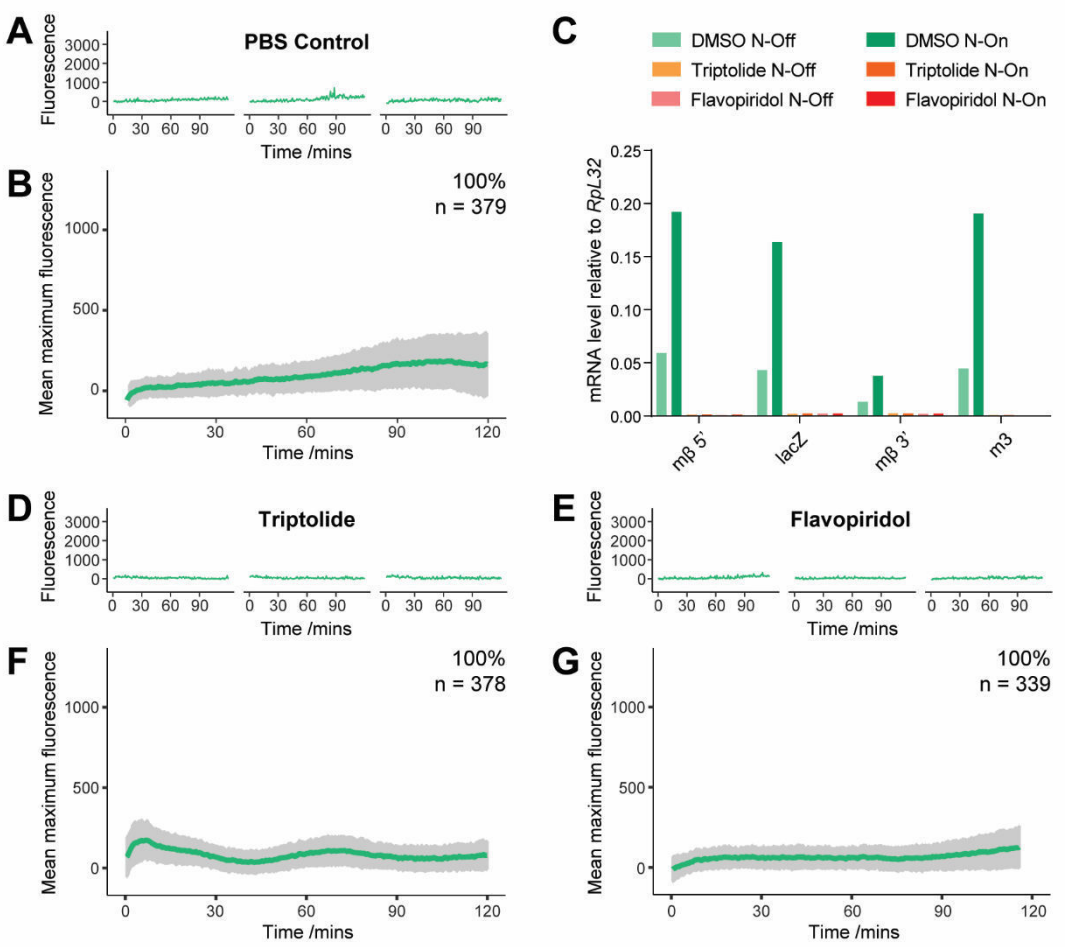

Figure 3.3. Observed foci are EGTA-dependent and represent transcription. (A and B) Transcription is not detected under control conditions (treatment with PBS only). (C) Triptolide and flavopiridol prevent transcription of *E(spl)mβ-HLH* and *E(spl)m3-HLH* under both Notch-ON ("N-On"; EGTA treatment) and Notch-OFF ("N-Off"; PBS control) conditions, measured with reverse transcription-qPCR. Positions of primers are as in Figure 3.1C. (D-G) Triptolide (D and F) and flavopiridol (E and G) prevent detection of transcription with live imaging. Graphs are example tracks illustrating maximum fluorescence intensity from individual cells (A, D and E) and mean maximum fluorescence with standard deviation for all cells (B, F and G). Notch is activated with EGTA treatment at time zero as in Figure 3.2. Percentages and n numbers (top right) indicate the number of cells analysed.

EGTA-induced Notch activation relies on the γ-secretase-mediated cleavage to release NICD and its subsequent transfer to the nucleus (Krejcí et al. 2009). There are varying estimates for how rapidly these steps occur (Kawahashi and Hayashi 2010; Ilagan et al. 2011). The mβ MS2 cells provide a powerful system for determining the time needed to elicit a transcriptional response to Notch, since the time when transcription foci first appear can be found for each cell after EGTA addition. Transcriptionally active periods for each cell were determined (Figure 3.4A-C), which showed that the majority of responding cells had initiated transcription within the first 10 to 15 minutes, and this was highly reproducible (Figure 3.4D and E). In contrast, the cessation of transcription was more variable, occurring between 30 and 60 minutes after Notch activation. It is notable however that the profiles were very similar between cells, with the majority showing activity which roughly increased and then decreased within 60 minutes. These results demonstrate that the Notch response is very rapid and highlight its reproducibility.

To investigate whether there was a relationship between the levels of transcription and the duration, the maximum focus intensity was compared with transcriptional start and end times on a cell-by-cell basis. Focus intensity was negatively correlated with transcriptional start time but positively correlated with transcriptional end time (Figure 3.4F and G), meaning that cells with higher levels of transcription were detected as responding earlier and had a longer response than those with lower levels. This could be due to technical detection limits, since enough transcripts must be present to cause sufficient fluorescence accumulation for detection, or due to biological reasons. For example, cells with lower amounts of Notch present may take longer to reach threshold levels of NICD required for transcription, leading to a slower and dimmer response, followed by faster depletion of NICD levels to terminate the response.

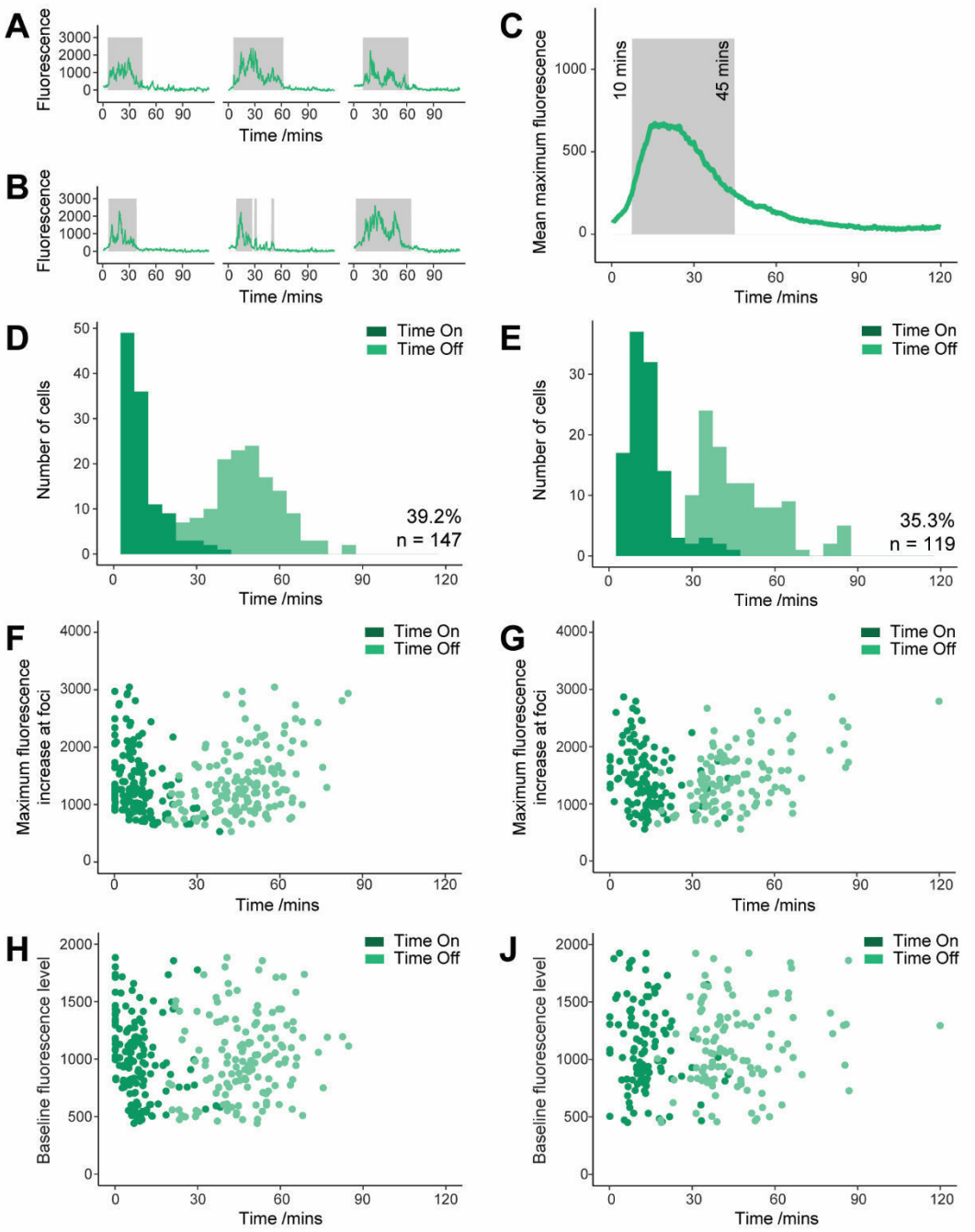

Figure 3.4. The timing of the Notch transcriptional response is reproducible. (A and B) Transcriptionally active periods (grey boxes) indicated with example tracks showing maximum fluorescence intensity for individual cells from two independent experiments. (C) Mean maximum fluorescence for responding cells from three pooled experiments (green line). Grey box indicates the transcriptionally active period determined from the mean results shown. Values given are the mean transcriptional start and end times determined for the responding cells from three experimental replicates. *Continued on next page.*

It was also important to investigate whether the baseline level of MCP-GFP fluorescence in each cell affected the timing of focus detection. Therefore, in a similar manner, the baseline fluorescence level was plotted against transcriptional start and end times (Figure 3.4H and J). While correlations were once again detected in one experiment (with transcriptional start time negatively and end time positively correlated with baseline fluorescence level), these were weaker than the correlations detected between the transcriptional timings and maximum focus intensity, and were not reproducible between experiments. Thus, it appeared that the varying concentrations of MCP-GFP in the cells did not affect the experimental detection of active transcription. And therefore, the transcription foci which were present for longer durations indeed represented the cells reaching higher peak transcription levels, rather than simply the cells with brighter or dimmer average levels of MCP-GFP.

Figure 3.4 continued (D and E) Histograms of transcriptional start ("Time On", dark green) and end ("Time Off", pale green) times from two independent experiments. Most cells start transcription within the first 15 minutes after Notch activation, while the end of transcription varies more between approximately 30 and 60 minutes. Percentages and n numbers (bottom right) indicate the number of responding cells. (F and G) Transcription level correlates negatively with the transcriptional start time (dark green) and positively with transcriptional end time (pale green). Maximum increase in fluorescence plotted for individual cells against time. (H and J) Baseline fluorescence level plotted for individual cells against time. Correlations were not reproducible across three replicates (two shown here). Pearson product moment correlation coefficients: r = -0.36, -0.24, -0.25, -0.13 for Time On, and r = 0.38, 0.39, 0.21, 0.032 for Time Off (F, G, H and J, respectively); p = $6x10^{-6}$, 0.008, 0.002, 0.1 for Time On, and p = $3x10^{-6}$, $2x10^{-5}$, 0.01, 0.7 for Time Off. Notch is activated by EGTA treatment for all data in this figure.

To verify that the blasticidin resistance cassette present in the engineered *E(spl)mβ-HLH* gene was not affecting the dynamics of the Notch response, it was removed by flippase-induced recombination (Figure 3.5A and B). A homogenous population of cells in which the cassette was removed were obtained by cell cloning. These cells responded to Notch activation in a similar manner to the original mβ MS2 cells, except that the transcription now extended through to the 3' portion of the engineered E(spl)mβ-HLH gene (Figure 3.5C). Live imaging confirmed that the dynamics of the response in these cells was similar (Video 3; Figure 3.5D and E), with transcription occurring rapidly in the responding cells and giving similar fluorescence profiles. The most notable difference was that the levels of transcription were slightly lower. Most likely as a result of this, as discussed above, the transcriptional start times detected were slightly later on average (compare Figure 3.5F with Figure 3.4D and E) and transcriptional end times were earlier (Figure 3.5F and G). It is possible that a more efficient transcription termination in the absence of the blasticidin resistance cassette was partly responsible for the earlier end time, and indeed possibly for the lower fluorescence intensity of transcription foci, since the efficient release of transcripts from the site would reduce the build-up of fluorescence. However, the similarity in the overall shape of the response argues that the 3' UTR does not make a major contribution to the qualitative dynamics of E(spl)mβ-HLH transcription. In other words, the normal processing of the 3' end of the transcript is not required for further transcription initiation or to regulate bursting behaviour.

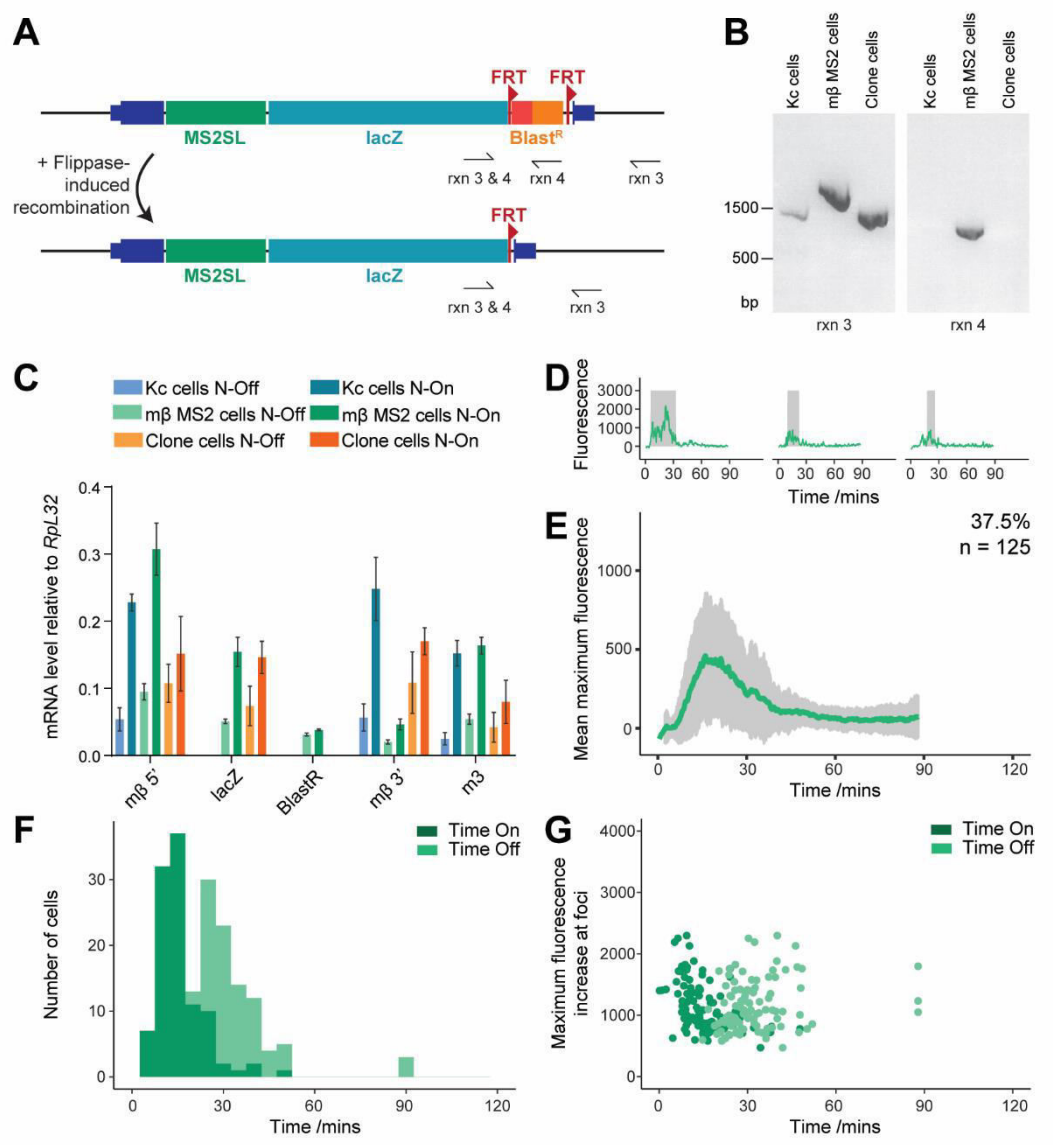

Figure 3.5. Removal of the blasticidin resistance cassette did not alter the speed of the detected transcriptional response. (A) Schematic illustrating flippase-induced recombination to remove the blasticidin resistance cassette. (B) Successful removal of the blasticidin resistance cassette from "Clone cells", demonstrated by genotyping PCR reactions. Positions of primers used are shown by half arrows in A. PCR product is reduced in size in Clone cells for reaction 3 ("rxn 3"), and is absent for reaction 4 ("rxn 4"). Un-transfected "Kc cells" and "mβ MS2 cells" before flippase-induced recombination are shown as controls. (C) Notch-responsive transcription of the edited *E(spl)mβ-HLH* gene from "Clone cells", demonstrated by reverse transcription-qPCR, with un-transfected "Kc cells" and "mβ MS2 cells" as controls. Positions of primers are as in Figure 3.1C. Data is shown for Notch-ON ("N-On"; EGTA treatment) and Notch-OFF ("N-Off"; PBS control) conditions. There is no transcription from the blasticidin resistance cassette in Clone cells, and the levels of transcription from the 3' end of the gene match the 5' end. Mean ± SEM; n = 2. *Continued on next page.*

3.2.3 Effects of MG132 on the dynamics of the Notch response

Pulse-chase experiments suggest that the termination of the Notch response is due to the degradation of NICD, and it is proposed that NICD becomes post-translationally modified and targeted to the proteasome (Fryer et al. 2002, 2004; Fortini 2009; Ilagan et al. 2011; Guruharsha et al. 2012). To gain insight into the speed of NICD degradation in the Kc167 cells, the amount of active NICD present at different times following Notch activation was assessed by analysing the amounts that co-immunoprecipitated with Su(H) (Figure 3.6A). Results showed that the amount of active NICD increased within 30 minutes of Notch activation, and the levels then decreased gradually over time. Rather than disappearing rapidly to account for the termination of transcription, the levels remained quite robust even at 120 minutes post-activation. This suggests that either there is a particular threshold of NICD required for transcription, or that NICD is becoming inactivated in another way such as post-translational modification. When the distribution of NICD in the cells was detected by immunofluorescence, it was enriched in the nuclei after activation and subsequently became restricted to discrete regions, which may indeed be sites of degradation (Figure 3.6B).

Figure 3.5 continued (D and E) The detected transcriptional response to EGTA-induced Notch activation is largely similar when the blasticidin cassette is removed. Graphs are example tracks of maximum fluorescence intensity from individual cells (D) and mean maximum fluorescence with standard deviation for all responding cells (E). Percentage and n number (top right) indicate the number of responding cells. (F) Histograms of transcriptional start ("Time On", dark green) and end ("Time Off", pale green) times from Clone cells. Start time is not altered but end time may be slightly earlier. (G) Maximum increase in fluorescence plotted for individual cells against time. As before, transcription level correlates negatively with the transcriptional start time (dark green) and positively with transcriptional end time (pale green). Pearson product moment correlation coefficients: $r = -0.44$ for Time On, and $r = 0.24$ for Time Off; $p < 0.05$.

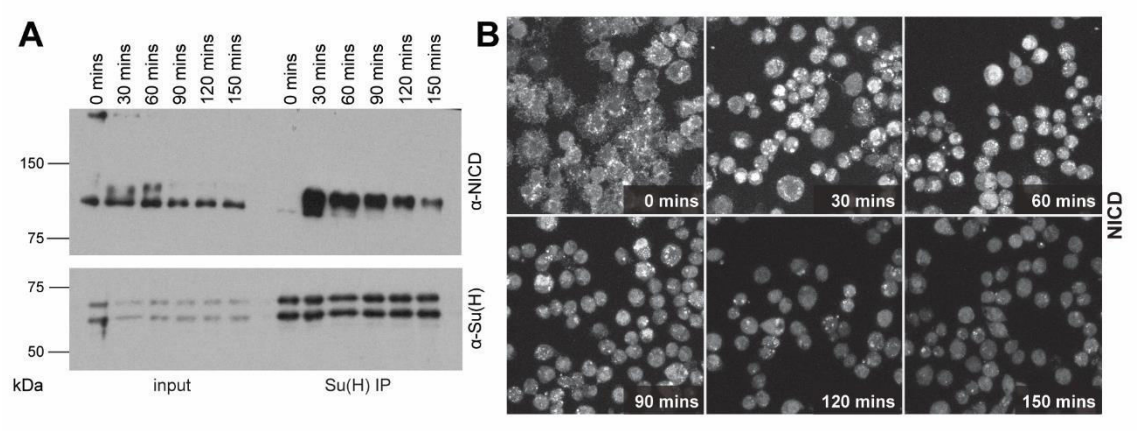

Figure 3.6. Active NICD levels decrease slowly over time. (A) Active NICD levels detected by co-immunoprecipitation with Su(H), shown on Western blot probed with NICD antibody, at the times indicated after EGTA-induced Notch activation. Western blot probed with Su(H) antibody is shown as a control. Input indicates protein samples taken before immunoprecipitation. Active NICD levels increase dramatically by 30 minutes after Notch activation, then decrease slowly. (B) Immunofluorescence staining of NICD in Kc167 cells at the indicated lengths of time after EGTA-induced Notch activation. NICD is observed on the membrane at zero minutes, and at decreasing levels in the nucleus and other compartments after Notch activation.

To investigate whether the decline in NICD levels was due to proteasomal degradation, cells were treated with MG132, a widely used proteasome inhibitor (Oberg et al. 2001; Wu et al. 2001; Sriuranpong et al. 2002; Chapman et al. 2006). Surprisingly, when Notch was activated in mβ MS2 cells pre-treated with MG132 for five hours, very few transcription foci were detected within the first 60 minutes, suggesting that the normal transcription response of *E(spl)mβ-HLH* did not occur (Figure 3.7A and C). The length of treatment was chosen to be similar to previous studies (Wu et al. 2001; Dale et al. 2003; McGill and McGlade 2003). Since the possibility of indirect effects occurring is likely to increase with time, it would instead have been an improvement to optimise the length of treatment by testing when the proteasome was successfully inhibited using a Western blot for ubiquitinated proteins (Lundgren et al. 2005). However, when MG132 was added only in conjunction with the EGTA and not before, the result was similar, with far fewer cells responding than normal.

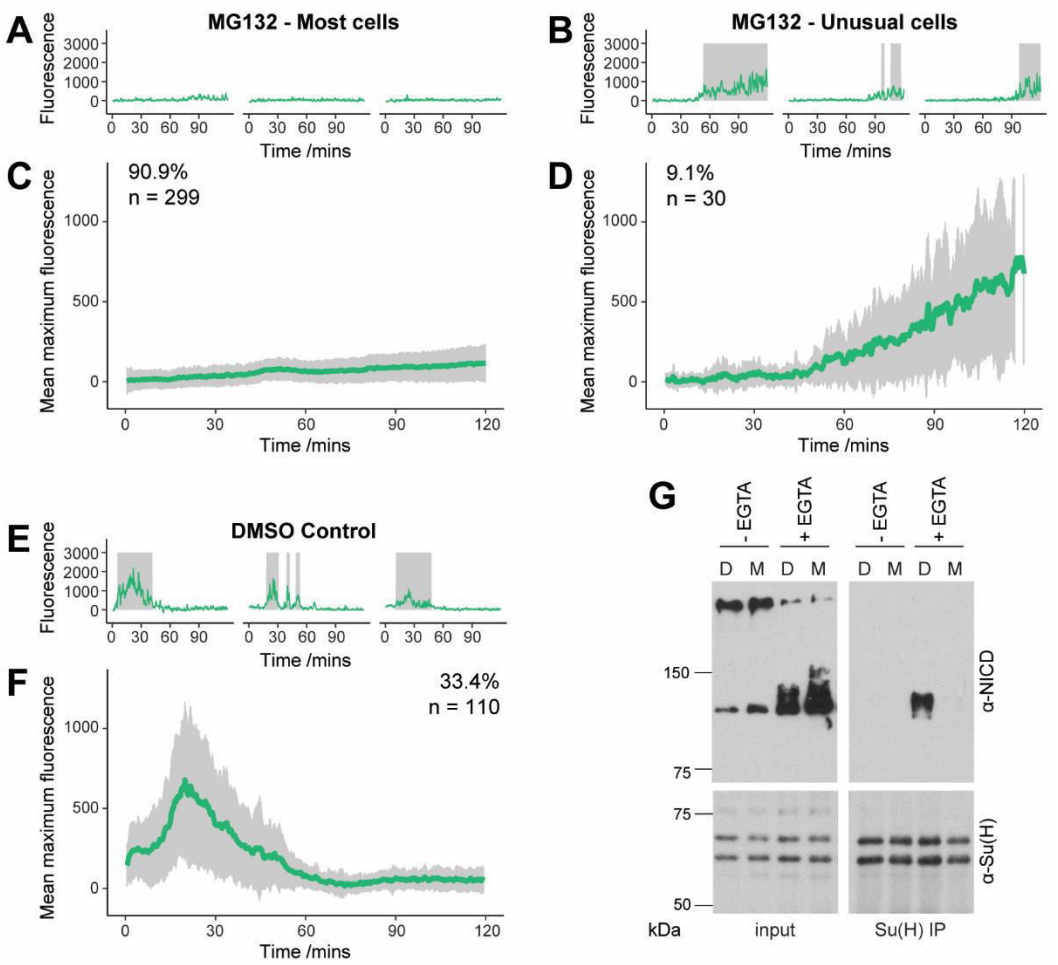

Figure 3.7. MG132 treatment disrupts transcription dynamics. (A-D) The transcriptional response to EGTA-induced Notch activation is disrupted by the inhibitor MG132. Most cells do not respond (A and C), while a small proportion show a delayed and increasing transcriptional response (B and D). (E and F) Control cells treated with DMSO have a normal transcriptional response to EGTA-induced Notch activation. Graphs are example tracks of maximum fluorescence intensity from individual cells (A, B and E) and mean maximum fluorescence with standard deviation for all cells in each category (C, D and F). Percentages and n numbers indicate the number of cells in each category. (G) Effect of MG132 on active NICD levels detected by co-immunoprecipitation with Su(H), shown on Western blot probed with NICD antibody, with ("+EGTA") and without ("-EGTA") 30-minute EGTA induction of Notch. Western blot probed with Su(H) antibody is shown as a control. Input indicates protein samples taken before immunoprecipitation. MG132 ("M") severely reduces the level of active NICD produced by EGTA treatment compared to controls with DMSO ("D").

Surprisingly, a small proportion of cells acquired foci after a considerable delay, suggesting that they had started transcribing *E(spl)mβ-HLH* much later than normal, and in these cases transcription levels gradually increased over time (Figure 3.7B and D; Video 4). This behaviour was observed in three independent experiments when MG132 was added for five hours (and also in the experiment where MG132 was added in conjunction with the EGTA), but always only occurred in less than 10% of the cells. This type of profile had not been observed before and did not occur in control experiments (Figure 3.7E and F), suggesting that it does reflect a real response in the presence of MG132, albeit with low penetrance.

The effects of MG132 were not consistent with a simple model where the drug had perturbed the proteasomal degradation of Notch. However, although MG132 has been primarily used as a proteasome inhibitor assumed to prevent NICD degradation (Oberg et al. 2001; Wu et al. 2001; Sriuranpong et al. 2002; Chapman et al. 2006), it was also shown previously to inhibit the γ-secretase cleavage of Notch (Brou et al. 2000; Taniguchi et al. 2002; Dale et al. 2003). It is possible therefore that MG132 has different effects dependent on concentration, and one of its targets appears to be the γ-secretase complex. It was therefore important to assess its effects on active NICD levels, so the levels of NICD that co-immunoprecipiated with Su(H) in the presence of MG132 were analysed. At 30 minutes after Notch activation, the amount of NICD present in the immunoprecipitate was severely reduced and barely detectable in the MG132-treated cells (Figure 3.7G). These results were replicated in two independent experiments and are therefore consistent with MG132 inhibiting the cleavage of Notch.

These data have two implications. Firstly, they confirm the Notch-dependency of the EGTA-induced transcriptional response, since a disrupted formation of the active Su(H) complex correlated with a disrupted transcriptional response. It is possible that the delayed transcriptional response observed in some cells was due to a slower cleavage of Notch, but this would need to be tested by assessing active NICD levels at different time points. Secondly, they highlight the need to use MG132 with caution when using it as a proteasome inhibitor in Notch studies.

3.2.4 The dynamic response to ligand-induced Notch activation

The results show that transcription is initiated very rapidly within 15 minutes of EGTA-induced Notch cleavage. Previous experiments in mammalian cells using split-luciferase to measure NICD-CSL association made a similar estimate for EGTA-mediated complex formation, but have estimated that ligand-induced NICD-CSL complexes appear much more slowly (Ilagan et al. 2011). To investigate how rapidly ligands can elicit a transcriptional response, a simple co-culture system was used to activate Notch by the ligand Delta. A *Drosophila* S2 cell line expressing Delta was plated first, then the mβ MS2 cells were added to the plate. The cells were imaged live throughout the process so that the behaviour of the mβ MS2 cells could be analysed as they made contact with the Delta-expressing S2 cells.

Clear transcription foci were observed in around 20% of the mβ MS2 cells after they settled onto the plate (Video 5; Figure 3.8C-F), suggesting that Notch had been activated and initiated transcription in those cells, and this behaviour was observed reproducibly. In agreement, no foci were detected in the absence of S2 cells, even when the mβ MS2 cells were manipulated in a similar manner (Figure 3.8G).

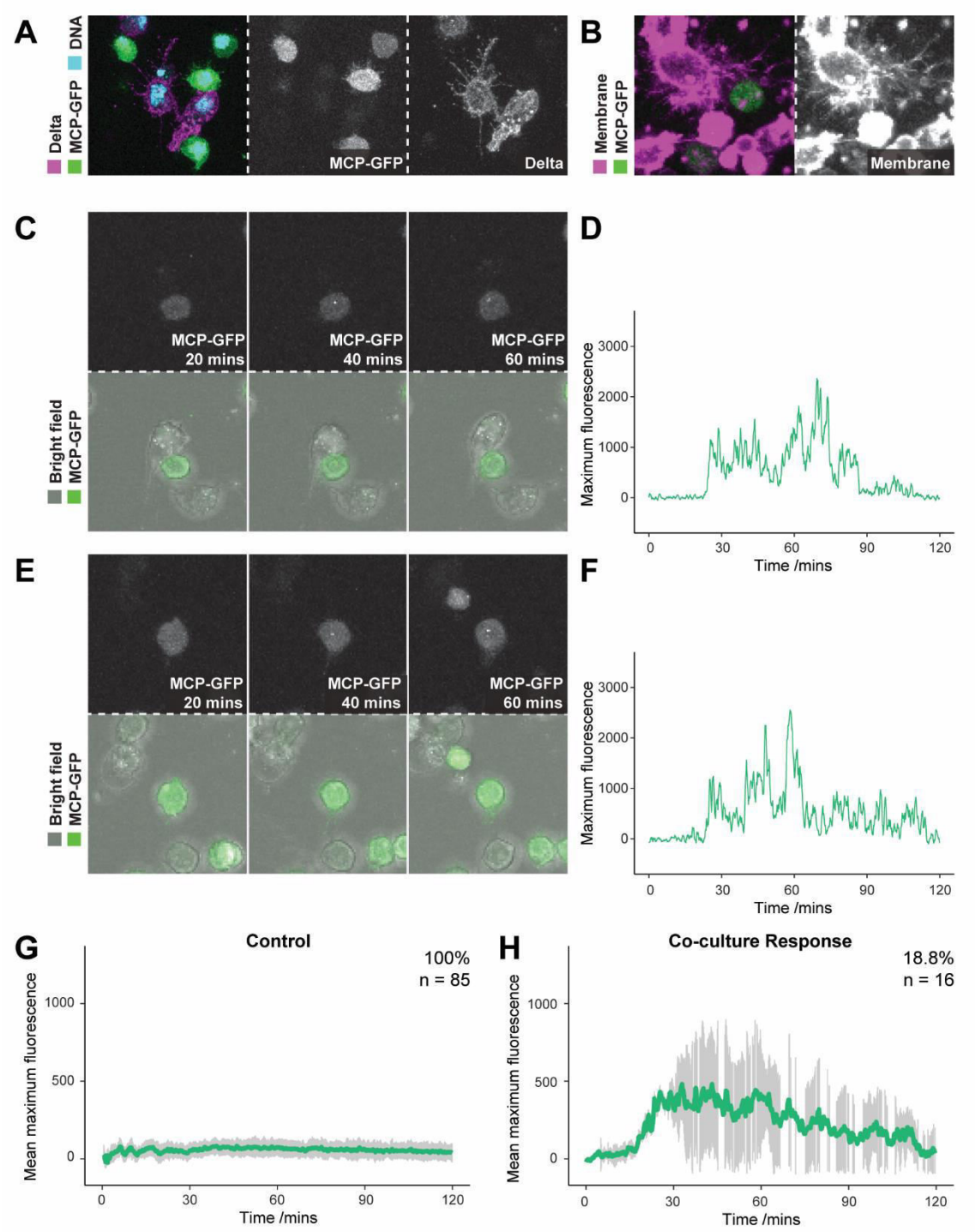

Figure 3.8. Ligand-induced Notch activation takes longer and can signal via cell projections. (A) Immunofluorescence staining of Delta (magenta) in co-cultured S2 and mβ MS2 cells. S2 cells express Delta from the inducible pMT promoter, while mβ MS2 cells show no staining. mβ MS2 cells are marked by their MCP-GFP expression (green) and DNA is stained with Hoechst (cyan). (B) Cells have many projections, shown by a live plasma membrane stain (magenta) of S2 cells. An mβ MS2 cell (green) is observed interacting with these projections. *Continued on next page.*

The transcription foci appeared quickly after addition of the mβ MS2 cells, and at first glance it appeared that some responding mβ MS2 cells were not in contact with any S2 cells, raising the question of how the receptor could have been activated (Figure 3.8E). However, closer examination revealed that there were dynamic cell projections on the surface of both the mβ MS2 cells and the Delta-expressing S2 cells. These were also detected in fixed cells (Figure 3.8A), and became even more apparent when a live plasma membrane stain was used (Figure 3.8B). It was therefore likely that all mβ MS2 cells touching the plate were in contact with an S2 cell via one or more projections. As illustrated by the examples in Figure 3.8C-F, the response levels were robust even for cells signalling through projections, and there were similar strong responses regardless of whether the cells were in close contact or more distant from one another. Due to the low sample size from these experiments, the effect of the extent of contact between the cells on the transcription levels or timing could not be analysed. Nonetheless, it is a remarkable result that transcription occurred at a sufficient level for detection even when signalling took place through contacts between cellular projections.

Figure 3.8 continued (C-F) The Notch transcriptional response can be triggered by ligand-induced activation, either from an adjacent cell (C and D) or at a greater distance, most likely via projections (E and F). Examples are shown by images of co-cultured S2 and mβ MS2 cells at the time points indicated in minutes after the mβ MS2 cells settled onto the plate (C and E), and their individual tracks of maximum fluorescence intensity, where time zero is the time the cells settled onto the plate (D and F). (G) No transcriptional response is observed in control experiments where S2 cells are excluded, shown as mean maximum fluorescence with standard deviation for all cells. (H) The ligand-induced transcriptional response occurs after a 20 to 30 minute delay, illustrated by the mean maximum fluorescence with standard deviation for the responding cells in a co-culture experiment. Time zero is the time the cells settled onto the plate. Percentages and n numbers (top right) indicate the number of cells analysed.

It took 20 to 30 minutes for the transcription foci to be detected after the first S2 cell contact, demonstrated by the mean maximum fluorescence intensity from the responding cells (Figure 3.8H). This is in contrast to EGTA-induced Notch activation, where transcription was detected within five minutes in some cells. The additional delay could be due to events upstream of the S3-S4 Notch cleavage. For example, it may take some time for the receptor and ligand to come close enough together and physically interact, or the additional S2 cleavage step could add a significant delay. Alternatively, if transcription can only start when a threshold level of active NICD is reached, it could take longer to reach this threshold if fewer receptors are activated during the same time frame.

Another notable difference following ligand-induced activation was that some mβ MS2 cells exhibited transcription foci for a prolonged period, as illustrated by the profile in Figure 3.8F. However others appear to switch off after a period of time, more similarly to what was seen with EGTA-induced signalling (Figure 3.8D). With the current dataset, it is difficult to tell whether the two cell types are continuously signalling to each other or whether the interaction provides a single pulse of Notch signalling. More data would be required to fully understand whether the termination of transcription depends on the termination of signalling or something more intrinsic to the *E(spl)mβ-HLH* gene.

3.3 Discussion

In this chapter, the MS2 system was used to investigate the transcriptional response to Notch signalling with fine temporal resolution. Chemical-induced cleavage of Notch was found to give reliable and detectable transcription in a subset of the cell population very rapidly, which subsequently switched off. Detectable transcription could also be achieved by ligand-induced Notch activation, but this involved a delay.

The MS2 system is inherently quantitative since the fluorescence intensity of transcription foci reflects the number of RNA molecules present. However, the lower limit of detection depends on the imaging conditions (Corrigan et al.

2016). By comparing the foci obtained with the MS2 system with those obtained from fluorescence *in situ* hybridisation experiments, some have estimated the lower detection limit to be around six nascent transcripts in the *Drosophila* embryo system (Garcia et al. 2013), while others have increased the number of *MS2 stem-loops* to achieve single molecule detection (Tantale et al. 2016). One concern was whether the varying levels of MCP-GFP expression in the Kc167 cells would affect the detection of different transcription levels. Despite no calibration experiments being performed, the lack of correlation between the maximum fluorescence value and the baseline fluorescence level for each cell promisingly suggested that the increase in fluorescence detected at transcription foci likely reflects the level of transcription, rather than an MCP-GFP concentration-dependent effect. Furthermore, there were no reproducible correlations between the timing or duration of detected transcription and baseline fluorescence level, suggesting that in this system, the range of MCP-GFP levels did not significantly affect the detection of active transcription. Further experiments are required to determine the absolute detection threshold for this system and thus find out whether the seemingly unresponsive cells are likely to be transcribing low levels of *E(spl)mβ-HLH* or not.

The number of MS2-labelled nascent transcripts located at the site of transcription at any one time depends on the initiation, elongation and termination rates of transcription. Attempts have been made to distinguish between these by comparing the dynamics produced by *MS2 stem-loops* inserted at the 5' or 3' end of the gene (Larson et al. 2011; Garcia et al. 2013; Fukaya et al. 2017). Additionally, fluorescence recovery after photobleaching (FRAP) has been used, since focus recovery reflects new initiation events (Muramoto et al. 2012). These studies concluded that initiation rate was stochastic and related to transcription factor binding events, while elongation rate was deterministic (but variable), yet it remains to be seen if this is universally true. This could mean that Notch signalling upregulates *E(spl)mβ-HLH* expression by increasing the number of initiation events via Su(H)-NICD-Mam complex binding to enhancers. However, *E(spl)mβ-HLH* is thought to be regulated by promoter-proximal pausing involving the co-repressor Groucho (Kaul et al. 2014, 2015), and is therefore likely to also be regulated by the release from pausing, as has been found for genes regulated by TNFα (Danko et al.

2013). Since it had been shown previously that depletion of Groucho by RNAi in Kc167 cells reduces Pol II pausing at *E(spl)mβ-HLH* (Kaul et al. 2014), it would be interesting to see if this manipulation changes the dynamics of transcription measured by the MS2 system.

Although transcriptional bursting has been shown to be a widespread phenomenon (Nicolas et al. 2017), individual bursts were not easily distinguished for *E(spl)mβ-HLH* in the Kc167 cells (see Figure 3.2A and B). With EGTA treatment, the majority of responding cells appeared to have one "on" period without discrete bursts (Figure 3.2A, left). And where some cells exhibited short "off" periods during their response (Figure 3.2A, right), the "bursts" in between differed in size greatly. In the experiments using ligand-induced activation, some plots appeared to have bursts (see Figure 3.8F), although a larger sample size would be needed to assess this computationally. These bursts could either have occurred due to lower levels of transcriptional activation induced by fewer molecules of released NICD, or they could result from pulses in the upstream signalling.

At first glance, it may appear that this supports a model where transcriptional output is regulated by burst size. However, it has been argued that at high burst frequencies individual bursts merge in an additive manner when measured by the MS2 system, giving misleading results (Fukaya et al. 2016; Wang et al. 2018), and it is possible that this is the case here. If the fluorescence produced by an individual burst falls below the detection limit, the transcription foci observed may represent only those cells experiencing transcription bursts in quick succession, and this would explain the large variability in transcription focus intensity observed. Mathematical modelling would be required to draw firm conclusions about bursting in this system.

Regardless of whether the differences in intensity observed are due to a different burst size or frequency, it will be interesting to identify what controls the level of the response. For example, the transcriptional output of *E(spl)mβ-HLH* may be determined by the concentration of active NICD in the cell, which could be tested for example by the expression of a fluorescently-tagged NICD protein. Alternatively, there may be a greater degree of stochasticity in the

response, intrinsic to the gene being transcribed. One way to distinguish between the effects of extrinsic and intrinsic factors is to observe cells with two transcription foci, formed as a result of both copies of the *E(spl)mβ-HLH* gene being edited. While the computational analysis of two foci within a single cell is complicated, by eye some cells were observed to have two active sites of transcription at once. When this occurred, the responses were similar, with the two foci responding to Notch activation within the normal time window. However, the exact intensity and duration of transcription appeared to differ within single cells, fitting with a model of stochastic transcription initiation, although further analysis is needed to confirm this.

While the intensity of the transcriptional response differed from cell to cell, the speed of the response was highly reproducible, with the majority of observed transcription being detectable within the first 15 minutes after chemical-induced Notch activation. This is in line with previous experiments in mammalian and *Drosophila* cells where NICD was detected in the nucleus or target genes were upregulated shortly after calcium chelation (Kawahashi and Hayashi 2010; Ilagan et al. 2011; Housden et al. 2013), confirming that the trafficking of NICD to the nucleus to activate target genes can occur very rapidly. Interestingly, different classes of genes were identified in the *Drosophila* cells, some of which had a more delayed response to Notch signalling (Housden et al. 2013), indicating that some genes may be less poised for transcription, perhaps due to a lack of Pol II pausing, and take longer to become activated. It would be very interesting to analyse a gene which exhibits a delayed response to Notch with the MS2 system to observe whether the dynamics differ from *E(spl)mβ-HLH*.

Another study identified that the mammalian target genes Hes1 and Hey1 respond differently to Notch signalling, with Hes1 responding to a short pulse of signalling while Hey1 requires a longer period of sustained signalling. The two modes of signalling were found to be elicited by the two ligands Delta-like1 and Delta-like4, respectively, making an exciting link between ligand expression and target gene activation (Nandagopal et al. 2018). However, the time resolution of this study was a matter of hours since it relied on the expression of reporter proteins, so it remains to be seen how different ligands could affect the Notch

response on a finer timescale. Additionally, it is unclear how a broad change in NICD level over a period of several hours is translated into the transcriptional outcome. The fact that *E(spl)mβ-HLH* responded more slowly with the MS2 system when Notch was activated by ligands on neighbouring cells suggests that cell-cell signalling events upstream of Notch cleavage take significant time to occur. A similar conclusion was drawn by others using a single-cell optogenetic approach, where the delay due to ligand-induced NICD production was estimated to be around 50 minutes (Isomura et al. 2017). An alternative explanation is that when fewer Notch receptors are cleaved it takes longer for enough NICD to accumulate for detectable transcription.

The results presented in this chapter are significant for the understanding of Notch signalling mechanisms for several reasons. Firstly, very few previous studies have analysed the Notch response with such high temporal resolution or on a single cell basis. It has become apparent for other signalling pathways that the temporal dynamics of signalling can encode additional information (Purvis and Lahav 2013). For example, the dynamics of transcription factor NF-κB activity (nuclear localisation) differ depending on the concentration of activating TNFα signalling in terms of the speed of response and number of oscillations, driving the expression of different target genes (Tay et al. 2010). And while it has been known for some time that the different outcomes driven by epidermal (EGF) and nerve (NGF) growth factors via the same cascade in rat adrenal PC-12 cells depend on the different dynamics of ERK activation (Marshall 1995), recent experiments in single cells highlight the heterogeneity of the response (Ryu et al. 2015). Therefore, it is possible that the temporal encoding of signalling information is widespread and should not be overlooked in the case of Notch signalling.

Secondly, while most cell fate decisions during development are thought to be governed by a rigid set of conditions and inputs, some examples appear to be stochastic (Losick and Desplan 2008), including many where Notch signalling is implicated. The process of lateral inhibition, whereby small differences in gene expression between neighbouring cells are amplified by feedback loops leading to the spatial separation of cells with the same fate, is thought to depend on an initial stochastic imbalance (Sjöqvist and Andersson 2017). Many examples of

lateral inhibition, such as in the patterning of epidermal sensory bristles in *Drosophila* (Corson et al. 2017) or inner ear hair cells in the mouse (Basch et al. 2016), depend on Notch signalling. Being able to measure and characterise the stochasticity and cell-to-cell variability in the transcriptional Notch response is thus helpful for understanding this type of cell fate decision.

Finally, unlike other signalling mechanisms that rely of diffusible extracellular signals, Notch signalling is thought to be restricted to neighbouring cells, since in most animals, both the receptor and ligands are transmembrane proteins. The surprising result that the Notch response could be stimulated from signalling via cell projections gives the possibility that Notch signalling could act over longer distances, which has been proposed by several recent studies. Lateral inhibition-driven bristle spacing in *Drosophila* has been found to rely on basal actin-based filopodia spanning several cell diameters (Cohen et al. 2010), and the development of zebrafish stripes involves Notch signalling via thin projections between the two cell types, xanthophores and melanophores (Hamada et al. 2014; Eom et al. 2015). Therefore, this is a useful observation strengthening the argument that Notch signalling can occur through very small contact areas. It would be interesting to compare how the transcriptional response differs when Notch signalling is activated by cell contacts compared to soluble ligands, as found in *C. elegans* (Chen and Greenwald 2004; Komatsu et al. 2008).

The experiments presented in this chapter are novel and illustrate a successful method for measuring the Notch response on a temporal and single cell level. This will be a valuable system in which to evaluate different aspects of Notch signalling such as the response to different levels of signalling or different ligands. With mathematical modelling this system could give insight into the regulation of transcription initiation, elongation and termination rates by Notch signalling, contributing to a greater understanding of transcription regulation during development.

4 CHROMATIN DYNAMICS IN THE NOTCH RESPONSE

4.1 Introduction

In chapter 3 the rapidity of the Notch response was illustrated, with Notch-dependent transcription occurring within 15 minutes of Notch cleavage. To allow target genes to be so receptive to Notch, yet appropriately constrained in the absence of signalling, the chromatin structure must be highly regulated. Notch signalling has been reported to interact with various chromatin modifiers (Takeuchi et al. 2007; Yatim et al. 2012; Yu et al. 2013), and changes in histone PTMs occur at enhancers during Notch activation (Castel et al. 2013; Wang et al. 2014a; Skalska et al. 2015). While these findings make it clear that chromatin structure regulation is crucial for Notch signalling, it is still unknown how the interplay of these factors brings about the correct response mechanistically. The experiments in this chapter aim to address how the chromatin structure influences Su(H) binding and how this is regulated.

By switching between different partners in the Notch-OFF and Notch-ON state, CSL has a complex association with the chromatin (Bray and Gomez-Lamarca 2018). Beyond the immediate co-repressors and co-activators that interact directly with CSL (Hairless and Mam in *Drosophila*), many additional chromatin regulators have been found to modify CSL function. To name a few, the demethylase LSD1 has been shown to be important both for repression and

activation of Notch targets (Wang et al. 2007; Di Stefano et al. 2011; Yatim et al. 2012), the histone chaperone CAF-1 modulated the binding of Su(H) to enhancers (Yu et al. 2013), and a SWI/SNF chromatin remodelling subunit Baf60c was required for Notch-dependent transcription in mouse embryos (Takeuchi et al. 2007).

Genome-wide studies led to the finding that CSL binding increases with Notch signalling at Notch-responsive enhancers (Krejcí et al. 2009; Wang et al. 2011; Castel et al. 2013; Wang et al. 2014a), but the mechanism for how this is caused was not known. Additionally, the chromatin states at Notch target genes have been identified and changes in histone PTMs have been found to occur in response to Notch signalling (Castel et al. 2013; Wang et al. 2014a; Skalska et al. 2015). In *Drosophila*, these changes have been most clearly observed at the Enhancer of split complex (*E(spl)-C*), a 60-kilobase region where 11 highly Notch-responsive genes are concentrated (Bailey and Posakony 1995; Cooper et al. 2000; Housden et al. 2013; Schaaf et al. 2013). Notch signalling dramatically upregulates H3K27 and H3K56 acetylation at this locus (Skalska et al. 2015). While these findings were ground-breaking, they do not reveal the underlying mechanisms for how they contribute to Notch-responsive transcription. For example, it is unclear what causes these chromatin changes and what functional effect they have on the cellular outcome.

In this chapter, the dynamic nature of the chromatin structure is studied, giving new insight into the features of Notch-responsive enhancers. A chromatin remodelling complex essential for the Notch response is identified, and the mechanistic basis for its involvement is examined.

4.2 Results

4.2.1 Ectopic Notch signalling causes largescale changes in chromatin structure

The *Drosophila* larval salivary gland has been used extensively with live imaging to study intranuclear dynamics due to its large nuclei (Yao et al. 2006, 2007, 2008). Endoreplication in this tissue results in polytene chromosomes; many

copies of the DNA are aligned such that each genomic locus occupies a single position (Rodman 1967). To take advantage of these characteristics, the Bray group set out to use live imaging tools to study mechanisms required for Notch-dependent transcription in the salivary gland. Normally there is no Notch activity in the third instar salivary gland (Notch-OFF), except in the imaginal ring, but Notch activity can be provided by the expression of a constitutively-active form of Notch, $N^{\Delta ECD}$ (Notch-ON; Gomez-Lamarca et al. 2018). As part of this project, the *E(spl)-C* was non-intrusively labelled using the ParB-INT system, where the fluorescently-labelled ParB protein binds and oligomerises at the INT DNA segment within the locus, allowing a single bright band of fluorescence to be visualised (Saad et al. 2014; Gomez-Lamarca et al. 2018). This makes it possible to observe changes at a specific Notch-regulated locus. Indeed, when the *E(spl)-C* was labelled on both homologous chromosomes with different fluorescent proteins, the overall architecture of the locus was visible (Figure 4.1A and B). Notably, in Notch-ON conditions, the two chromosomes appeared more open with more intermingling between them (Figure 4.1B). This correlates with the increased activity of the *E(spl)-C* genes (shown by changes in mRNA production in Gomez-Lamarca et al. 2018).

To observe Notch-activated transcription *in situ*, the MS2 system was adapted for use in the salivary gland. In a similar manner to that outlined in chapter 3, the genomic *E(spl)mβ-HLH* gene was tagged with *MS2 stem-loops* using CRISPR gene editing (see Materials and methods). Combining this with a ubiquitously-expressed MCP-GFP should allow transcription to be visualised in the salivary gland. In agreement with *E(spl)mβ-HLH* being a direct transcriptional target of Notch, transcription foci were only observed in the Notch-ON condition (Figure 4.1C), where their distribution was similar to that seen with the GFP ParB-INT system (Figure 4.1B). It is unclear at present whether each transcription focus observed reflects a single strand of DNA transcribing the gene, or whether the DNA is clustered into hubs of transcription activity. It is estimated that there are up to around 1000 copies of the DNA in these polytene chromosomes (Rodman 1967). As there are fewer than 1000 foci detected, it is more than likely that they represent clustered transcription sites, although it remains possible that only a subset of the DNA copies are utilised for transcription, so that each fluorescent focus is an

individual transcription initiation site. Super-resolution microscopy techniques (Cho et al. 2016), perhaps combined with mutants affecting the number of salivary gland endoreplication cycles (Weng et al. 2003), could help to resolve this.

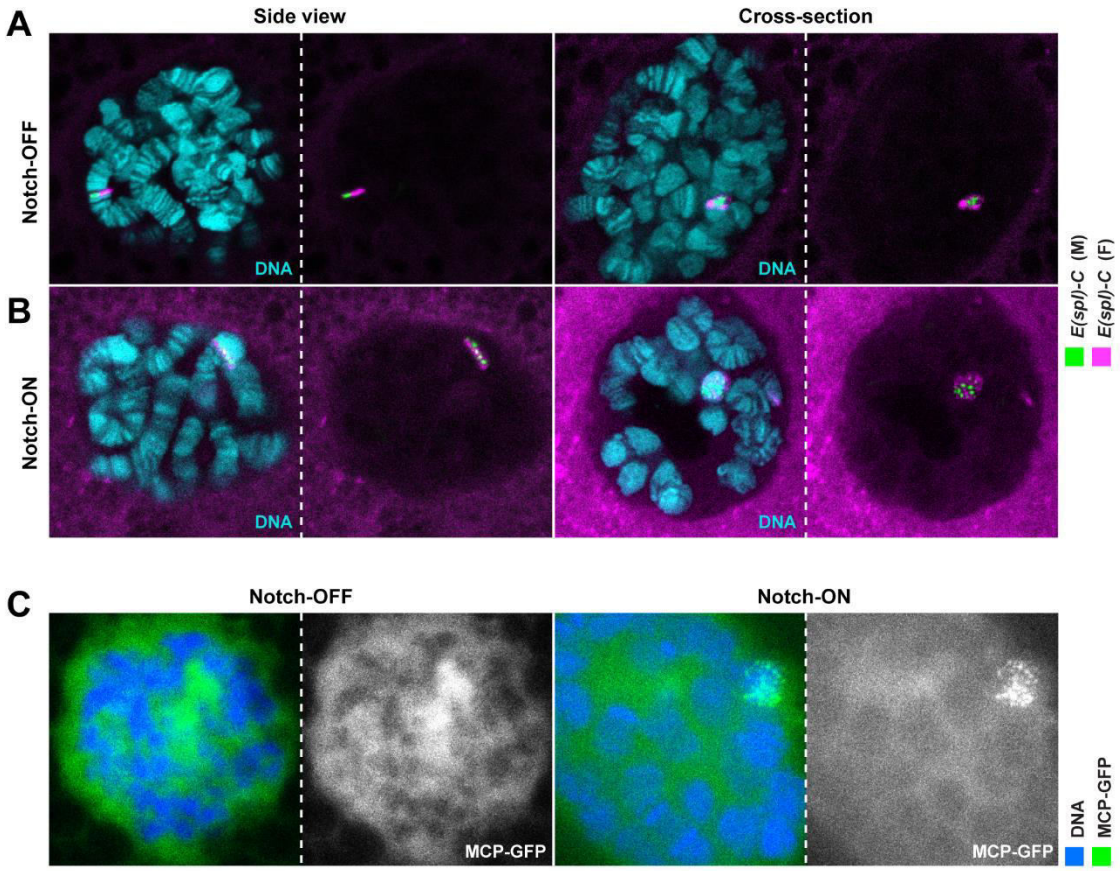

Figure 4.1. The *E(spl)-C* changes structure in Notch-ON nuclei. (A and B) Live imaging of ParB1-mCherry (magenta) and ParB2-GFP (green) expressed with *1151-Gal4* in Notch-OFF (A; $N^{\Delta ECD}$ expression) and Notch-ON (B; LacZ expression) larval salivary gland nuclei. ParB proteins bind to their respective INT DNA sequences in the *E(spl)-C* on the two homologous chromosomes (Saad et al. 2014; Gomez-Lamarca et al. 2018). (C) Live imaging of MCP-GFP (green) expressed ubiquitously and localising to *E(spl)mβ-HLH* transcripts via *MS2 stem-loops* in the Notch-ON ($N^{\Delta ECD}$ expression) condition. In control conditions (Notch-OFF; LacZ expression), MCP-GFP is seen in the space outside of the chromosomes and in the nucleolus. DNA is stained with Hoechst 33342 (cyan, A and B; blue, C).

Considering the apparent changes observed at the *E(spl)-C* in response to Notch signalling, it was hypothesised that the chromatin itself may be altered to allow this upregulation of Notch-dependent transcription. Therefore, GFP-tagged histone proteins were used to assess both the general structure of the chromosomes and the presence of histone variants at the *E(spl)-C* under Notch-ON and Notch-OFF conditions (Figure 4.2; Henikoff et al. 2000; Ahmad and Henikoff 2002). In order to do this, the histones were expressed using *1151-Gal4* along with either $N^{\Delta ECD}$ (Notch-ON) or LacZ in the Notch-OFF control and the salivary gland nuclei were imaged. Without Notch signalling, both the canonical histone H3-GFP and histone variant H3.3-GFP were present at low levels at the *E(spl)-C* compared to surrounding regions (Figure 4.2A and C, Notch-OFF). However, under Notch-ON conditions, the relative levels of H3.3-GFP were greatly increased at the *E(spl)-C* compared to surrounding regions (Figure 4.2A, Notch-ON). This was highly reproducible, as seen from quantifications of relative fluorescence intensity across the locus in images taken from multiple nuclei in live salivary glands (Figure 4.2B). No such change was detected when the effects on histone H3 were examined in a similar manner (Figure 4.2C and D).

It should be noted that the changes detected represent changes in histone-GFP levels within or in the vicinity of the 60-kilobase region and cannot distinguish between histones incorporated at gene bodies versus intergenic regions. However, histone H3.3 has been associated with actively-transcribed genes and can be incorporated into the chromatin independently of DNA replication (Ahmad and Henikoff 2002; Wirbelauer et al. 2005). To verify that the Notch-dependent increase in H3.3-GFP was replication-independent, a mutant form of histone H3.3 was used, $H3.3^{core}$-GFP, which is only incorporated in a replication-independent manner (Ahmad and Henikoff 2002). Indeed with $H3.3^{core}$-GFP the same effects were seen as with H3.3-GFP. Little $H3.3^{core}$-GFP was present at the *E(spl)-C* in Notch-OFF conditions (Figure 4.2E and F, Notch-OFF), and high levels were recruited in Notch-ON nuclei (Figure 4.2E and F, Notch-ON). This argues that the local increase in H3.3 concentration at the *E(spl)-C* is not due to an increased level of endoreplication at this locus and likely reflects incorporation associated with Notch-induced gene activation.

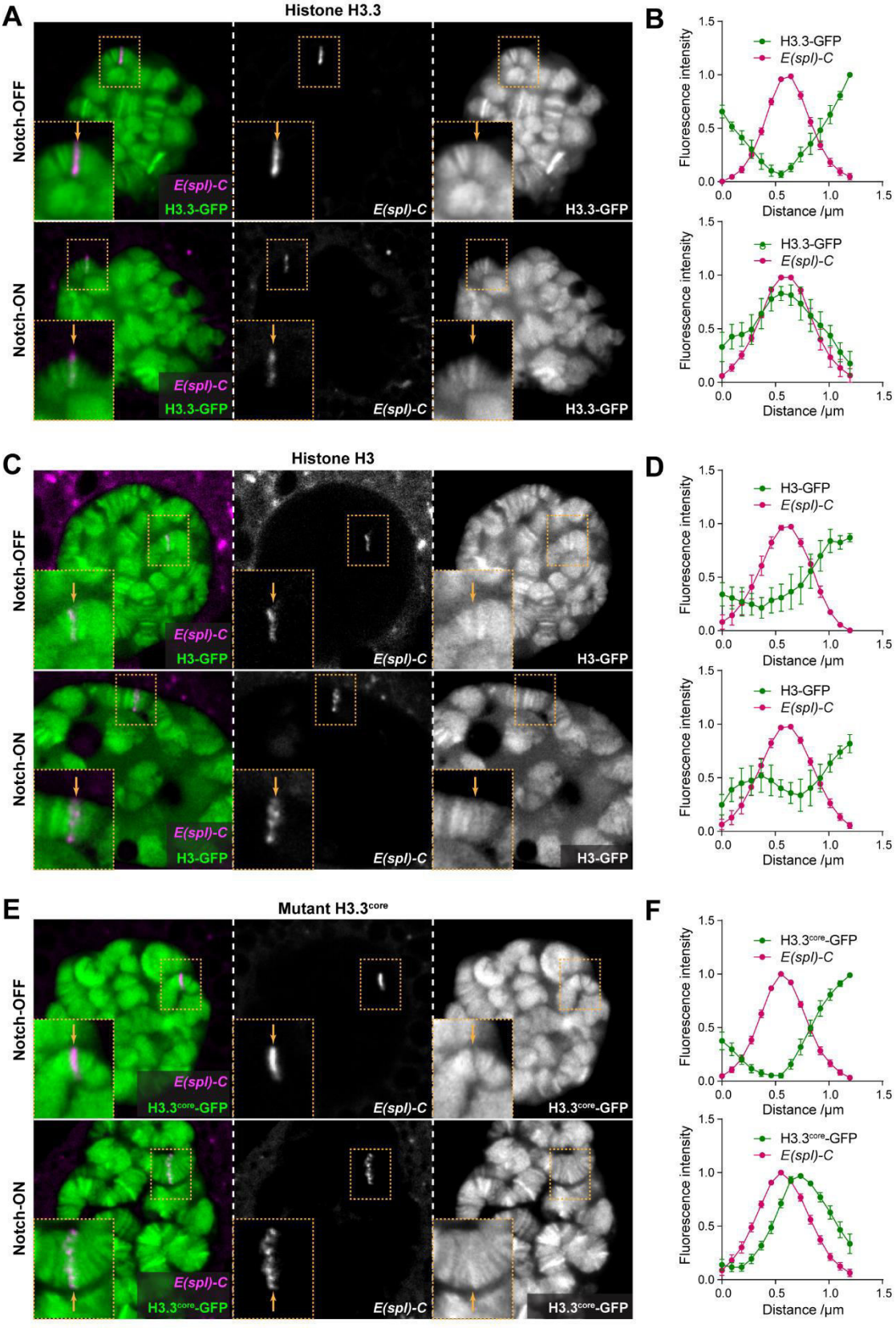

Figure 4.2. Histone H3.3 levels increase at the *E(spl)-C* in Notch-ON nuclei. *Legend on next page.*

4.2.2 The BRM chromatin remodelling complex promotes high chromatin accessibility at Notch-regulated enhancers

The changes in *E(spl)-C* architecture and the incorporation of histone H3.3 in the vicinity of Notch-regulated genes suggest the involvement of chromatin remodelling complexes or histone chaperones. As well as the change in histone H3.3 levels, Notch activation in the salivary gland promotes a robust and detectable recruitment of Su(H)-GFP to the *E(spl)-C* when imaged live (Figure 4.3A; Gomez-Lamarca et al. 2018). This band of fluorescence is not observed in the Notch-OFF condition and thus represents increased recruitment of activating complexes. This was therefore used as a powerful assay to investigate which chromatin regulators might be required. Su(H) recruitment was assessed under conditions where different chromatin remodellers and histone chaperones were depleted by RNAi, to identify whether any of these manipulations would prevent this Notch-dependent effect on Su(H). In most cases, little or no change was detected. For example, depletion of components in the ISWI, NuRD or INO80 chromatin remodelling complexes (Bouazoune and Brehm 2006) failed to perturb Su(H) recruitment (Figure 4.3). Likewise, knockdown of chromatin assembly factors (CAFs) associated with canonical replication-coupled nucleosome assembly (Burgess and Zhang 2013) or

---

Figure 4.2 continued (A, C and E) Live imaging of histone-GFP (green) and ParB-mCherry (magenta) expressed in larval salivary gland nuclei using *1151-Gal4*. H3.3-GFP levels are increased at the *E(spl)-C* in Notch-ON nuclei (A; $N^{\Delta ECD}$ expression) compared to control Notch-OFF nuclei (A; LacZ expression). The same is seen with $H3.3^{core}$-GFP (E), but there is little change in H3-GFP between Notch-OFF and Notch-ON nuclei (C). ParB-mCherry marks the *E(spl)-C* as in Figure 4.1A and B. Yellow dotted box contains the *E(spl)-C* and yellow arrow indicates the position of the *E(spl)-C* on the chromosome. (B, D and F) Quantifications (see Materials and methods for details) of relative fluorescence intensity of histone-GFP and ParB-mCherry across the *E(spl)-C* in Notch-OFF (upper) and Notch-ON (lower) conditions. Mean ± SEM; n ≥ 5.

chaperones associated with histone H3.3 deposition such as DEK (Sawatsubashi et al. 2010) and Yemanuclein (YEM; Orsi et al. 2013) had no effect (Figure 4.3).

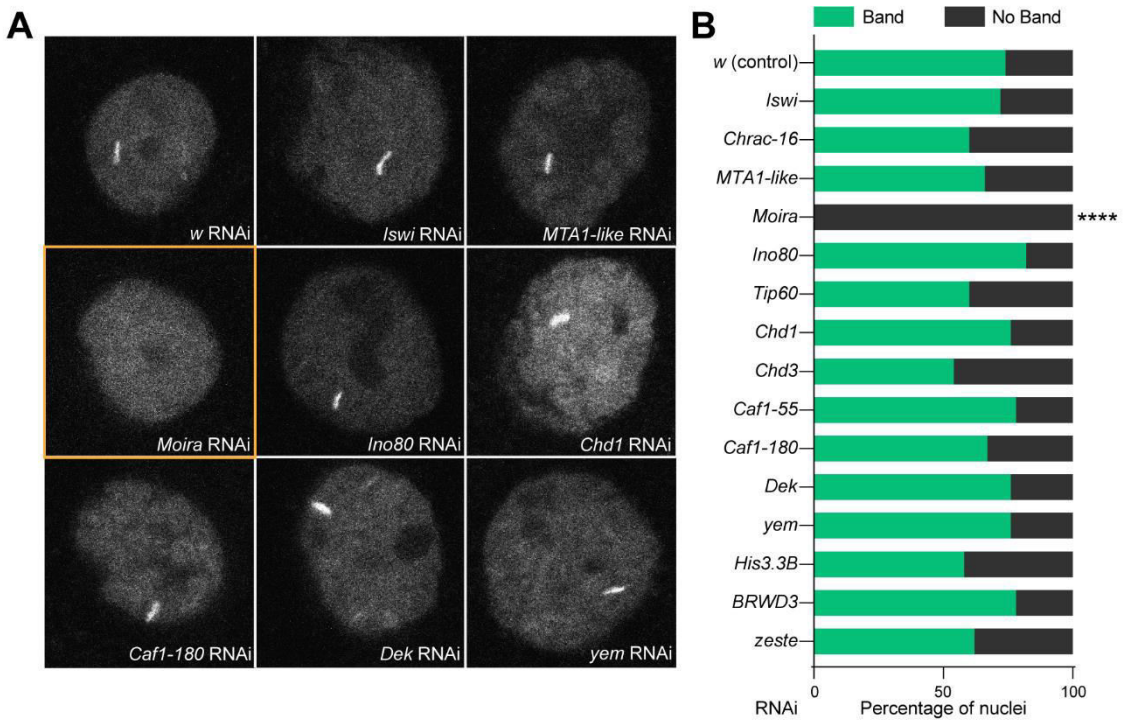

Figure 4.3. Chromatin remodelling factors required for Su(H) recruitment. (A) Effects from depleting chromatin remodellers and histone chaperones, as indicated, by RNAi on recruitment of Su(H)-GFP in Notch-ON nuclei ($N^{\Delta ECD}$ expression). In all conditions shown except *Moira* RNAi, nuclei exhibit a bright accumulation of Su(H)-GFP at a single locus when imaged live. (B) Percentage of Notch-ON nuclei retaining a single clear band of Su(H)-GFP when the indicated RNAi was co-expressed with $N^{\Delta ECD}$. For each genotype, 5 nuclei in each of ten glands were scored (50 nuclei total). **** *Moira* RNAi resulted in a significant number of nuclei losing the fluorescent band when compared to the *w* RNAi control; $p<0.0001$, two-tailed Fisher's exact test.

However, manipulation of the BRM SWI/SNF chromatin remodelling complex had a striking effect. Knockdown of the core components Moira and Snr1 (Mohrmann and Verrijzer 2005) by RNAi reduced Su(H) recruitment, with *Moira* RNAi preventing any visible localisation of Su(H)-GFP in all nuclei (Figure 4.3) and *Snr1* RNAi preventing a single clear band of recruitment in most nuclei (Figure 4.4A and B). Additionally, all visible recruitment of Su(H)-GFP was prevented by the expression of a dominant negative form of the Brm ATPase, BrmK804R (Figure 4.4A and B; Elfring et al. 1998).

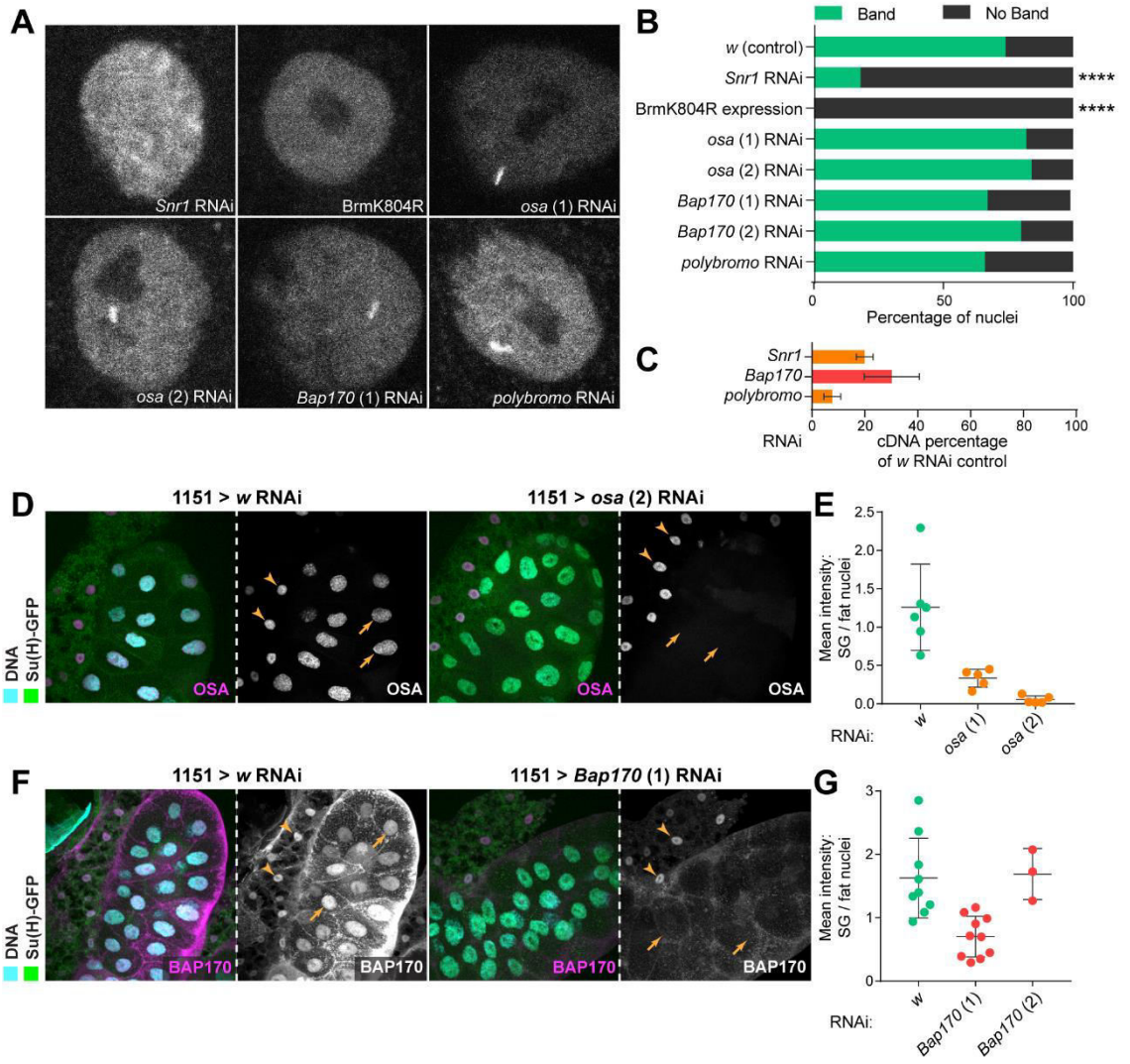

Figure 4.4. Core components of the BRM complex are required for Su(H) recruitment. (A) Effects from perturbing BRM complex components, as indicated, on recruitment of Su(H)-GFP in Notch-ON nuclei ($N^{\Delta ECD}$ expression). All show depletion by RNAi except BrmK804R, which is dominant-negative Brm expression. Only the core components of the BRM complex affected the accumulation of Su(H)-GFP at the *E(spl)-C*. (B) Percentage of Notch-ON nuclei retaining a single clear band of Su(H)-GFP when the indicated manipulation was performed in the presence of $N^{\Delta ECD}$ expression. **** Manipulation of core components resulted in a significant number of nuclei losing the fluorescent band when compared to the *w* RNAi control; $p<0.0001$, two-tailed Fisher's exact test. (C) Effect of *Snr1, Bap170* (1) and *polybromo* RNAi in salivary glands on *Snr1, Bap170* and *polybromo* cDNA levels respectively, measured by reverse transcription-qPCR; percentage cDNA compared to *w* RNAi control. All reduce their respective cDNA levels, with *polybromo* RNAi causing a greater reduction than *Snr1*, despite not having an effect on Su(H) recruitment. Mean ± SEM; $n \geq 2$. *Continued on next page.*

Two types of BRM complexes have been characterised in *Drosophila*, BAP and PBAP. These are distinguished by the presence of OSA in BAP and of BAP170 and Polybromo in PBAP (Mohrmann and Verrijzer 2005). However when these BAP or PBAP-specific components were depleted, no effect on Su(H) recruitment was detected. Depletion of OSA, BAP170 or Polybromo by RNAi did not prevent the band of Su(H)-GFP recruitment, despite clear reductions in their RNA and protein levels (Figure 4.4C-G). The knockdown of Polybromo led to a greater reduction in RNA levels than that of Snr1 (Figure 4.4C), and no OSA protein remained detectable after depletion by one of the RNAi lines (Figure 4.4D and E). This evidence suggests that either the two complexes can compensate for each other or that the specialised subunits are not necessary for the Notch-mediated effects on chromatin.

Since the BRM complex is known as a chromatin remodeller which functions to alter chromatin structure, the molecular approach ATAC (Assay for Transposase Accessible Chromatin; Buenrostro et al. 2015) was used to assess whether there were any local changes in chromatin accessibility at the *E(spl)-C* under several conditions. The results were analysed using qPCR with probes targeted to a number of regions across the *E(spl)-C* (regions illustrated in Figure 4.5A). Firstly, ATAC was performed in Notch-OFF and Notch-ON conditions, where Notch was activated by $N^{\Delta ECD}$ expression controlled by *1151-Gal4* (Figure 4.5B;

Figure 4.4 continued (D and F) Immunofluorescence staining of OSA (D, magenta) and BAP170 (F, magenta) in salivary glands expressing *osa* (2) and *Bap170* (1) RNAi respectively, compared to *w* RNAi control glands. *osa* (2) RNAi depletes all detectable OSA protein and *Bap170* (1) RNAi removes most BAP170 protein. Yellow arrows indicate salivary gland nuclei and yellow arrowheads indicate fat cell nuclei for comparison where RNAi is not expressed. (E and G) Quantifications of OSA (E) and BAP170 (G) nuclear levels from maximum projection images of immunofluorescence staining, with salivary gland nuclei normalised to fat cell nuclei. (1) and (2) denote different *osa* and *Bap170* RNAi stocks used.

data was published in Gomez-Lamarca et al. 2018). The results showed that there is a dramatic increase in accessibility across large portions of the *E(spl)-C* in Notch-ON nuclei. Strong increases were detected at the enhancer regions, even though these are already relatively accessible in the Notch-OFF state compared to surrounding regions. The distal *E(spl)m8-HLH* region of the *E(spl)-C,* as well as other non-Notch-responsive regions did not change in accessibility, in agreement with the fact that these genes are not upregulated by Notch in this tissue.

Secondly, Su(H) was depleted by RNAi to assess its role in chromatin accessibility (Figure 4.5C). The same regions across the *E(spl)-C* that became more accessible with Notch activity were found to increase in accessibility with *Su(H)* RNAi, showing that Su(H) has the effect of suppressing accessibility in the absence of Notch signalling. It is likely that this occurs through the recruitment of co-repressors via Hairless, since a loss of these factors has been shown previously to de-repress target genes (Nagel et al. 2005; Chan et al. 2017). Therefore, the depletion of Su(H) most likely caused a loss of these co-repressors at the *E(spl)-C* and de-repression. The accessibility did not increase with *Su(H)* RNAi to the same extent as in the Notch-ON nuclei, highlighting that the effects of Notch on accessibility cannot solely be explained by a loss of repression.

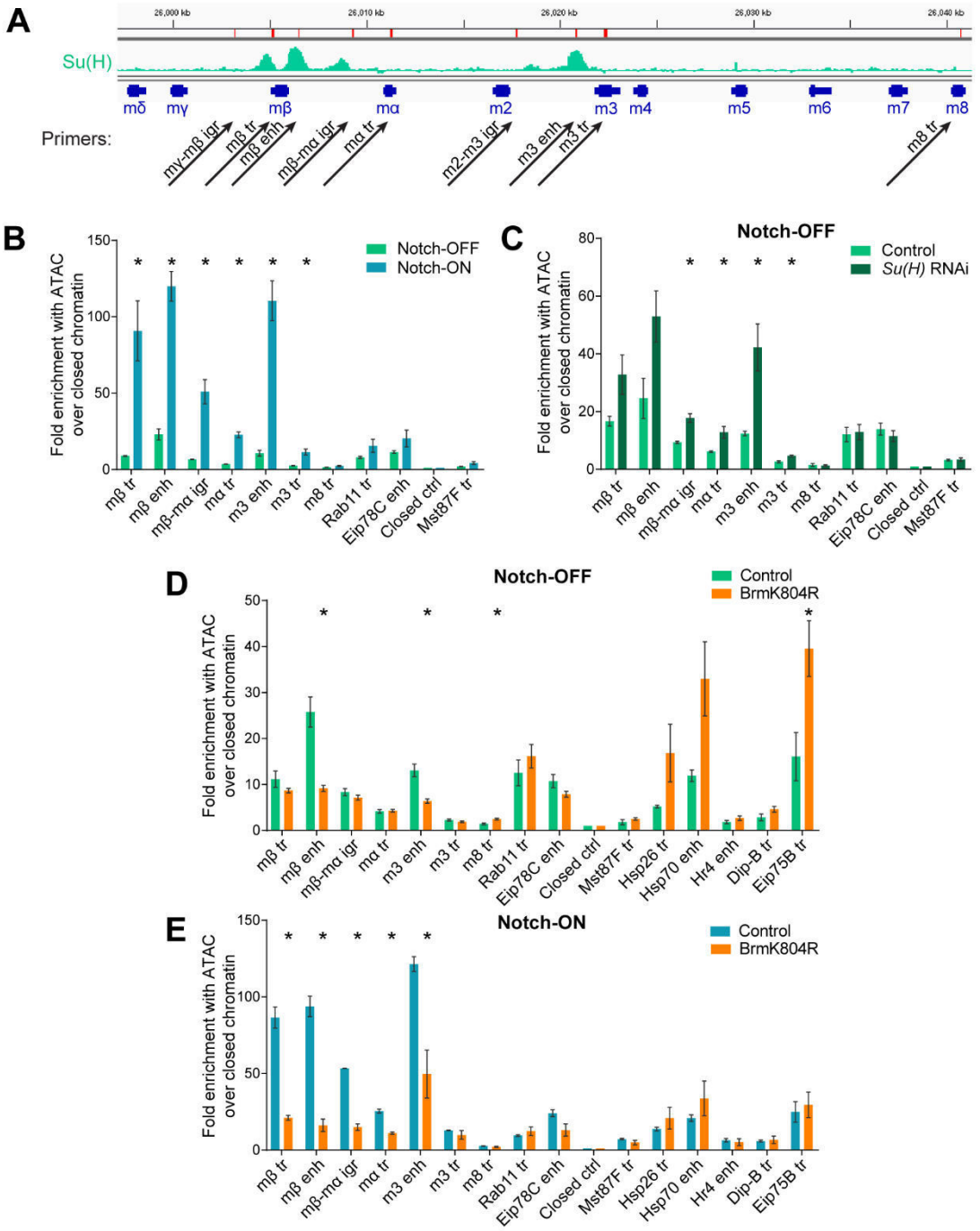

Figure 4.5. Chromatin accessibility of the *E(spl)-C* is regulated by Notch signalling and dependent on the BRM complex. (A) Genomic region encompassing the *E(spl)-C*; green graphs indicate ChIP enrichment for Su(H) in Kc167 cells (Log_2 scale is -0.5 to 2.9; data obtained by Jin Li and published in Skalska et al. 2015); gene models are depicted in dark blue. Positions of primer pairs used in qPCR experiments are indicated with black arrows. Abbreviations are as follows: "igr" = intergenic region, "tr" = transcribed region and "enh" = enhancer. *Continued on next page.*

Finally, chromatin accessibility was measured in the presence of BrmK804R expression to test whether the BRM complex regulates accessibility. Despite the BRM complex being known as a general chromatin remodeller, which could have very widespread effects across the genome, expression of BrmK804R had a surprisingly local effect on accessibility measured with ATAC. The accessibilities of the *E(spl)mβ-HLH* and *E(spl)m3-HLH* enhancer regions were strongly reduced in both Notch-OFF (Figure 4.5D) and Notch-ON (Figure 4.5E) conditions. The effects in the Notch-ON condition were the most dramatic, with BrmK804R mostly abolishing the large increases in accessibility induced by Notch across the *E(spl)-C*, so that the locus resembled that in the Notch-OFF condition. These results demonstrate that the BRM complex is necessary to maintain a degree of accessibility at enhancers, even before the cells experience Notch signalling, and is then essential for the Notch activity-dependent increase in accessibility of the *E(spl)-C*.

Figure 4.5 continued (B-E) Chromatin accessibility in salivary gland nuclei measured by ATAC-qPCR under several conditions; fold enrichment at the indicated regions compared to a "Closed ctrl" region. Notch signalling (B; $N^{\Delta ECD}$ expression) and Su(H) depletion by RNAi (C) both caused increases in accessibility across the *E(spl)-C* without significant changes at control regions. Expression of dominant-negative Brm, BrmK804R, led to reduced accessibility of *E(spl)mβ-HLH* and *E(spl)m3-HLH* enhancer regions in Notch-OFF conditions (D), and to a more widespread reduction in accessibility across the *E(spl)-C* in Notch-ON conditions (E; $N^{\Delta ECD}$ expression). This is in contrast to other inducible enhancers and genes where BrmK804R expression caused either little change or an increase in accessibility. "Rab11 tr" and "Mst87F tr" represent highly and lowly-expressed control genes respectively which do not respond to Notch. "Eip78C enh", "Hr4 enh", "Dip-B tr" and "Eip75B tr" are ecdysone-responsive enhancers and genes (Skalska et al. 2015). "Hsp26 tr" and "Hsp70 enh" are regions near to heat shock-responsive promoters (Boehm et al. 2003). Note the difference in scale between D and E – the changes observed at heat-shock regions are similar in both. Mean ± SEM; n = 3; * $p<0.05$ with two-tailed Welch's t-test compared to controls which express LacZ.

To determine whether the BRM complex plays the same role at other inducible genes, several additional regions were analysed, including heat-shock and ecdysone-responsive enhancers and genes. In contrast to the Notch-responsive regions in the *E(spl)-C*, these other regions showed no decrease in accessibility in the presence of BrmK804R and, in some cases, actually showed an increase in accessibility (Figure 4.5D and E). This was particularly clear at the heat-shock promoters of the *Hsp26* and *Hsp70* genes, which showed an increase in accessibility in both the Notch-OFF and Notch-ON experiments, suggesting that chromatin remodelling by the BRM complex acts to inhibit these genes. These data suggest that SWI/SNF chromatin remodelling has different effects depending on the regulatory mechanisms operating, and demonstrate that there is some specificity in the role that the BRM complex plays at Notch-regulated loci.

4.2.3 The BRM complex is also required at Notch-regulated targets in Kc167 cells

To test whether the BRM complex is similarly required in another context, its role was investigated in Kc167 cells, where Notch signalling can be acutely manipulated by chemical treatments. As characterised in detail in chapter 3, Notch signalling is rapidly activated by the calcium chelator EGTA (Rand et al. 2000). As in the salivary gland, gene activation is accompanied by an increase in Su(H) recruitment, detectable by chromatin immunoprecipitation (ChIP; Skalska et al. 2015). To test the involvement of the BRM complex in this context, the core components Brm and Snr1 were depleted by RNAi (Figure 4.6A) and the effects on Su(H) recruitment were analysed by ChIP with qPCR. Both in Notch-OFF (Figure 4.6B) and Notch-ON (Figure 4.6C) cells, the level of Su(H) recruitment was decreased when Brm and Snr1 were depleted, showing that the BRM complex is essential for Su(H) recruitment. The transcription of the target genes *E(spl)mβ-HLH* and *E(spl)m3-HLH*, which are usually strongly induced following Notch activation, was also decreased by *brm* RNAi (Figure 4.6D).

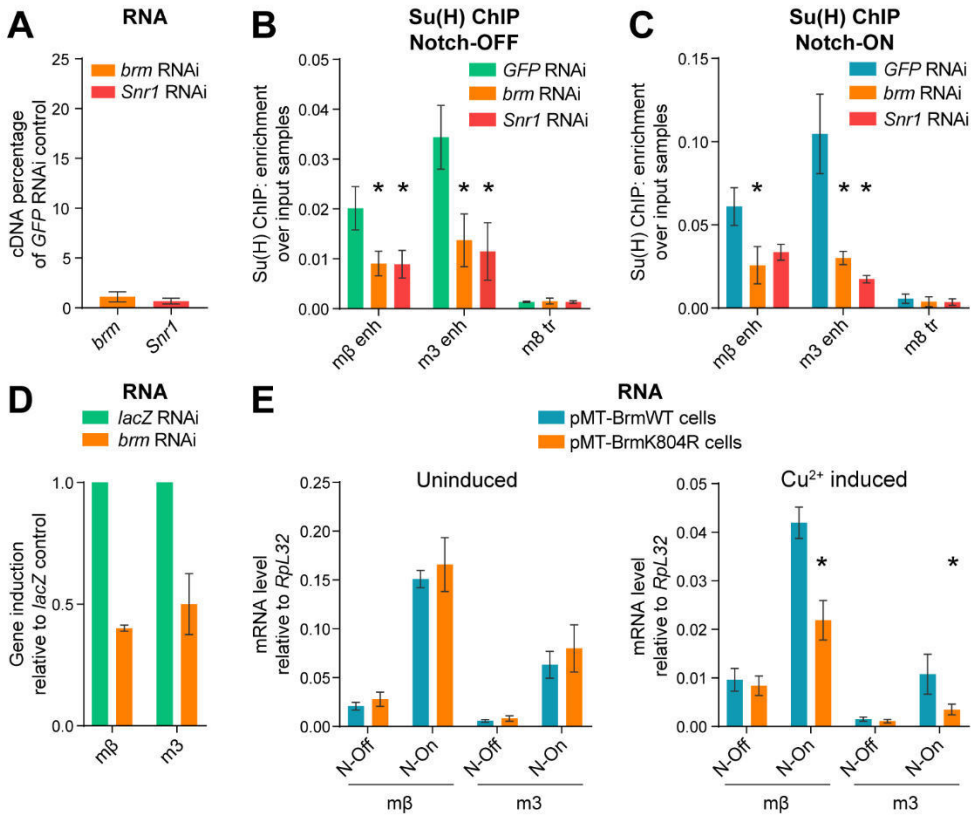

Figure 4.6. The BRM complex is required for Su(H) recruitment and Notch-dependent transcription in Kc167 cells. (A) Effects of *brm* and *Snr1* RNAi on *brm* and *Snr1* cDNA levels respectively, measured by reverse transcription-qPCR in Kc167 cells; percentage cDNA compared to *GFP* RNAi control. The knockdowns were highly effective, with only 1-2% of *brm* and *Snr1* cDNA remaining detectable. (B and C) Knockdown of core components of the BRM complex reduced Su(H) recruitment both in Notch-OFF (B) and Notch-ON (C; EGTA treatment) conditions. Fold enrichment of Su(H) occupancy at the indicated positions detected by ChIP-qPCR, relative to input, in Kc167 cells treated with *brm*, *Snr1* or *GFP* RNAi as a control. These data were obtained during the rotation project and were therefore submitted for the MRes degree. Mean ± SEM; n = 3 (B) and 2 (C); * $p<0.05$ with one-tailed student's t-test compared to GFP RNAi control. (D) Effects of *brm* RNAi on *E(spl)mβ-HLH* ("mβ") and *E(spl)m3-HLH* ("m3") induction by Notch activation (EGTA treatment) measured by reverse transcription-qPCR, shown as fold difference to *lacZ* RNAi control. Mean ± SEM; n = 3. (E) Effects of BrmK804R expression on *E(spl)mβ-HLH* ("mβ") and *E(spl)m3-HLH* ("m3") expression measured by reverse transcription-qPCR. Expression was analysed in stable cell lines containing pMT-inducible BrmWT or BrmK804R in the absence (left, "Uninduced") or presence of copper sulfate (right, "Cu^{2+} induced"). The responses of *E(spl)mβ-HLH* and *E(spl)m3-HLH* to Notch activation ("Non" = EGTA treatment, "Noff" = PBS control) were reduced in the BrmK804R-expressing cells compared to BrmWT-expressing cells, only when induced with copper (right graph). Mean ± SEM; n = 2 (left) and 3 (right); * $p<0.05$ with one-tailed student's t-test comparing BrmWT and BrmK804R.

In order to confirm that the ATPase activity of the BRM complex was essential, stable cell lines were made expressing BrmK804R or the wild type form, BrmWT as a control from the copper-inducible pMT promoter (Yu et al. 2014). Expression of *E(spl)mβ-HLH* and *E(spl)m3-HLH* was rapidly induced by Notch activation in control conditions (Figure 4.6E, Uninduced). However, following copper-induced expression of BrmK804R, cells had a significantly reduced upregulation of *E(spl)mβ-HLH* and *E(spl)m3-HLH* compared to cells expressing BrmWT (Figure 4.6E, Cu^{2+} induced). This shows that the ATPase function of the BRM complex is key to the Notch response in these cells.

4.2.4 Nucleosome turnover increases in response to Notch signalling and is BRM complex-dependent

Chromatin remodellers are thought to slide, replace or eject nucleosomes (Längst and Manelyte 2015). Additionally, the histone variant H3.3 has been associated with nucleosome turnover (Huang and Zhu 2014; Deaton et al. 2016). A short pulse of activity in Kc167 cells induced by EGTA treatment was sufficient to bring about a change in chromatin accessibility measured with ATAC (Figure 4.7A), suggesting that Notch-dependent chromatin changes may be very dynamic and have an ongoing requirement for chromatin remodelling. The effect of Notch activation here was smaller than in the salivary gland, partly due to difficulties of the technique. In an ATAC experiment, the chromatin is tagmented in live nuclei for 30 minutes. Thus, the brief and reversible nature of the EGTA-induced Notch response (demonstrated in chapter 3) was more difficult to detect with this method. Nonetheless, these results indicated that the mechanisms controlling the Notch response may be similar in Kc167 cells.

Given the results showing changes in accessibility and histone H3.3 levels, experiments were performed to measure nucleosome turnover. To do this, the CATCH-IT technique was used, which relies on the incorporation of a methionine analogue called azidohomoalanine into newly-synthesised proteins (Deal et al. 2010; Teves et al. 2012). Click chemistry is used to biotinylated this residue so that any chromatin containing newly-synthesised histones can therefore be isolated (Figure 4.7B and C).

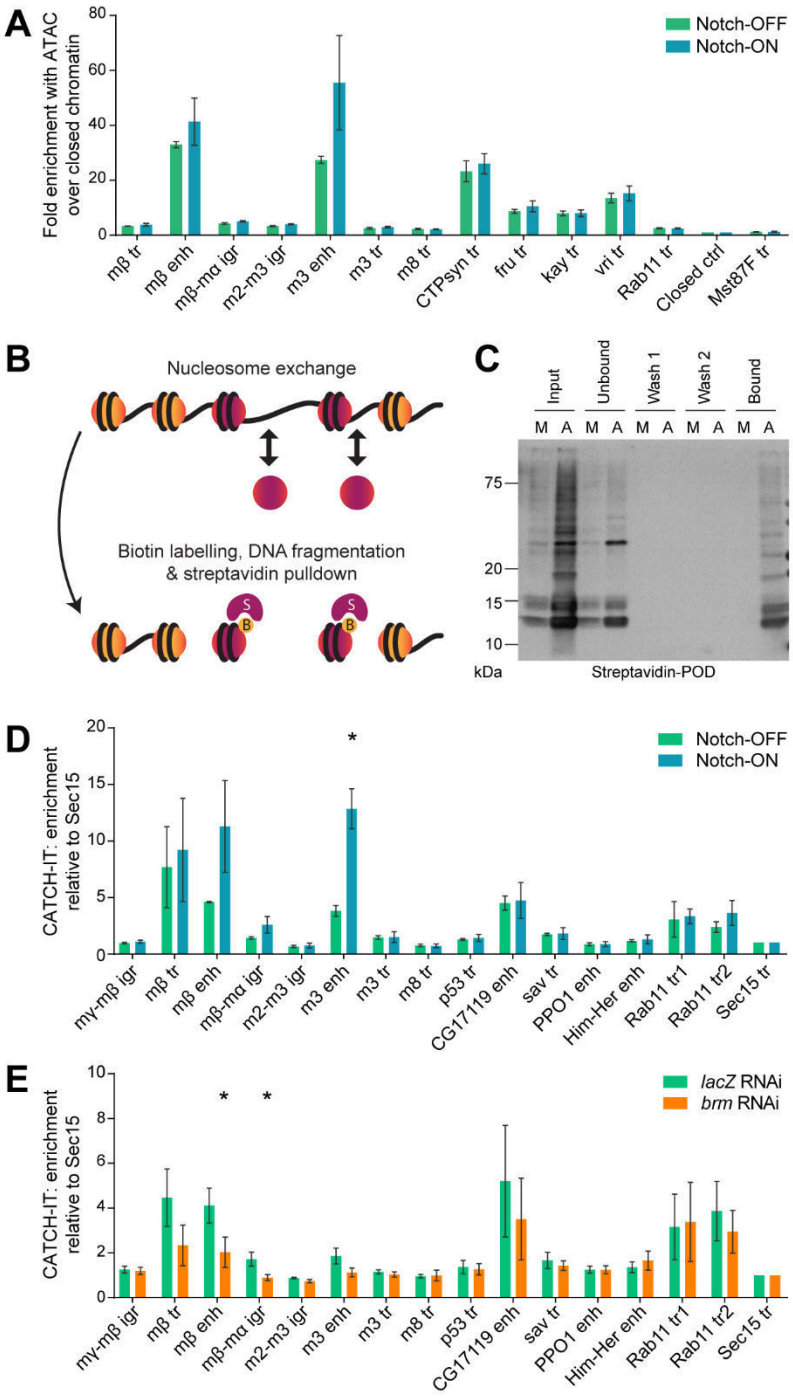

Figure 4.7. Nucleosome turnover at Su(H)-bound enhancers is increased in Notch-ON cells and is dependent on the BRM complex. (A) Chromatin accessibility across the *E(spl)-C* in Notch-ON (30-minute EGTA treatment) and Notch-OFF (PBS control) Kc167 cells detected by ATAC-qPCR. Fold enrichment of the indicated regions compared to a "Closed ctrl" region. "CTPsyn tr", "fru tr", "kay tr" and "vri tr" are highly accessible control regions which do not respond to Notch. Mean ± SEM; n = 3. (B) Schematic illustrating the CATCH-IT technique. DNA incorporating newly-synthesised nucleosomes is labelled and isolated. *Continued on next page.*

CATCH-IT was performed in Kc167 cells by incubating the cells with media containing azidohomoalanine after a period of methionine starvation, in the presence or absence of NICD. To achieve this, NICD was expressed from the copper-inducible pMT promoter (Skalska et al. 2015). Differential levels of histone turnover were detected across the *E(spl)-C*. Notably, the Su(H)-binding enhancer regions had high levels of nucleosome turnover compared to surrounding regions, and this turnover was significantly increased in the presence of NICD (Figure 4.7D). This increase did not occur at control regions, including an unresponsive Su(H)-bound enhancer at *CG17119*, and regions within the *Rab11* gene (UTR and intron), chosen for their high levels of "enhancer"-like chromatin marks and nucleosome turnover in the data published for S2 cells (Deal et al. 2010).

Figure 4.7 continued (C) Samples from different fractions of the CATCH-IT DNA isolation procedure shown on a Western blot probed with streptavidin-peroxidase. "A" denotes samples which have had azidohomoalanine added and "M" denotes methionine controls. "A" samples contain higher levels of biotinylated proteins and while some of these remain unbound from the streptavidin beads, biotinylated proteins are only bound in "A" and not "M" samples. (D) Nucleosome turnover measured by CATCH-IT-qPCR; fold enrichment over input samples compared to "Sec15 tr" control region. Su(H)-bound enhancers show increased nucleosome turnover in response to Notch signalling. Notch signalling is activated in Kc167 cells by 6 hours of copper-induced NICD expression ("Notch-ON") with copper excluded in the control ("Notch-OFF"). Mean ± SEM; n = 2; * $p<0.05$ with two-tailed student's t-test compared to Notch-OFF. (E) *brm* RNAi reduces nucleosome turnover at Notch-responsive regions. CATCH-IT-qPCR results as in D after *brm* or *lacZ* RNAi as a control. Mean ± SEM; n = 5 for all primers, except "p53 tr", "CG17119 enh", "sav tr" and "Rab11 tr1" where n = 3; * $p<0.05$ with one-tailed student's t-test compared to *lacZ* RNAi. Positions of *E(spl)-C* primers in the genome are shown in Figure 4.5A. "p53 tr", "CG17119 enh" and "sav tr" are control regions located near an unresponsive Su(H) binding site. "PPO1 enh" and "Him-Her enh" are Su(H)-binding enhancers which are not occupied by Su(H) in Kc167 cells (Skalska et al. 2015). "Rab11 tr1", "Rab11 tr2" and "Sec15 tr" are additional non-Notch-responsive control regions.

Brm was then depleted by RNAi to test whether knockdown of the BRM complex would affect the levels of nucleosome turnover measured with CATCH-IT. Brm depletion resulted in a localised decrease in histone turnover at the Notch-responsive regions with relatively little change at control regions (Figure 4.7E), strengthening the evidence that the BRM complex has a critical role in Notch signalling and providing a mechanism by which this may occur.

Given that histone H3.3 recruitment was increased in Notch-ON cells *in vivo*, it is possible that the increased turnover can be explained by a replacement of histone H3 with the histone variant H3.3. The levels of histone H3.3 were therefore measured specifically at different genomic regions by expressing V5-tagged histone proteins in Kc167 cells (Figure 4.8A) and performing ChIP (Wirbelauer et al. 2005). When H3-V5 and H3.3-V5 were expressed from a constitutive promoter, differential levels of the two variants were found across the *E(spl)-C* (Figure 4.8D-F). Histone H3.3 predominated over histone H3 at the Notch-responsive regions of the *E(spl)-C*. This included the transcribed regions of the two target genes *E(spl)mβ-HLH* (mβ tr) and *E(spl)m3-HLH* (m3 tr) and nearby enhancer regions (mβ enh, mβ-mα igr and m3 enh). However, the levels of the two variants were similar at the unresponsive *E(spl)m8-HLH* region (m8 tr). Notch signalling, when induced by either EGTA treatment (Figure 4.8D) or NICD expression (Figure 4.8E), did not result in a detectable change in levels of either histone protein at the regions tested, despite clearly inducing target gene expression (Figure 4.8B and C). The effects of Brm depletion were also minor, with *brm* RNAi giving slight reductions in histone H3.3 levels within gene bodies but no change at the enhancers (Figure 4.8F).

Together, these data argue that there is no gross change in the overall levels of histones H3 or H3.3 during an acute Notch response, and that the BRM complex is not essential for H3.3 incorporation at enhancers. Thus, the BRM complex-dependent Notch-responsive accessibility at Su(H)-bound enhancers cannot be explained by a simple model of histone H3.3 replacement.

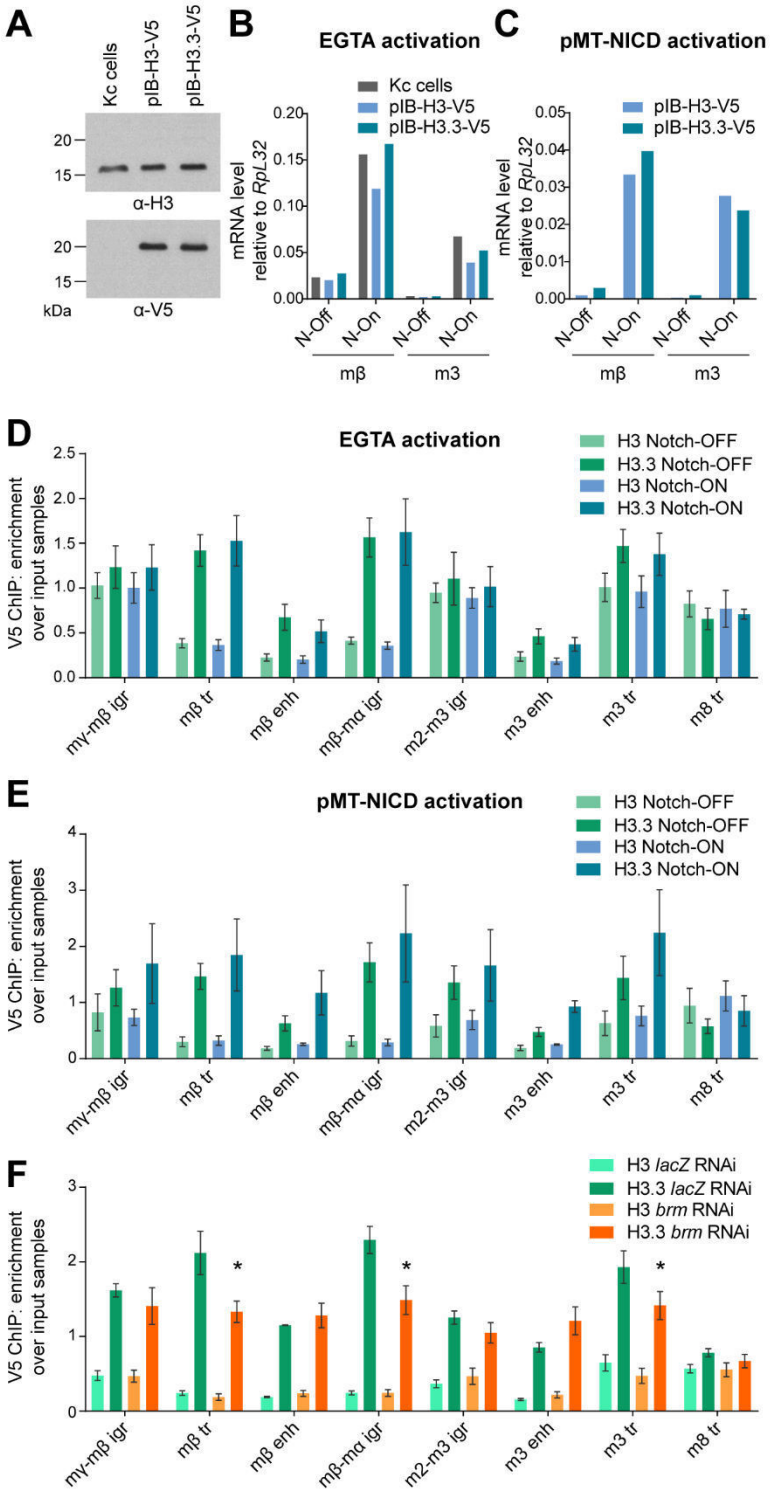

Figure 4.8. Notch activation or BRM complex depletion does not affect the overall distribution of histones H3 and H3.3. (A) H3-V5 ("pIB-H3-V5") and H3.3-V5 ("pIB-H3.3-V5") expression in stable cell lines compared to un-transfected "Kc cells". Western blots probed with H3 and V5 antibodies. V5-tagged histones have a larger molecular weight and are not detectable in the H3 blot due to low levels of expression in comparison to endogenous histone H3. *Continued on next page.*

The experiments above measure the steady-state levels of histones, but do not give insight into their rates of turnover. To investigate the dynamics of the two histone variants in the Kc167 cells, expression of H3-V5 and H3.3-V5 from the pMT promoter was induced for varying lengths of time, allowing their incorporation over shorter timescales to be measured. By approximately 90 minutes to three hours after their induction, the labelled histones had started to be incorporated into the chromatin, as can be seen from the increasing levels of ChIP enrichment and different levels of incorporation of H3.3-V5 between regions (Figure 4.9A-D; compare mβ tr, mβ enh and m3 enh with m8 tr). This pattern of H3.3-V5 incorporation replicated the pattern seen across the *E(spl)-C* with CATCH-IT, while the levels of H3-V5 incorporation were lower and largely uniform. Crucially, the incorporation of H3-V5 and H3.3-V5 was greatly reduced following depletion of Brm, in agreement with the BRM complex having a key role in nucleosome turnover (Figure 4.9F). This abolished the pattern of differential H3.3-V5 incorporation between regions such that the Notch-responsive enhancer regions (mβ enh and m3 enh) had similar levels of H3.3-V5 incorporation to the unresponsive *E(spl)m8-HLH* region (m8 tr).

Figure 4.8 continued (B and C) Effects of Notch activation by EGTA (B) or copper-inducible NICD expression (C) on *E(spl)mβ-HLH* ("mβ") and *E(spl)m3-HLH* ("m3") expression in stable cell lines expressing H3-V5 and H3.3-V5, measured by reverse transcription-qPCR. Both methods of activation strongly induce both genes. "N-On" denotes EGTA or copper treatment and "N-Off" denotes PBS alone or no copper. (D-F) V5 ChIP-qPCR in Kc167 cells expressing H3-V5 or H3.3-V5 from a ubiquitous promoter, with Notch signalling activated by EGTA (D) or copper-inducible NICD expression (E), or with Brm depleted by RNAi (F); fold enrichment over input samples. Notch activation caused no detectable change in levels compared to controls treated with PBS (D) or no copper (E). The changes caused by Brm depletion compared to *lacZ* RNAi control were minimal and did not take place at enhancers (F) Mean ± SEM; n = 3 (D and F) and 2 (E). * $p<0.05$ with two-tailed student's t-test compared to control.

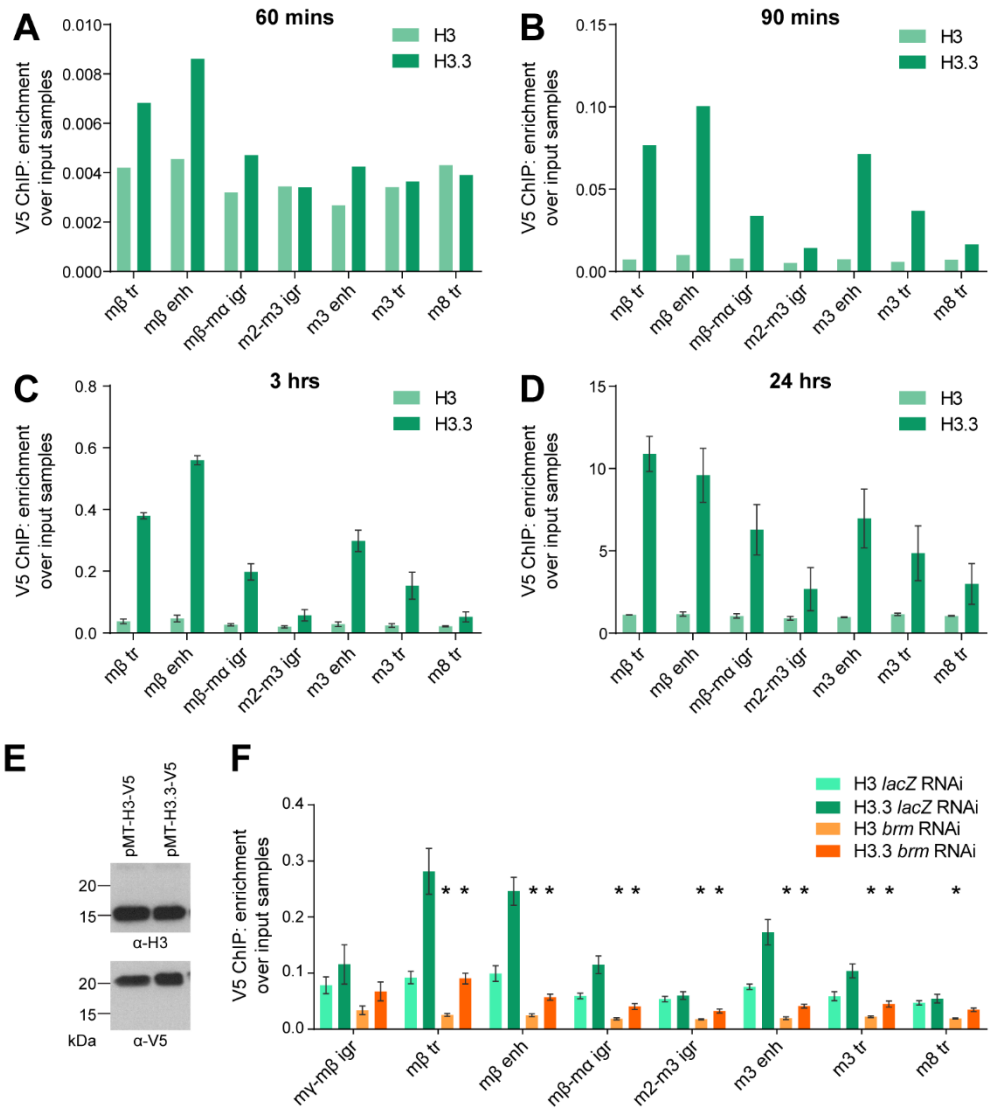

Figure 4.9. Histone H3.3 is incorporated rapidly at Notch-responsive enhancers in a BRM complex-dependent manner. (A-D) V5 ChIP-qPCR in stable cell lines with H3-V5 and H3.3-V5 expression induced by copper from the pMT promoter for 60 minutes (A), 90 minutes (B), 3 hours (C) and 24 hours (D), shown as fold enrichment over input samples. Differential incorporation of H3.3-V5 across the *E(spl)-C* is clear after 90 minutes. Experiment performed only once at 60 and 90 minute time points (A and B). Mean ± SEM; n = 2 (C and D). (E) H3-V5 and H3.3-V5 expression induced for 24 hours in stable cell lines, demonstrated by Western blots probed with H3 and V5 antibodies. (F) *brm* RNAi reduces dynamic incorporation of histones H3 and H3.3. V5 ChIP-qPCR after *lacZ* or *brm* RNAi treatment in cells with H3-V5 or H3.3-V5 expression induced for 3 hours, shown as fold enrichment over input samples. Mean ± SEM; n = 3. * $p<0.05$ with two-tailed Welch's t-test compared to *lacZ* RNAi control.

4.3 Discussion

Changes in gene expression are likely to rely on dynamic rearrangements of chromatin. The goal of the experiments here was to investigate how such chromatin dynamics contribute to the Notch response. Using live imaging and molecular techniques, it has been possible to show that Notch activity brings about largescale changes at the responding *E(spl)-C*, including a broad increase in histone variant H3.3 levels, a large increase in accessibility and enhanced nucleosome turnover. Screening a set of chromatin modifiers identified the BRM SWI/SNF chromatin remodelling complex as a crucial component for the Notch response. It regulates the accessibility of Notch-responsive genomic regions, Su(H) occupancy and the transcriptional output of Notch-responsive genes. Furthermore, the BRM complex was required for nucleosome turnover broadly across the genome.

It has been known for some time that Su(H) occupancy increases in response to Notch signalling (Krejci and Bray 2007; Castel et al. 2013; Wang et al. 2014a), challenging the dated view that Su(H) is stably bound to the DNA while the co-repressors are displaced by NICD and the co-activators (Borggrefe and Oswald 2009). However, the mechanisms leading to this increased dynamic recruitment of Su(H) were unknown. Previous studies have correlated Su(H) binding sites with histone PTMs (Skalska et al. 2015), but it is not clear that an increase in a particular histone PTM (such as H3K27 or H3K56 acetylation) could be causative for an increase in Su(H) binding. The ATAC data presented in this chapter provide a clear rationale for the Su(H) recruitment observed in the salivary gland and it is therefore highly likely that Notch-responsive Su(H) occupancy is controlled by chromatin accessibility. To distinguish between cause and effect, *Su(H)* RNAi was performed, which highlighted that the role of Su(H) in the Notch-OFF state is to inhibit accessibility rather than promote it. This is likely to occur via the co-repressor Hairless with its partners, since removal of these factors is also known to lead to de-repression (Nagel et al. 2005; Chan et al. 2017). The repressive state may depend on the maintenance of certain histone PTMs, as has been argued in mammalian cells (Oswald et al. 2016), or on the recruitment of other classes of chromatin remodeller to counteract the BRM complex and inhibit chromatin accessibility.

A number of studies have previously made links between SWI/SNF chromatin remodelling and Notch signalling (Kadam and Emerson 2003; Armstrong et al. 2005; Das et al. 2007; Takeuchi et al. 2007). In particular, BRM has been found to bind to Notch-responsive enhancers (Kadam and Emerson 2003), and Baf60c has been shown to physically interact with RBPJ in mammalian cells (Takeuchi et al. 2007). However, the mechanistic role of SWI/SNF remodelling in the Notch response has not been established. Additionally, SWI/SNF remodelling has been shown to both positively (Takeuchi et al. 2007) and negatively (Das et al. 2007) regulate Notch target gene expression in different systems. The data presented in this chapter provide a possible answer for this discrepancy. It was demonstrated that both in Notch-ON and the Notch-OFF states, the BRM complex promotes chromatin accessibility and Su(H) recruitment. Therefore, since Su(H) acts to repress target genes in the Notch-OFF state, it is possible that some Notch target genes are de-repressed by removal of BRM complex activity.

While the number of studies which have reported links between SWI/SNF chromatin remodelling and Notch is relatively small, there is robust literature documenting connections between SWI/SNF complexes and cancer (for review see Nair and Kumar 2012; Hodges et al. 2016), with around 20% of human malignancies having mutations in SWI/SNF subunits (Kadoch et al. 2013). Since Notch signalling also has a complex role in cancer, in some cases acting as an oncogene and in others as a tumour suppressor (Yuan et al. 2015; Aster et al. 2017), it is possible that some cancer phenotypes could be explained by the interaction of the two. For example, SWI/SNF remodelling has been found to be required for triple negative breast cancer (Wu et al. 2015), a disease in which Notch signalling has an established role (Speiser et al. 2013; Locatelli and Curigliano 2017). Both SWI/SNF remodelling and Notch signalling have gained interest as therapeutic opportunities for cancer (Yuan et al. 2015; St Pierre and Kadoch 2017), so perhaps a combinatorial approach could hold the key to an effective treatment.

SWI/SNF complexes fall into two subclasses, BAF and PBAF-like complexes, which are conserved throughout eukaryotic evolution and called BAP and PBAP in *Drosophila* (Mohrmann and Verrijzer 2005). BAP and PBAP are thought to

act on different sites in the genome, with OSA (BAP-specific) and Polybromo (PBAP-specific) subunits displaying distinct but overlapping patterns on polytene chromosomes (Mohrmann et al. 2004). The two complexes have also been found to have specialised functions in development (Terriente-Félix and de Celis 2009; He et al. 2014). However in this study, BAP and PBAP-specific subunits did not appear to be necessary for the function of the BRM complex in Notch signalling. This could be explained if there is some redundancy between the complexes and either complex is able to function in Notch signalling, which could be tested by the dual knockdown of BAP and PBAP-specific subunits. However, a previous study found that the removal of OSA, BAP170 and Polybromo together did not phenocopy *brm* null mutants in oogenesis (Carrera et al. 2008b). Thus, an alternative explanation may be that the core components of the BRM complex have some BAP and PBAP-independent roles. The intricacy of BRM complex function is exemplified by its known ATPase-independent functions (Kwok et al. 2015; Jordán-Pla et al. 2018).

The mechanism by which SWI/SNF complexes remodel the chromatin *in vivo* is not well established. It has been shown that removal of SWI/SNF function leads to changes in nucleosome positioning, disfavouring precise nucleosome placement (Moshkin et al. 2012; Shi et al. 2014), but whether this occurs through a sliding or eviction-based means is not clear. The data presented in this chapter suggest that the BRM complex is required for nucleosome turnover at Notch-responsive enhancers. Nucleosome turnover could be promoted in several ways: either by the active eviction of nucleosomes from the chromatin, the sliding of nucleosomes to less favourable positions where they become dissociated from the DNA, or the displacement of nucleosomes by the movement or incorporation of others. Regardless of the precise mechanism, these data illustrate the dynamic nature of nucleosomes and highlight that static views of nucleosome occupancy cannot give the whole picture.

The difference between the static and dynamic view is demonstrated by the histone ChIP experiments in Kc167 cells. While Notch signalling and *brm* RNAi did not appear to dramatically change the levels of histones H3-V5 and H3.3-V5 when they were expressed constitutively, the dynamics of histone incorporation became apparent when the tagged histones were expressed transiently. The

incorporation of histone H3.3-V5 mirrored the results found with CATCH-IT, with higher levels of incorporation at Notch-responsive enhancer regions. Both H3-V5 and H3.3-V5 levels were reduced by *brm* RNAi. The effect of *brm* RNAi was more dramatic for H3.3-V5 and led to similar levels of incorporation at all regions tested. Further experiments would be required to establish whether an even longer period of histone expression would give results more similar to expression from the constitutive promoter and whether the removal of copper induction would result in histone levels being depleted differentially.

The result shown in Figure 4.2 that histone H3.3 levels are increased by Notch activity in the vicinity of the *E(spl)-C* in the salivary gland was intriguing, as it suggested that histone H3.3 could be part of the mechanism controlling the Notch response. However, histone H3.3 is known to be deposited at actively-transcribed gene bodies, enhancers and telomeres by different mechanisms (Campos and Reinberg 2010), so it was not clear at this macroscopic level which regions within the *E(spl)-C* were incorporating an increased level of histone H3.3. The data from Kc167 cells suggest that histone H3.3 may be involved in BRM complex-dependent nucleosome turnover. However, the dynamic incorporation of histone H3 was also affected by *brm* RNAi, showing that the mechanism is unlikely to involve histone H3.3 exclusively. Furthermore, the only essential function for histone H3.3 is in male fertility in *Drosophila* and upregulation of histone H3 has been shown to compensate for a lack of histone H3.3 (Sakai et al. 2009). Therefore, it is likely that the increase in histone H3.3 recruitment and turnover can be compensated by similar changes in histone H3 when it is not present.

4.3.1 Model

In light of the data presented in this chapter, the following model is proposed and illustrated in Figure 4.10. Su(H) competes with nucleosomes for binding to the DNA at enhancers and is unable to bind to closed chromatin. The BRM complex actively promotes nucleosome turnover at enhancer regions to encourage Su(H) binding and maintain accessibility of these regions. In the absence of Notch signalling, Su(H) recruits repressive factors which ultimately limit the accessibility of the DNA and counteract the BRM complex. This

balance between the BRM complex and repressive factors maintains genes in a highly-responsive state, able to change their chromatin and transcription status incredibly rapidly. Upon Notch signalling, the nucleosome turnover at enhancer regions increases, allowing more Su(H) recruitment to occur. This may be required to recruit sufficient levels of transcriptional machinery for rapid transcriptional activation.

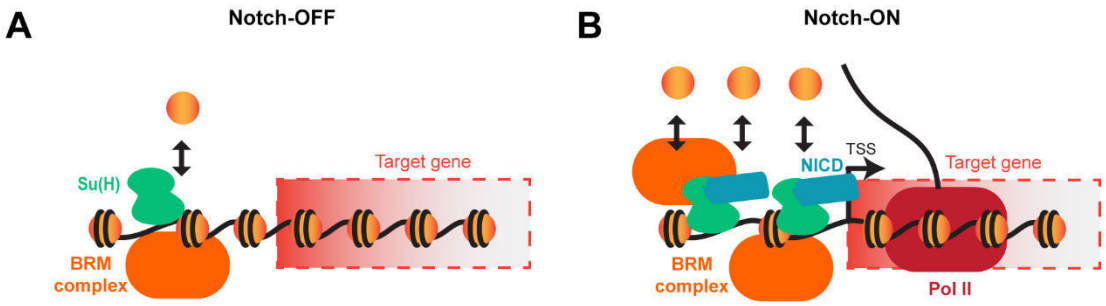

Figure 4.10. Model of BRM complex action in the Notch response. (A) In the absence of Notch signalling, the BRM complex maintains the accessibility of Notch-responsive enhancers to allow Su(H) recruitment by promoting nucleosome turnover. (B) When Notch signalling is activated, the nucleosome turnover at Notch-responsive enhancers increases, increasing the accessibility of the chromatin and allowing more Su(H) to bind. The BRM complex is essential for the process to occur. Target genes are activated via co-activators.

Since the BRM complex appears to play a key role in nucleosome turnover, it is plausible that the BRM complex itself is responsible for the Notch-dependent increase in nucleosome turnover. However, another possibility is that the BRM complex is required only to set up the Notch-OFF accessibility of enhancers and that another factor drives the opening of the chromatin in response to Notch signalling. To test this, a system is required in which Notch signalling can be activated and the BRM complex subsequently sequestered or rendered inactive. If the BRM complex is required continuously to maintain the high accessibility of enhancers in the Notch-ON state, removal of BRM complex activity would switch off the Notch response. One option to achieve this would be to control the localisation of the dominant negative BrmK804R protein with an optogenetically-controlled nuclear import signal (Wehler et al. 2016), assuming the protein could be modified to remain cytoplasmic in the dark.

The studies performed in this chapter have addressed the mechanisms by which Notch signalling activates the *E(spl)-C* genes. However, it will be important to understand to what extent the BRM complex is necessary at other Notch targets and in other contexts. While many Notch targets increase Su(H) binding in the Notch-ON state, other Su(H)-bound sites do not respond in this way (Castel et al. 2013). It will be very interesting to see whether BRM complex involvement could be a determining factor for the type of response. Genome-wide ChIP-seq for Su(H) in the presence of BrmK804R would identify how widespread the necessity of the BRM complex is. This has the potential to improve our understanding of how Notch targets are specified in a context-dependent manner.

5 CONCLUSIONS AND OUTLOOK

In this thesis, progress has been made in understanding two key features of the Notch signalling response. Firstly, insight has been gained into the temporal dynamics of the transcriptional response using a live imaging approach. This has also raised a number of questions, especially in the context of ligand-induced activation, where small areas of contact are sufficient for signalling but there is a temporal delay in transcription. Secondly, our understanding of the role of chromatin remodelling in the Notch response has been advanced, with mechanistic details regarding chromatin accessibility and nucleosome turnover at enhancers coming to light. It remains to be seen how widely these mechanisms apply.

5.1 Most significant findings

The use of the MS2 system to analyse the Notch signalling response of the target gene *E(spl)mβ-HLH* led to unprecedented temporal information about its transcription. Active transcription was observed in real time, and thus it was found that most cells with detectable responses switch on transcription within 15 minutes of chemical-induced Notch cleavage, and later switch it off again. Interestingly, there was a large heterogeneity in the level of transcription detected between cells. And while the start of transcription was fairly reproducible between cells, there was more heterogeneity in the times that cells

switched off transcription, with cells that transcribed *E(spl)mβ-HLH* at higher peak levels having detectable transcription for longer periods.

Studies of the chromatin structure gave significant insight into the mechanistic role of the BRM SWI/SNF chromatin remodelling complex in Notch signalling. It was discovered that the BRM complex controls chromatin accessibility and thereby CSL recruitment at Notch-responsive enhancers. BRM complex remodelling was found to be required for nucleosome turnover broadly, and Notch signalling promoted local increases in nucleosome turnover at Notch-responsive enhancers, suggesting that the Notch response involves an increase in SWI/SNF-dependent nucleosome turnover. These findings are relevant for understanding the mechanisms used by SWI/SNF chromatin remodellers to change chromatin structure, as well as for understanding the CSL switch from repression to activation during Notch signalling.

5.2 Main unanswered questions

The MS2 system provided a useful tool for characterising the transcriptional response to Notch, but it remains unclear what caused the heterogeneous levels of transcription between single cells within the same population. It is possible that the experimental design may have contributed to the different levels detected, for example if the cooperative binding of MCP-GFP to the *MS2 stem-loops* caused small differences in transcriptional output to be amplified. And different levels of Notch expression or activation may cause different levels of transcription to occur between cells. Furthermore, it is not known how the temporal dynamics of the response may change with different levels of Notch signalling. This could be tested by expressing different levels of NICD in these cells to identify how the level of NICD impacts the response. For example, if the levels of signalling are lower, transcriptional bursts may become distinguishable, or the level of transcription may be reduced in all cells, with fewer cells having detectable levels of transcription. Mathematical modelling could help to distinguish whether the level of NICD affects the rate of transcription initiation, pause release or elongation.

Another question is how the upstream activation of Notch affects the transcriptional response. It was shown that ligand-induced Notch activation resulted in a delayed response, which could be attributed to the time taken for establishing cell contact, cleavage of the receptor or the dynamics of NICD trafficking to the nucleus. Further similar studies could provide more insight into how the contact area between cells or the number of neighbours influences the transcriptional response. It is currently unknown whether the ligands Delta and Serrate could promote different transcription dynamics, which could be tested in this system. It would also be possible to tag different genes with the MS2 system to find out how the dynamics of different Notch targets differ, since previous data has shown that target genes can be categorised into different classes based on their response profiles to a pulse of signalling (Housden et al. 2013). Combining these studies could make new links between the mode of upstream activation and different transcriptional behaviours.

Notch signalling activates different genes in different cell types and tissues, and so a major question in the field is how this is controlled. Rather than target genes simply being on or off, it is possible that the transcriptional dynamics vary between cell types. The *E(spl)mβ-HLH* gene was CRISPR-edited *in vivo* during this PhD and can therefore be analysed with the MS2 system in different live *Drosophila* tissues. Furthermore, combining the MS2 system with studies of CSL dynamics *in vivo* (Gomez-Lamarca et al. 2018) could help to identify how local transcription factor binding events affect transcription dynamics. Additionally, observing Notch target transcription in an endogenous system where signalling directs cell fate, such as the process of neurogenesis in the embryo, where lateral inhibition between cells leads to neuroblast selection (Wech et al. 1999), could give new insight into the regulation of cell fate choices by Notch signalling. It is likely that the precise dynamics of transcription are important for this kind of dynamic developmental process.

It will also be important to find out whether SWI/SNF chromatin remodelling is required for Notch signalling in different contexts, which could be tested using dominant-negative forms of the ATPase subunit (de la Serna et al. 2001; Zraly et al. 2006; Marathe et al. 2013). It is plausible that SWI/SNF chromatin remodelling determines which genes respond to Notch in different cell types by

promoting enhancer accessibility to CSL, and genome-wide studies of CSL binding profiles in the presence or absence of SWI/SNF function could address this. While SWI/SNF remodelling has been linked to transcription factor binding in other signalling pathways (Lee et al. 2002; Nagaich et al. 2004), it is unknown whether this involves the same nucleosome turnover-mediated mechanism or not. Correlating genome-wide nucleosome turnover levels with different transcription factor binding profiles could identify for which classes of transcription factor nucleosome turnover is important.

Considering that SWI/SNF complexes are likely to play a key role in determining target gene selection, there is a major question over how they are recruited specifically to the DNA. The presence of a bromodomain, which binds to acetylated histones, suggests that histone PTMs may be crucial for SWI/SNF targeting, and inhibition of the bromodomain has cellular consequences (Fedorov et al. 2015). In *Drosophila*, the protein Zeste has been shown to recruit the SWI/SNF complex (Kal et al. 2000; Déjardin and Cavalli 2004). However, Zeste depletion did not affect CSL binding in the salivary gland, so further studies are needed to fully understand the recruitment of SWI/SNF complexes to Notch-responsive enhancers. The increase in local nucleosome turnover in response to Notch signalling suggests that Notch activation may lead to increased SWI/SNF complex recruitment. Since there have been previous reports of SWI/SNF complex components interacting with CSL or NICD (Takeuchi et al. 2007; Yatim et al. 2012), it is likely that the active CSL complex can recruit SWI/SNF either directly or indirectly. ChIP studies may be able to confirm this.

While the majority of this thesis has focused on the Notch-induced transcriptional activation mechanism, the MS2 experiments highlight the fact that the switching off of Notch targets is important too, since Notch targets do not remain active indefinitely. It is believed that Notch-dependent transcription is terminated by post-translational modification and degradation of NICD (Fortini 2009; Guruharsha et al. 2012). However, questions remain about how quickly this occurs and MS2 provides a useful system in which to study this. For example, mutations of specific residues or domains in NICD could perturb this process and the resulting transcriptional response could be analysed.

Questions also remain about the chromatin changes that occur after a Notch response. The ATAC data showing that CSL depletion increases chromatin accessibility confirmed that CSL acts with co-repressors to reduce activity in the Notch-OFF state. It remains to be seen exactly how SWI/SNF chromatin remodelling influences the balance between activation and repression during a Notch response. By promoting nucleosome turnover, it may facilitate the rapid switching of chromatin states (for example via changes in histone density or PTMs), allowing Notch targets to be quickly inactivated upon the termination of signalling. Since different classes of chromatin remodelling complex may have different effects on the chromatin, the balance between activation and repression may also involve the balance of different chromatin remodellers.

5.3 Future outlook

The use of modern tools and techniques during this PhD has allowed the Notch response to be studied from a dynamic perspective, resulting in novel findings. The continued development and utilisation of innovative methods are expected to drive further Notch signalling and developmental biology research in the near future. Two techniques of note are CRISPR gene editing and optogenetics, discussed here.

CRISPR gene editing along with new imaging techniques are opening up new avenues for developmental biology research. The MS2 system has now been used in multiple studies to analyse developmental gene expression in the *Drosophila* embryo (Garcia et al. 2013; Lucas et al. 2013; Bothma et al. 2014, 2015; Fukaya et al. 2016). So far, these studies have all made use of reporter constructs. However, the proof-of-concept demonstrated in this thesis that the MS2 system can be used to analyse endogenous transcription levels by CRISPR-editing paves the way for more genes to be analysed with this approach. The combination of high-throughput screening based on CRISPR with the MS2 system, as has already been established with RNA-seq (Adamson et al. 2016; Dixit et al. 2016; Jaitin et al. 2016), could even lead to advances in biomedical research in the future.

So far, experiments studying the Notch response *in vivo* have relied on chronic Notch activation, where the transcriptional response is ongoing. However, the ability to perturb Notch signalling with temporal control paired with the MS2 system would allow questions to be answered about how quickly the transcriptional response to Notch occurs. Optogenetics, referring to the class of techniques where cell biology is controlled by light, provides an opportunity to achieve this. Recent advances in optogenetic techniques have revealed mechanistic insight into developmental processes (Johnson and Toettcher 2018). For example, the temporal dynamics of Bicoid-dependent transcription in the *Drosophila* embryo have been uncovered using a light-responsive fusion protein (Huang et al. 2017). An optogenetic tool to control Notch signalling would thus be of great benefit to the field, particularly if combined with high-resolution or single molecule tracking in a tissue such as the salivary gland (Gomez-Lamarca et al. 2018). This could allow the different steps of Notch activation and subsequent inactivation to be dissected temporally.

6 References

Adamson B, Norman TM, Jost M, Cho MY, Nuñez JK, Chen Y, Villalta JE, Gilbert LA, Horlbeck MA, Hein MY, et al. 2016. A Multiplexed Single-Cell CRISPR Screening Platform Enables Systematic Dissection of the Unfolded Protein Response. *Cell* **167**: 1867–1882.e21.

Ahmad K, Henikoff S. 2002. The Histone Variant H3.3 Marks Active Chromatin by Replication-Independent Nucleosome Assembly. *Mol Cell* **9**: 1191–1200.

Almer A, Rudolph H, Hinnen A, Hörz W. 1986. Removal of positioned nucleosomes from the yeast PHO5 promoter upon PHO5 induction releases additional upstream activating DNA elements. *EMBO J* **5**: 2689–96.

Armstrong JA, Sperling AS, Deuring R, Manning L, Moseley SL, Papoulas O, Piatek CI, Doe CQ, Tamkun JW. 2005. Genetic Screens for Enhancers of brahma Reveal Functional Interactions Between the BRM Chromatin-Remodeling Complex and the Delta-Notch Signal Transduction Pathway in Drosophila. *Genetics* **170**: 1761–1774.

Aster JC, Pear WS, Blacklow SC. 2017. The Varied Roles of Notch in Cancer. *Annu Rev Pathol Mech Dis* **12**: 245–275.

Atherton TJ, Kerbyson DJ. 1999. Size invariant circle detection. *Image Vis Comput* **17**: 795–803.

Bailey AM, Posakony JW. 1995. Suppressor of hairless directly activates transcription of enhancer of split complex genes in response to Notch receptor activity. *Genes Dev* **9**: 2609–22.

Bakshi R, Hassan MQ, Pratap J, Lian JB, Montecino MA, van Wijnen AJ, Stein JL, Imbalzano AN, Stein GS. 2010. The human SWI/SNF complex associates with RUNX1 to control transcription of hematopoietic target genes. *J Cell Physiol* **225**: 569–76.

Ballaré C, Castellano G, Gaveglia L, Althammer S, González-Vallinas J, Eyras E, Le Dily F, Zaurin R, Soronellas D, Vicent GP, et al. 2013a. Nucleosome-driven transcription factor binding and gene regulation. *Mol Cell* **49**: 67–79.

Ballaré C, Zaurin R, Vicent GP, Beato M. 2013b. More help than hindrance: nucleosomes aid transcriptional regulation. *Nucleus* **4**: 189–94.

Banaszynski LA, Wen D, Dewell S, Whitcomb SJ, Lin M, Diaz N, Elsässer SJ, Chapgier A, Goldberg AD, Canaani E, et al. 2013. Hira-dependent histone H3.3 deposition facilitates PRC2 recruitment at developmental loci in ES cells. *Cell* **155**: 107–20.

Barolo S, Stone T, Bang AG, Posakony JW. 2002. Default repression and Notch signaling: Hairless acts as an adaptor to recruit the corepressors Groucho and dCtBP to Suppressor of Hairless. *Genes Dev* **16**: 1964–1976.

Barozzi I, Simonatto M, Bonifacio S, Yang L, Rohs R, Ghisletti S, Natoli G. 2014. Coregulation of Transcription Factor Binding and Nucleosome Occupancy through DNA Features of Mammalian Enhancers. *Mol Cell* **54**: 844–857.

Bartman CR, Hsu SC, Hsiung CC-S, Raj A, Blobel GA. 2016. Enhancer Regulation of Transcriptional Bursting Parameters Revealed by Forced Chromatin Looping. *Mol Cell* **62**: 237–247.

Basch ML, Brown RM, Jen H-I, Semerci F, Depreux F, Edlund RK, Zhang H, Norton CR, Gridley T, Cole SE, et al. 2016. Fine-tuning of Notch signaling sets the boundary of the organ of Corti and establishes sensory cell fates. *Elife* **5**.

Basson MA. 2012. Signaling in cell differentiation and morphogenesis. *Cold Spring Harb Perspect Biol* **4**.

Bertrand E, Chartrand P, Schaefer M, Shenoy SM, Singer RH, Long RM. 1998. Localization of ASH1 mRNA particles in living yeast. *Mol Cell* **2**: 437–45.

Bier E, De Robertis EM. 2015. BMP gradients: A paradigm for morphogen-mediated developmental patterning. *Science (80-)* **348**: aaa5838-aaa5838.

Blokzijl A, Dahlqvist C, Reissmann E, Falk A, Moliner A, Lendahl U, Ibáñez CF. 2003. Cross-talk between the Notch and TGF-beta signaling pathways mediated by interaction of the Notch intracellular domain with Smad3. *J Cell Biol* **163**: 723–8.

Boeger H, Griesenbeck J, Kornberg RD. 2008. Nucleosome retention and the stochastic nature of promoter chromatin remodeling for transcription. *Cell* **133**: 716–26.

Boeger H, Griesenbeck J, Strattan JS, Kornberg RD. 2003. Nucleosomes unfold completely at a transcriptionally active promoter. *Mol Cell* **11**: 1587–98.

Boeger H, Griesenbeck J, Strattan JS, Kornberg RD. 2004. Removal of promoter nucleosomes by disassembly rather than sliding in vivo. *Mol Cell* **14**: 667–73.

Boehm AK, Saunders A, Werner J, Lis JT. 2003. Transcription factor and polymerase recruitment, modification, and movement on dhsp70 in vivo in the minutes following heat shock. *Mol Cell Biol* **23**: 7628–37.

Bonnefoy E, Orsi GA, Couble P, Loppin B. 2007. The Essential Role of Drosophila HIRA for De Novo Assembly of Paternal Chromatin at Fertilization. *PLoS Genet* **3**: e182.

Borggrefe T, Oswald F. 2009. The Notch signaling pathway: Transcriptional regulation at Notch target genes. *Cell Mol Life Sci* **66**: 1631–1646.

Bos TJ, Nussbacher JK, Aigner S, Yeo GW. 2016. Tethered Function Assays as Tools to Elucidate the Molecular Roles of RNA-Binding Proteins. *Adv Exp Med Biol* **907**: 61–88.

Bothma JP, Garcia HG, Esposito E, Schlissel G, Gregor T, Levine M. 2014. Dynamic regulation of eve stripe 2 expression reveals transcriptional bursts in living Drosophila embryos. *Proc Natl Acad Sci U S A* **111**: 10598–603.

Bothma JP, Garcia HG, Ng S, Perry MW, Gregor T, Levine M. 2015. Enhancer additivity and non-additivity are determined by enhancer strength in the Drosophila embryo. *Elife* **4**.

Böttcher R, Hollmann M, Merk K, Nitschko V, Obermaier C, Philippou-Massier J, Wieland I, Gaul U, Förstemann K. 2014. Efficient chromosomal gene modification with CRISPR/cas9 and PCR-based homologous recombination donors in cultured Drosophila cells. *Nucleic Acids Res* **42**: e89.

Bouazoune K, Brehm A. 2006. ATP-dependent chromatin remodeling complexes in Drosophila. *Chromosom Res* **14**: 433–449.

Bray SJ. 2016. Notch signalling in context. *Nat Rev Mol Cell Biol* **17**: 722–735.

Bray SJ, Gomez-Lamarca M. 2018. Notch after cleavage. *Curr Opin Cell Biol* **51**: 103–109.

Brou C, Logeat F, Gupta N, Bessia C, LeBail O, Doedens JR, Cumano A, Roux P, Black RA, Israël A. 2000. A novel proteolytic cleavage involved in Notch signaling: the role of the disintegrin-metalloprotease TACE. *Mol Cell* **5**: 207–16.

Brown CR, Mao C, Falkovskaia E, Law JK, Boeger H. 2011. In vivo role for the chromatin-remodeling enzyme SWI/SNF in the removal of promoter nucleosomes by disassembly rather than sliding. *J Biol Chem* **286**: 40556–65.

Buckley MS, Kwak H, Zipfel WR, Lis JT. 2014. Kinetics of promoter Pol II on Hsp70 reveal stable pausing and key insights into its regulation. *Genes Dev* **28**: 14–9.

Buenrostro JD, Wu B, Chang HY, Greenleaf WJ. 2015. ATAC-seq: A Method for Assaying Chromatin Accessibility Genome-Wide. In *Current Protocols in Molecular Biology*, Vol. 109 of, p. 21.29.1-21.29.9, John Wiley & Sons, Inc., Hoboken, NJ, USA.

Bultman S, Gebuhr T, Yee D, La Mantia C, Nicholson J, Gilliam A, Randazzo F, Metzger D, Chambon P, Crabtree G, et al. 2000. A Brg1 null mutation in the mouse reveals functional differences among mammalian SWI/SNF complexes. *Mol Cell* **6**: 1287–95.

Burgess RJ, Zhang Z. 2013. Histone chaperones in nucleosome assembly and human disease. *Nat Struct Mol Biol* **20**: 14–22.

Campos EI, Reinberg D. 2010. New chaps in the histone chaperone arena. *Genes Dev* **24**: 1334–8.

Cannavò E, Khoueiry P, Garfield DA, Geeleher P, Zichner T, Gustafson EH, Ciglar L, Korbel JO, Furlong EEM. 2016. Shadow Enhancers Are Pervasive Features of Developmental Regulatory Networks. *Curr Biol* **26**: 38–51.

Carr A, Biggin MD. 1999. A comparison of in vivo and in vitro DNA-binding specificities suggests a new model for homeoprotein DNA binding in Drosophila embryos. *EMBO J* **18**: 1598–608.

Carrera I, Janody F, Leeds N, Duveau F, Treisman JE. 2008a. Pygopus activates Wingless target gene transcription through the mediator complex subunits Med12 and Med13. *Proc Natl Acad Sci U S A* **105**: 6644–9.

Carrera I, Zavadil J, Treisman JE. 2008b. Two subunits specific to the PBAP chromatin remodeling complex have distinct and redundant functions during drosophila development. *Mol Cell Biol* **28**: 5238–50.

Cartailler J, Reingruber J. 2015. Facilitated diffusion framework for transcription factor search with conformational changes. *Phys Biol* **12**: 046012.

Carter R, Drouin G. 2009. Structural differentiation of the three eukaryotic RNA polymerases. *Genomics* **94**: 388–396.

Castel D, Mourikis P, Bartels SJJ, Brinkman AB, Tajbakhsh S, Stunnenberg HG. 2013. Dynamic binding of RBPJ is determined by Notch signaling status. *Genes Dev* **27**: 1059–71.

Castro B, Barolo S, Bailey AM, Posakony JW. 2005. Lateral inhibition in proneural clusters: cis-regulatory logic and default repression by Suppressor of Hairless. *Development* **132**: 3333–3344.

Chan K-M, Fang D, Gan H, Hashizume R, Yu C, Schroeder M, Gupta N, Mueller S, James CD, Jenkins R, et al. 2013. The histone H3.3K27M mutation in pediatric glioma reprograms H3K27 methylation and gene expression. *Genes Dev* **27**: 985–90.

Chan SKK, Cerda-Moya G, Stojnic R, Millen K, Fischer B, Fexova S, Skalska L, Gomez-Lamarca M, Pillidge Z, Russell S, et al. 2017. Role of co-repressor genomic landscapes in shaping the Notch response ed. M. Snyder. *PLOS Genet* **13**: e1007096.

Chao S-H, Fujinaga K, Marion JE, Taube R, Sausville EA, Senderowicz AM, Peterlin BM, Price DH. 2000. Flavopiridol Inhibits P-TEFb and Blocks HIV-1 Replication. *J Biol Chem* **275**: 28345–28348.

Chapman G, Liu L, Sahlgren C, Dahlqvist C, Lendahl U. 2006. High levels of Notch signaling down-regulate Numb and Numblike. *J Cell Biol* **175**: 535–40.

Cheloufi S, Elling U, Hopfgartner B, Jung YL, Murn J, Ninova M, Hubmann M, Badeaux AI, Euong Ang C, Tenen D, et al. 2015. The histone chaperone CAF-1 safeguards somatic cell identity. *Nature* **528**: 218–24.

Chen J, Ghazawi FM, Li Q. 2010. Interplay of bromodomain and histone acetylation in the regulation of p300-dependent genes. *Epigenetics* **5**: 509–15.

Chen J, Zhang Z, Li L, Chen B-C, Revyakin A, Hajj B, Legant W, Dahan M, Lionnet T, Betzig E, et al. 2014. Single-Molecule Dynamics of Enhanceosome Assembly in Embryonic Stem Cells. *Cell* **156**: 1274–1285.

Chen N, Greenwald I. 2004. The lateral signal for LIN-12/Notch in C. elegans vulval development comprises redundant secreted and transmembrane DSL proteins. *Dev Cell* **6**: 183–92.

Chen W-Y, Shih H-T, Liu K-Y, Shih Z-S, Chen L-K, Tsai T-H, Chen M-J, Liu H, Tan BC-M, Chen C-Y, et al. 2015. Intellectual disability-associated dBRWD3 regulates gene expression through inhibition of HIRA/YEM-mediated chromatin deposition of histone H3.3. *EMBO Rep* **16**: 528–38.

Chen X, Xu H, Yuan P, Fang F, Huss M, Vega VB, Wong E, Orlov YL, Zhang W, Jiang J, et al. 2008. Integration of External Signaling Pathways with the Core Transcriptional Network in Embryonic Stem Cells. *Cell* **133**: 1106–1117.

Cho W-K, Jayanth N, Mullen S, Tan TH, Jung YJ, Cissé II. 2016. Super-resolution imaging of fluorescently labeled, endogenous RNA Polymerase II in living cells with CRISPR/Cas9-mediated gene editing. *Sci Rep* **6**: 35949.

Chuang LSH, Ito K, Ito Y. 2013. RUNX family: Regulation and diversification of roles through interacting proteins. *Int J Cancer* **132**: 1260–1271.

Chubb JR, Trcek T, Shenoy SM, Singer RH. 2006. Transcriptional pulsing of a developmental gene. *Curr Biol* **16**: 1018–25.

Clapier CR, Iwasa J, Cairns BR, Peterson CL. 2017. Mechanisms of action and regulation of ATP-dependent chromatin-remodelling complexes. *Nat Rev Mol Cell Biol* **18**: 407–422.

Clapier CR, Kasten MM, Parnell TJ, Viswanathan R, Szerlong H, Sirinakis G, Zhang Y, Cairns BR. 2016. Regulation of DNA Translocation Efficiency within the Chromatin Remodeler RSC/Sth1 Potentiates Nucleosome Sliding and Ejection. *Mol Cell* **62**: 453–461.

Cohen M, Georgiou M, Stevenson NL, Miodownik M, Baum B. 2010. Dynamic filopodia transmit intermittent Delta-Notch signaling to drive pattern refinement during lateral inhibition. *Dev Cell* **19**: 78–89.

Coleman RT, Struhl G. 2017. Causal role for inheritance of H3K27me3 in maintaining the OFF state of a Drosophila HOX gene. *Science* **356**.

Collins KJ, Yuan Z, Kovall RA. 2014. Structure and function of the CSL-KyoT2 corepressor complex: a negative regulator of Notch signaling. *Structure* **22**: 70–81.

Cooper MTD, Tyler DM, Furriols M, Chalkiadaki A, Delidakis C, Bray S. 2000. Spatially Restricted Factors Cooperate with Notch in the Regulation of Enhancer of split Genes. *Dev Biol* **221**: 390–403.

Corrigan AM, Tunnacliffe E, Cannon D, Chubb JR. 2016. A continuum model of transcriptional bursting. *Elife* **5**.

Corson F, Couturier L, Rouault H, Mazouni K, Schweisguth F. 2017. Self-organized Notch dynamics generate stereotyped sensory organ patterns in *Drosophila*. *Science (80-)* **356**: eaai7407.

Creyghton MP, Cheng AW, Welstead GG, Kooistra T, Carey BW, Steine EJ, Hanna J, Lodato MA, Frampton GM, Sharp PA, et al. 2010. Histone H3K27ac separates active from poised enhancers and predicts developmental state. *Proc Natl Acad Sci U S A* **107**: 21931–6.

D'Souza B, Meloty-Kapella L, Weinmaster G. 2010. Canonical and non-canonical Notch ligands. *Curr Top Dev Biol* **92**: 73–129.

Dai J, Hyland EM, Yuan DS, Huang H, Bader JS, Boeke JD. 2008. Probing nucleosome function: a highly versatile library of synthetic histone H3 and H4 mutants. *Cell* **134**: 1066–78.

Dale JK, Maroto M, Dequeant M-L, Malapert P, McGrew M, Pourquie O. 2003. Periodic Notch inhibition by Lunatic Fringe underlies the chick segmentation clock. *Nature* **421**: 275–278.

Danko CG, Hah N, Luo X, Martins AL, Core L, Lis JT, Siepel A, Kraus WL. 2013. Signaling pathways differentially affect RNA polymerase II initiation, pausing, and elongation rate in cells. *Mol Cell* **50**: 212–22.

Dar RD, Razooky BS, Singh A, Trimeloni T V, McCollum JM, Cox CD, Simpson ML, Weinberger LS. 2012. Transcriptional burst frequency and burst size are equally modulated across the human genome. *Proc Natl Acad Sci U S A* **109**: 17454–9.

Das A V, James J, Bhattacharya S, Imbalzano AN, Antony ML, Hegde G, Zhao X, Mallya K, Ahmad F, Knudsen E, et al. 2007. SWI/SNF chromatin remodeling ATPase Brm regulates the differentiation of early retinal stem cells/progenitors by influencing Brn3b expression and Notch signaling. *J Biol Chem* **282**: 35187–201.

De Angelis RW, Maluf NK, Yang Q, Lambert JR, Bain DL. 2015. Glucocorticoid Receptor–DNA Dissociation Kinetics Measured *in Vitro* Reveal Exchange on the Second Time Scale. *Biochemistry* **54**: 5306–5314.

de la Serna IL, Carlson KA, Imbalzano AN. 2001. Mammalian SWI/SNF complexes promote MyoD-mediated muscle differentiation. *Nat Genet* **27**: 187–190.

Deal RB, Henikoff JG, Henikoff S. 2010. Genome-Wide Kinetics of Nucleosome Turnover Determined by Metabolic Labeling of Histones. *Science (80-)* **328**: 1161–1164.

Deaton AM, Gómez-Rodríguez M, Mieczkowski J, Tolstorukov MY, Kundu S, Sadreyev RI, Jansen LE, Kingston RE. 2016. Enhancer regions show high histone H3.3 turnover that changes during differentiation. *Elife* **5**.

Dechassa ML, Sabri A, Pondugula S, Kassabov SR, Chatterjee N, Kladde MP, Bartholomew B. 2010. SWI/SNF has intrinsic nucleosome disassembly activity that is dependent on adjacent nucleosomes. *Mol Cell* **38**: 590–602.

Degner JF, Pai AA, Pique-Regi R, Veyrieras J-B, Gaffney DJ, Pickrell JK, De Leon S, Michelini K, Lewellen N, Crawford GE, et al. 2012. DNase I sensitivity QTLs are a major determinant of human expression variation. *Nature* **482**: 390–4.

Deindl S, Hwang WL, Hota SK, Blosser TR, Prasad P, Bartholomew B, Zhuang X. 2013. ISWI Remodelers Slide Nucleosomes with Coordinated Multi-Base-Pair Entry Steps and Single-Base-Pair Exit Steps. *Cell* **152**: 442–452.

Déjardin J, Cavalli G. 2004. Chromatin inheritance upon Zeste-mediated Brahma recruitment at a minimal cellular memory module. *EMBO J* **23**: 857–68.

Deng W, Lee J, Wang H, Miller J, Reik A, Gregory PD, Dean A, Blobel GA. 2012. Controlling long-range genomic interactions at a native locus by targeted tethering of a looping factor. *Cell* **149**: 1233–44.

Di Stefano L, Walker JA, Burgio G, Corona DF V., Mulligan P, Naar AM, Dyson NJ. 2011. Functional antagonism between histone H3K4 demethylases in vivo. *Genes Dev* **25**: 17–28.

Dixit A, Parnas O, Li B, Chen J, Fulco CP, Jerby-Arnon L, Marjanovic ND, Dionne D, Burks T, Raychowdhury R, et al. 2016. Perturb-Seq: Dissecting Molecular Circuits with Scalable Single-Cell RNA Profiling of Pooled Genetic Screens. *Cell* **167**: 1853–1866.e17.

Dixon JR, Selvaraj S, Yue F, Kim A, Li Y, Shen Y, Hu M, Liu JS, Ren B. 2012. Topological domains in mammalian genomes identified by analysis of chromatin interactions. *Nature* **485**: 376–80.

Doudna JA, Charpentier E. 2014. The new frontier of genome engineering with CRISPR-Cas9. *Science (80-)* **346**: 1258096–1258096.

Dror I, Rohs R, Mandel□Gutfreund Y. 2016. How motif environment influences transcription factor search dynamics: Finding a needle in a haystack. *Bioessays* **38**: 605.

Elfring LK, Daniel C, Papoulas O, Deuring R, Sarte M, Moseley S, Beek SJ, Waldrip WR, Daubresse G, DePace A, et al. 1998. Genetic analysis of brahma: the Drosophila homolog of the yeast chromatin remodeling factor SWI2/SNF2. *Genetics* **148**: 251–65.

ENCODE Project Consortium TEP. 2012. An integrated encyclopedia of DNA elements in the human genome. *Nature* **489**: 57–74.

Eom DS, Bain EJ, Patterson LB, Grout ME, Parichy DM. 2015. Long-distance communication by specialized cellular projections during pigment pattern development and evolution. *Elife* **4**.

Esnault C, Ghavi-Helm Y, Brun S, Soutourina J, Van Berkum N, Boschiero C, Holstege F, Werner M. 2008. Mediator-Dependent Recruitment of TFIIH Modules in Preinitiation Complex. *Mol Cell* **31**: 337–346.

Eychenne T, Novikova E, Barrault M-B, Alibert O, Boschiero C, Peixeiro N, Cornu D, Redeker V, Kuras L, Nicolas P, et al. 2016. Functional interplay between Mediator and TFIIB in preinitiation complex assembly in relation to promoter architecture. *Genes Dev* **30**: 2119–2132.

Fascher KD, Schmitz J, Hörz W. 1990. Role of trans-activating proteins in the generation of active chromatin at the PHO5 promoter in S. cerevisiae. *EMBO J* **9**: 2523–8.

Fazzio TG, Tsukiyama T. 2003. Chromatin remodeling in vivo: evidence for a nucleosome sliding mechanism. *Mol Cell* **12**: 1333–40.

Fedorov O, Castex J, Tallant C, Owen DR, Martin S, Aldeghi M, Monteiro O, Filippakopoulos P, Picaud S, Trzupek JD, et al. 2015. Selective targeting of the BRG/PB1 bromodomains impairs embryonic and trophoblast stem cell maintenance. *Sci Adv* **1**: e1500723.

Felsenfeld G. 1992. Chromatin as an essential part of the transcriptional mechanim. *Nature* **355**: 219–224.

Flores G V, Duan H, Yan H, Nagaraj R, Fu W, Zou Y, Noll M, Banerjee U. 2000. Combinatorial signaling in the specification of unique cell fates. *Cell* **103**: 75–85.

Fortini ME. 2009. Notch signaling: the core pathway and its posttranslational regulation. *Dev Cell* **16**: 633–47.

Fortini ME, Rebay I, Caron LA, Artavanis-Tsakonas S. 1993. An activated Notch receptor blocks cell-fate commitment in the developing Drosophila eye. *Nature* **365**: 555–557.

Fryer CJ, Archer TK. 1998. Chromatin remodelling by the glucocorticoid receptor requires the BRG1 complex. *Nature* **393**: 88–91.

Fryer CJ, Lamar E, Turbachova I, Kintner C, Jones KA. 2002. Mastermind mediates chromatin-specific transcription and turnover of the Notch enhancer complex. *Genes Dev* **16**: 1397–411.

Fryer CJ, White JB, Jones KA. 2004. Mastermind recruits CycC:CDK8 to phosphorylate the Notch ICD and coordinate activation with turnover. *Mol Cell* **16**: 509–20.

Fukaya T, Lim B, Levine M. 2016. Enhancer Control of Transcriptional Bursting. *Cell* **166**: 358–368.

Fukaya T, Lim B, Levine M. 2017. Rapid Rates of Pol II Elongation in the Drosophila Embryo. *Curr Biol* **27**: 1387–1391.

Galbraith MD, Allen MA, Bensard CL, Wang X, Schwinn MK, Qin B, Long HW, Daniels DL, Hahn WC, Dowell RD, et al. 2013. HIF1A employs CDK8-mediator to stimulate RNAPII elongation in response to hypoxia. *Cell* **153**: 1327–39.

Garcia HG, Tikhonov M, Lin A, Gregor T. 2013. Quantitative imaging of transcription in living Drosophila embryos links polymerase activity to patterning. *Curr Biol* **23**: 2140–5.

Ghavi-Helm Y, Klein FA, Pakozdi T, Ciglar L, Noordermeer D, Huber W, Furlong EEM. 2014. Enhancer loops appear stable during development and are associated with paused polymerase. *Nature* **512**: 96–100.

Gilmour DS, Lis JT. 1986. RNA polymerase II interacts with the promoter region of the noninduced hsp70 gene in Drosophila melanogaster cells. *Mol Cell Biol* **6**: 3984–9.

Giorgetti L, Siggers T, Tiana G, Caprara G, Notarbartolo S, Corona T, Pasparakis M, Milani P, Bulyk ML, Natoli G. 2010. Noncooperative Interactions between Transcription Factors and Clustered DNA Binding Sites Enable Graded Transcriptional Responses to Environmental Inputs. *Mol Cell* **37**: 418–428.

Goldberg AD, Banaszynski LA, Noh K-M, Lewis PW, Elsaesser SJ, Stadler S, Dewell S, Law M, Guo X, Li X, et al. 2010. Distinct factors control histone variant H3.3 localization at specific genomic regions. *Cell* **140**: 678–91.

Golding I, Paulsson J, Zawilski SM, Cox EC. 2005. Real-time kinetics of gene activity in individual bacteria. *Cell* **123**: 1025–36.

Gomez-Lamarca MJ, Falo-Sanjuan J, Stojnic R, Abdul Rehman S, Muresan L, Jones ML, Pillidge Z, Cerda-Moya G, Yuan Z, Baloul S, et al. 2018. Activation of the Notch Signaling Pathway In Vivo Elicits Changes in CSL Nuclear Dynamics. *Dev Cell* **44**: 611–623.e7.

González M, Martín-Ruíz I, Jiménez S, Pirone L, Barrio R, Sutherland JD. 2011. Generation of stable Drosophila cell lines using multicistronic vectors. *Sci Rep* **1**: 75.

Gordon WR, Vardar-Ulu D, Histen G, Sanchez-Irizarry C, Aster JC, Blacklow SC. 2007. Structural basis for autoinhibition of Notch. *Nat Struct Mol Biol* **14**: 295–300.

Gordon WR, Zimmerman B, He L, Miles LJ, Huang J, Tiyanont K, McArthur DG, Aster JC, Perrimon N, Loparo JJ, et al. 2015. Mechanical Allostery: Evidence for a Force Requirement in the Proteolytic Activation of Notch. *Dev Cell* **33**: 729–36.

Graves HK, Wang P, Lagarde M, Chen Z, Tyler JK. 2016. Mutations that prevent or mimic persistent post-translational modifications of the histone H3 globular domain cause lethality and growth defects in Drosophila. *Epigenetics Chromatin* **9**: 9.

Grøntved L, Madsen MS, Boergesen M, Roeder RG, Mandrup S. 2010. MED14 tethers mediator to the N-terminal domain of peroxisome proliferator-activated receptor gamma and is required for full transcriptional activity and adipogenesis. *Mol Cell Biol* **30**: 2155–69.

Grossman SR, Engreitz J, Ray JP, Nguyen TH, Hacohen N, Lander ES. 2018. Positional specificity of different transcription factor classes within enhancers. *Proc Natl Acad Sci U S A* **115**: E7222–E7230.

Grossman SR, Zhang X, Wang L, Engreitz J, Melnikov A, Rogov P, Tewhey R, Isakova A, Deplancke B, Bernstein BE, et al. 2017. Systematic dissection of genomic features determining transcription factor binding and enhancer function. *Proc Natl Acad Sci* **114**: E1291–E1300.

Günesdogan U, Jäckle H, Herzig A. 2010. A genetic system to assess in vivo the functions of histones and histone modifications in higher eukaryotes. *EMBO Rep* **11**: 772–6.

GURDON JB. 1962. The developmental capacity of nuclei taken from intestinal epithelium cells of feeding tadpoles. *J Embryol Exp Morphol* **10**: 622–40.

Guruharsha KG, Kankel MW, Artavanis-Tsakonas S. 2012. The Notch signalling system: recent insights into the complexity of a conserved pathway. *Nat Rev Genet* **13**: 654–66.

Ha M, Kraushaar DC, Zhao K. 2014. Genome-wide analysis of H3.3 dissociation reveals high nucleosome turnover at distal regulatory regions of embryonic stem cells. *Epigenetics Chromatin* **7**: 38.

Haberle V, Stark A. 2018. Eukaryotic core promoters and the functional basis of transcription initiation. *Nat Rev Mol Cell Biol* 1.

Hamada H, Watanabe M, Lau HE, Nishida T, Hasegawa T, Parichy DM, Kondo S. 2014. Involvement of Delta/Notch signaling in zebrafish adult pigment stripe patterning. *Development* **141**: 318–324.

Hansen JC, Tse C, Wolffe AP. 1998. Structure and function of the core histone N-termini: more than meets the eye. *Biochemistry* **37**: 17637–41.

Hass MR, Liow H-H, Chen X, Sharma A, Inoue YU, Inoue T, Reeb A, Martens A, Fulbright M, Raju S, et al. 2015. SpDamID: Marking DNA Bound by Protein Complexes Identifies Notch-Dimer Responsive Enhancers. *Mol Cell* **59**: 685–97.

He J, Xuan T, Xin T, An H, Wang J, Zhao G, Li M. 2014. Evidence for Chromatin-Remodeling Complex PBAP-Controlled Maintenance of the Drosophila Ovarian Germline Stem Cells ed. S.R. Singh. *PLoS One* **9**: e103473.

Heck BW, Zhang B, Tong X, Pan Z, Deng W-M, Tsai C-C. 2012. The transcriptional corepressor SMRTER influences both Notch and ecdysone signaling during Drosophila development. *Biol Open* **1**: 182–96.

Henikoff S, Ahmad K, Platero JS, van Steensel B. 2000. Heterochromatic deposition of centromeric histone H3-like proteins. *Proc Natl Acad Sci U S A* **97**: 716–21.

Henikoff S, Shilatifard A. 2011. Histone modification: cause or cog? *Trends Genet* **27**: 389–396.

Henriques T, Gilchrist DA, Nechaev S, Bern M, Muse GW, Burkholder A, Fargo DC, Adelman K. 2013. Stable pausing by RNA polymerase II provides an opportunity to target and integrate regulatory signals. *Mol Cell* **52**: 517–28.

Ho JWK, Jung YL, Liu T, Alver BH, Lee S, Ikegami K, Sohn K-A, Minoda A, Tolstorukov MY, Appert A, et al. 2014. Comparative analysis of metazoan chromatin organization. *Nature* **512**: 449–52.

Hodges C, Kirkland JG, Crabtree GR. 2016. The Many Roles of BAF (mSWI/SNF) and PBAF Complexes in Cancer. *Cold Spring Harb Perspect Med* **6**.

Hödl M, Basler K. 2009. Transcription in the Absence of Histone H3.3. *Curr Biol* **19**: 1221–1226.

Hota SK, Bruneau BG. 2016. ATP-dependent chromatin remodeling during mammalian development. *Development* **143**: 2882–97.

Housden BE, Fu AQ, Krejci A, Bernard F, Fischer B, Tavaré S, Russell S, Bray SJ. 2013. Transcriptional Dynamics Elicited by a Short Pulse of Notch Activation Involves Feed-Forward Regulation by E(spl)/Hes Genes ed. J. Lewis. *PLoS Genet* **9**: e1003162.

Housden BE, Millen K, Bray SJ. 2012. Drosophila Reporter Vectors Compatible with ΦC31 Integrase Transgenesis Techniques and Their Use to Generate New Notch Reporter Fly Lines. *G3 (Bethesda)* **2**: 79–82.

Hsieh JJ, Zhou S, Chen L, Young DB, Hayward SD. 1999. CIR, a corepressor linking the DNA binding factor CBF1 to the histone deacetylase complex. *Proc Natl Acad Sci U S A* **96**: 23–8.

Huang A, Amourda C, Zhang S, Tolwinski NS, Saunders TE. 2017. Decoding temporal interpretation of the morphogen Bicoid in the early Drosophila embryo. *Elife* **6**.

Huang C, Zhu B. 2014. H3.3 turnover: a mechanism to poise chromatin for transcription, or a response to open chromatin? *Bioessays* **36**: 579–84.

Ilagan MXG, Lim S, Fulbright M, Piwnica-Worms D, Kopan R. 2011. Real-time imaging of notch activation with a luciferase complementation-based reporter. *Sci Signal* **4**: rs7.

Imhof A, Yang XJ, Ogryzko V V, Nakatani Y, Wolffe AP, Ge H. 1997. Acetylation of general transcription factors by histone acetyltransferases. *Curr Biol* **7**: 689–92.

Isomura A, Ogushi F, Kori H, Kageyama R. 2017. Optogenetic perturbation and bioluminescence imaging to analyze cell-to-cell transfer of oscillatory information. *Genes Dev* **31**: 524–535.

Ivanauskiene K, Delbarre E, McGhie JD, Küntziger T, Wong LH, Collas P. 2014. The PML-associated protein DEK regulates the balance of H3.3 loading on chromatin and is important for telomere integrity. *Genome Res* **24**: 1584–94.

Jaitin DA, Weiner A, Yofe I, Lara-Astiaso D, Keren-Shaul H, David E, Salame TM, Tanay A, van Oudenaarden A, Amit I. 2016. Dissecting Immune Circuits by Linking CRISPR-Pooled Screens with Single-Cell RNA-Seq. *Cell* **167**: 1883–1896.e15.

Jang MK, Mochizuki K, Zhou M, Jeong H-S, Brady JN, Ozato K. 2005. The Bromodomain Protein Brd4 Is a Positive Regulatory Component of P-TEFb and Stimulates RNA Polymerase II-Dependent Transcription. *Mol Cell* **19**: 523–534.

Jin S, Mutvei AP, Chivukula I V, Andersson ER, Ramsköld D, Sandberg R, Lee KL, Kronqvist P, Mamaeva V, Ostling P, et al. 2013. Non-canonical Notch signaling activates IL-6/JAK/STAT signaling in breast tumor cells and is controlled by p53 and IKKα/IKKβ. *Oncogene* **32**: 4892–902.

Jin Y, Rodriguez AM, Wyrick JJ. 2009. Genetic and genomewide analysis of simultaneous mutations in acetylated and methylated lysine residues in histone H3 in Saccharomyces cerevisiae. *Genetics* **181**: 461–72.

Johnson HE, Toettcher JE. 2018. Illuminating developmental biology with cellular optogenetics. *Curr Opin Biotechnol* **52**: 42–48.

Jordán-Pla A, Yu S, Waldholm J, Källman T, Östlund Farrants A-K, Visa N. 2018. SWI/SNF regulates half of its targets without the need of ATP-driven nucleosome remodeling by Brahma. *BMC Genomics* **19**: 367.

Kadam S, Emerson BM. 2003. Transcriptional Specificity of Human SWI/SNF BRG1 and BRM Chromatin Remodeling Complexes. *Mol Cell* **11**: 377–389.

Kadoch C, Hargreaves DC, Hodges C, Elias L, Ho L, Ranish J, Crabtree GR. 2013. Proteomic and bioinformatic analysis of mammalian SWI/SNF complexes identifies extensive roles in human malignancy. *Nat Genet* **45**: 592–601.

Kagey MH, Newman JJ, Bilodeau S, Zhan Y, Orlando DA, van Berkum NL, Ebmeier CC, Goossens J, Rahl PB, Levine SS, et al. 2010. Mediator and cohesin connect gene expression and chromatin architecture. *Nature* **467**: 430–5.

Kakarougkas A, Jeggo PA. 2014. DNA DSB repair pathway choice: an orchestrated handover mechanism. *Br J Radiol* **87**: 20130685.

Kal AJ, Mahmoudi T, Zak NB, Verrijzer CP. 2000. The Drosophila brahma complex is an essential coactivator for the trithorax group protein zeste. *Genes Dev* **14**: 1058–71.

Kao HY, Ordentlich P, Koyano-Nakagawa N, Tang Z, Downes M, Kintner CR, Evans RM, Kadesch T. 1998. A histone deacetylase corepressor complex regulates the Notch signal transduction pathway. *Genes Dev* **12**: 2269–77.

Kaplan N, Moore IK, Fondufe-Mittendorf Y, Gossett AJ, Tillo D, Field Y, LeProust EM, Hughes TR, Lieb JD, Widom J, et al. 2009. The DNA-encoded nucleosome organization of a eukaryotic genome. *Nature* **458**: 362–366.

Kaplan T, Li X-Y, Sabo PJ, Thomas S, Stamatoyannopoulos JA, Biggin MD, Eisen MB. 2011. Quantitative Models of the Mechanisms That Control Genome-Wide Patterns of Transcription Factor Binding during Early Drosophila Development ed. G.S. Barsh. *PLoS Genet* **7**: e1001290.

Kaul A, Schuster E, Jennings BH. 2014. The Groucho Co-repressor Is Primarily Recruited to Local Target Sites in Active Chromatin to Attenuate Transcription ed. S. Russell. *PLoS Genet* **10**: e1004595.

Kaul AK, Schuster EF, Jennings BH. 2015. Recent insights into Groucho co-repressor recruitment and function. *Transcription* **6**: 7–11.

Kawahashi K, Hayashi S. 2010. Dynamic intracellular distribution of Notch during activation and asymmetric cell division revealed by functional fluorescent fusion proteins. *Genes to Cells* **15**: 749–759.

Kazemian M, Pham H, Wolfe SA, Brodsky MH, Sinha S. 2013. Widespread evidence of cooperative DNA binding by transcription factors in Drosophila development. *Nucleic Acids Res* **41**: 8237–52.

Kharchenko P V, Alekseyenko AA, Schwartz YB, Minoda A, Riddle NC, Ernst J, Sabo PJ, Larschan E, Gorchakov AA, Gu T, et al. 2011. Comprehensive analysis of the chromatin landscape in Drosophila melanogaster. *Nature* **471**: 480–5.

Klein T, Arias AM. 1999. The vestigial gene product provides a molecular context for the interpretation of signals during the development of the wing in Drosophila. *Development* **126**: 913–25.

Klose R, Berger C, Moll I, Adam MG, Schwarz F, Mohr K, Augustin HG, Fischer A. 2015. Soluble Notch ligand and receptor peptides act antagonistically during angiogenesis. *Cardiovasc Res* **107**: 153–163.

Komatsu H, Chao MY, Larkins-Ford J, Corkins ME, Somers GA, Tucey T, Dionne HM, White JQ, Wani K, Boxem M, et al. 2008. OSM-11 Facilitates LIN-12 Notch Signaling during Caenorhabditis elegans Vulval Development ed. J. Ahringer. *PLoS Biol* **6**: e196.

Kopan R, Ilagan MXG. 2009. The canonical Notch signaling pathway: unfolding the activation mechanism. *Cell* **137**: 216–33.

Kornberg RD. 1974. Chromatin structure: a repeating unit of histones and DNA. *Science* **184**: 868–71.

Kraushaar DC, Jin W, Maunakea A, Abraham B, Ha M, Zhao K. 2013. Genome-wide incorporation dynamics reveal distinct categories of turnover for the histone variant H3.3. *Genome Biol* **14**: R121.

Krebs AR, Imanci D, Hoerner L, Gaidatzis D, Burger L, Schübeler D. 2017. Genome-wide Single-Molecule Footprinting Reveals High RNA Polymerase II Turnover at Paused Promoters. *Mol Cell* **67**: 411–422.e4.

Krejcí A, Bernard F, Housden BE, Collins S, Bray SJ. 2009. Direct response to Notch activation: signaling crosstalk and incoherent logic. *Sci Signal* **2**: ra1.

Krejci A, Bray S. 2007. Notch activation stimulates transient and selective binding of Su(H)/CSL to target enhancers. *Genes Dev* **21**: 1322–1327.

Kunzelmann S, Böttcher R, Schmidts I, Förstemann K. 2016. A Comprehensive Toolbox for Genome Editing in Cultured Drosophila melanogaster Cells. *G3 (Bethesda)* **6**: 1777–85.

Kurth P, Preiss A, Kovall RA, Maier D. 2011. Molecular analysis of the notch repressor-complex in Drosophila: characterization of potential hairless binding sites on suppressor of hairless. *PLoS One* **6**: e27986.

Kwok RS, Li YH, Lei AJ, Edery I, Chiu JC. 2015. The Catalytic and Non-catalytic Functions of the Brahma Chromatin-Remodeling Protein Collaborate to Fine-Tune Circadian Transcription in Drosophila. *PLoS Genet* **11**: e1005307.

Lagha M, Bothma JP, Esposito E, Ng S, Stefanik L, Tsui C, Johnston J, Chen K, Gilmour DS, Zeitlinger J, et al. 2013. Paused Pol II coordinates tissue morphogenesis in the Drosophila embryo. *Cell* **153**: 976–87.

Lamparter D, Marbach D, Rueedi R, Bergmann S, Kutalik Z. 2017. Genome-Wide Association between Transcription Factor Expression and Chromatin Accessibility Reveals Regulators of Chromatin Accessibility ed. T. Wang. *PLOS Comput Biol* **13**: e1005311.

Längst G, Manelyte L. 2015. Chromatin Remodelers: From Function to Dysfunction. *Genes (Basel)* **6**: 299–324.

Larson DR, Fritzsch C, Sun L, Meng X, Lawrence DS, Singer RH. 2013. Direct observation of frequency modulated transcription in single cells using light activation. *Elife* **2**: e00750.

Larson DR, Zenklusen D, Wu B, Chao JA, Singer RH. 2011. Real-time observation of transcription initiation and elongation on an endogenous yeast gene. *Science* **332**: 475–8.

Lebrecht D, Foehr M, Smith E, Lopes FJP, Vanario-Alonso CE, Reinitz J, Burz DS, Hanes SD. 2005. Bicoid cooperative DNA binding is critical for embryonic patterning in Drosophila. *Proc Natl Acad Sci U S A* **102**: 13176–81.

Lee BH, Stallcup MR. 2017. Glucocorticoid receptor binding to chromatin is selectively controlled by the coregulator Hic-5 and chromatin remodeling enzymes. *J Biol Chem* **292**: 9320–9334.

Lee C, Sorensen EB, Lynch TR, Kimble J. 2016. C. elegans GLP-1/Notch activates transcription in a probability gradient across the germline stem cell pool. *Elife* **5**.

Lee D, Kim JW, Seo T, Hwang SG, Choi E-J, Choe J. 2002. SWI/SNF Complex Interacts with Tumor Suppressor p53 and Is Necessary for the Activation of p53-mediated Transcription. *J Biol Chem* **277**: 22330–22337.

Lee DK, Duan HO, Chang C. 2001. Androgen receptor interacts with the positive elongation factor P-TEFb and enhances the efficiency of transcriptional elongation. *J Biol Chem* **276**: 9978–84.

Lee H-H, Frasch M, Goto T, Bodmer R. 2005. Nuclear integration of positive Dpp signals, antagonistic Wg inputs and mesodermal competence factors during Drosophila visceral mesoderm induction. *Development* **132**: 1429–42.

Lee J-E, Wang C, Xu S, Cho Y-W, Wang L, Feng X, Baldridge A, Sartorelli V, Zhuang L, Peng W, et al. 2013. H3K4 mono- and di-methyltransferase MLL4 is required for enhancer activation during cell differentiation. *Elife* **2**: e01503.

Levine M, Cattoglio C, Tjian R. 2014. Looping back to leap forward: transcription enters a new era. *Cell* **157**: 13–25.

Levine M, Tjian R. 2003. Transcription regulation and animal diversity. *Nature* **424**: 147–151.

Lewis PW, Elsaesser SJ, Noh K-M, Stadler SC, Allis CD. 2010. Daxx is an H3.3-specific histone chaperone and cooperates with ATRX in replication-independent chromatin assembly at telomeres. *Proc Natl Acad Sci* **107**: 14075–14080.

Li G, Reinberg D. 2011. Chromatin higher-order structures and gene regulation. *Curr Opin Genet Dev* **21**: 175–86.

Li M, Hada A, Sen P, Olufemi L, Hall MA, Smith BY, Forth S, McKnight JN, Patel A, Bowman GD, et al. 2015. Dynamic regulation of transcription factors by nucleosome remodeling. *Elife* **4**.

Li X-Y, Thomas S, Sabo PJ, Eisen MB, Stamatoyannopoulos JA, Biggin MD. 2011. The role of chromatin accessibility in directing the widespread, overlapping patterns of Drosophila transcription factor binding. *Genome Biol* **12**: R34.

Lia G, Praly E, Ferreira H, Stockdale C, Tse-Dinh YC, Dunlap D, Croquette V, Bensimon D, Owen-Hughes T. 2006. Direct observation of DNA distortion by the RSC complex. *Mol Cell* **21**: 417–25.

Lickwar CR, Mueller F, Hanlon SE, McNally JG, Lieb JD. 2012. Genome-wide protein-DNA binding dynamics suggest a molecular clutch for transcription factor function. *Nature* **484**: 251–5.

Lieberman BA, Nordeen SK. 1997. DNA intersegment transfer, how steroid receptors search for a target site. *J Biol Chem* **272**: 1061–8.

Ling X, Harkness TA, Schultz MC, Fisher-Adams G, Grunstein M. 1996. Yeast histone H3 and H4 amino termini are important for nucleosome assembly in vivo and in vitro: redundant and position-independent functions in assembly but not in gene regulation. *Genes Dev* **10**: 686–99.

Lis JT, Mason P, Peng J, Price DH, Werner J. 2000. P-TEFb kinase recruitment and function at heat shock loci. *Genes Dev* **14**: 792–803.

Liu L, Xu Y, He M, Zhang M, Cui F, Lu L, Yao M, Tian W, Benda C, Zhuang Q, et al. 2014. Transcriptional Pause Release Is a Rate-Limiting Step for Somatic Cell Reprogramming. *Cell Stem Cell* **15**: 574–588.

Lobry C, Oh P, Aifantis I. 2011. Oncogenic and tumor suppressor functions of Notch in cancer: it's NOTCH what you think. *J Exp Med* **208**: 1931–5.

Locatelli M, Curigliano G. 2017. Notch inhibitors and their role in the treatment of triple negative breast cancer. *Curr Opin Oncol* **29**: 411–427.

Lorch Y, Maier-Davis B, Kornberg RD. 2006. Chromatin remodeling by nucleosome disassembly in vitro. *Proc Natl Acad Sci U S A* **103**: 3090–3.

Losick R, Desplan C. 2008. Stochasticity and cell fate. *Science* **320**: 65–8.

Lucas T, Ferraro T, Roelens B, De Las Heras Chanes J, Walczak AM, Coppey M, Dostatni N. 2013. Live imaging of bicoid-dependent transcription in Drosophila embryos. *Curr Biol* **23**: 2135–9.

Luger K, Suto RK, Clarkson MJ, Tremethick DJ. 2000. Crystal structure of a nucleosome core particle containing the variant histone H2A.Z. *Nat Struct Biol* **7**: 1121–1124.

Lundgren J, Masson P, Mirzaei Z, Young P. 2005. Identification and characterization of a Drosophila proteasome regulatory network. *Mol Cell Biol* **25**: 4662–75.

Madsen MS, Siersbaek R, Boergesen M, Nielsen R, Mandrup S. 2014. Peroxisome Proliferator-Activated Receptor and C/EBP Synergistically Activate Key Metabolic Adipocyte Genes by Assisted Loading. *Mol Cell Biol* **34**: 939–954.

Maier D, Chen AX, Preiss A, Ketelhut M. 2008. The tiny Hairless protein from Apis mellifera: a potent antagonist of Notch signaling in Drosophila melanogaster. *BMC Evol Biol* **8**: 175.

Major RJ, Irvine KD. 2005. Influence of Notch on dorsoventral compartmentalization and actin organization in the Drosophila wing. *Development* **132**: 3823–33.

Majumder A, Syed KM, Joseph S, Scambler PJ, Dutta D. 2015. Histone Chaperone HIRA in Regulation of Transcription Factor RUNX1. *J Biol Chem* **290**: 13053–63.

Marathe HG, Mehta G, Zhang X, Datar I, Mehrotra A, Yeung KC, de la Serna IL. 2013. SWI/SNF enzymes promote SOX10- mediated activation of myelin gene expression. *PLoS One* **8**: e69037.

Marshall CJ. 1995. *Specificity of Receptor Tyrosine Kinase Signaling: Transient versus Sustained Extracellular Signal-Regulated Kinase Activation Review*.

Martin AM, Pouchnik DJ, Walker JL, Wyrick JJ. 2004. Redundant roles for histone H3 N-terminal lysine residues in subtelomeric gene repression in Saccharomyces cerevisiae. *Genetics* **167**: 1123–32.

Maze I, Wenderski W, Noh K-M, Bagot RC, Tzavaras N, Purushothaman I, Elsässer SJ, Guo Y, Ionete C, Hurd YL, et al. 2015. Critical Role of Histone Turnover in Neuronal Transcription and Plasticity. *Neuron* **87**: 77–94.

McGill MA, McGlade CJ. 2003. Mammalian numb proteins promote Notch1 receptor ubiquitination and degradation of the Notch1 intracellular domain. *J Biol Chem* **278**: 23196–203.

McKay DJ, Klusza S, Penke TJR, Meers MP, Curry KP, McDaniel SL, Malek PY, Cooper SW, Tatomer DC, Lieb JD, et al. 2015. Interrogating the function of metazoan histones using engineered gene clusters. *Dev Cell* **32**: 373–86.

McKittrick E, Gafken PR, Ahmad K, Henikoff S. 2004. Histone H3.3 is enriched in covalent modifications associated with active chromatin. *Proc Natl Acad Sci U S A* **101**: 1525–30.

McKnight JN, Jenkins KR, Nodelman IM, Escobar T, Bowman GD. 2011. Extranucleosomal DNA binding directs nucleosome sliding by Chd1. *Mol Cell Biol* **31**: 4746–59.

McNally AG, Poplawski SG, Mayweather BA, White KM, Abel T. 2016. Characterization of a Novel Chromatin Sorting Tool Reveals Importance of Histone Variant H3.3 in Contextual Fear Memory and Motor Learning. *Front Mol Neurosci* **9**: 11.

Mikkelsen TS, Ku M, Jaffe DB, Issac B, Lieberman E, Giannoukos G, Alvarez P, Brockman W, Kim T-K, Koche RP, et al. 2007. Genome-wide maps of chromatin state in pluripotent and lineage-committed cells. *Nature* **448**: 553–60.

Min IM, Waterfall JJ, Core LJ, Munroe RJ, Schimenti J, Lis JT. 2011. Regulating RNA polymerase pausing and transcription elongation in embryonic stem cells. *Genes Dev* **25**: 742–54.

Mirny LA. 2010. Nucleosome-mediated cooperativity between transcription factors. *Proc Natl Acad Sci U S A* **107**: 22534–9.

Mito Y, Henikoff JG, Henikoff S. 2005. Genome-scale profiling of histone H3.3 replacement patterns. *Nat Genet* **37**: 1090–1097.

Mitra P, Pereira LA, Drabsch Y, Ramsay RG, Gonda TJ. 2012. Estrogen receptor-α recruits P-TEFb to overcome transcriptional pausing in intron 1 of the MYB gene. *Nucleic Acids Res* **40**: 5988–6000.

Mizuguchi G, Shen X, Landry J, Wu W-H, Sen S, Wu C. 2004. ATP-Driven Exchange of Histone H2AZ Variant Catalyzed by SWR1 Chromatin Remodeling Complex. *Science (80-)* **303**: 343–348.

Mohrmann L, Langenberg K, Krijgsveld J, Kal AJ, Heck AJR, Verrijzer CP. 2004. Differential targeting of two distinct SWI/SNF-related Drosophila chromatin-remodeling complexes. *Mol Cell Biol* **24**: 3077–88.

Mohrmann L, Verrijzer CP. 2005. Composition and functional specificity of SWI2/SNF2 class chromatin remodeling complexes. *Biochim Biophys Acta - Gene Struct Expr* **1681**: 59–73.

Molina N, Suter DM, Cannavo R, Zoller B, Gotic I, Naef F. 2013. Stimulus-induced modulation of transcriptional bursting in a single mammalian gene. *Proc Natl Acad Sci U S A* **110**: 20563–8.

Moorman C, Sun L V., Wang J, de Wit E, Talhout W, Ward LD, Greil F, Lu X-J, White KP, Bussemaker HJ, et al. 2006. Hotspots of transcription factor colocalization in the genome of Drosophila melanogaster. *Proc Natl Acad Sci* **103**: 12027–12032.

Moshkin YM, Chalkley GE, Kan TW, Reddy BA, Ozgur Z, van Ijcken WFJ, Dekkers DHW, Demmers JA, Travers AA, Verrijzer CP. 2012. Remodelers organize cellular chromatin by counteracting intrinsic histone-DNA sequence preferences in a class-specific manner. *Mol Cell Biol* **32**: 675–88.

Moshkin YM, Mohrmann L, van Ijcken WFJ, Verrijzer CP. 2007. Functional differentiation of SWI/SNF remodelers in transcription and cell cycle control. *Mol Cell Biol* **27**: 651–61.

Muramoto T, Cannon D, Gierlinski M, Corrigan A, Barton GJ, Chubb JR. 2012. Live imaging of nascent RNA dynamics reveals distinct types of transcriptional pulse regulation. *Proc Natl Acad Sci U S A* **109**: 7350–5.

Muse GW, Gilchrist DA, Nechaev S, Shah R, Parker JS, Grissom SF, Zeitlinger J, Adelman K. 2007. RNA polymerase is poised for activation across the genome. *Nat Genet* **39**: 1507–1511.

Nagaich AK, Walker DA, Wolford R, Hager GL. 2004. Rapid periodic binding and displacement of the glucocorticoid receptor during chromatin remodeling. *Mol Cell* **14**: 163–74.

Nagel AC, Krejci A, Tenin G, Bravo-Patiño A, Bray S, Maier D, Preiss A. 2005. Hairless-mediated repression of notch target genes requires the combined activity of Groucho and CtBP corepressors. *Mol Cell Biol* **25**: 10433–41.

Nair SS, Kumar R. 2012. Chromatin remodeling in cancer: a gateway to regulate gene transcription. *Mol Oncol* **6**: 611–9.

Nakamura Y, Yamamoto K, He X, Otsuki B, Kim Y, Murao H, Soeda T, Tsumaki N, Deng JM, Zhang Z, et al. 2011. Wwp2 is essential for palatogenesis mediated by the interaction between Sox9 and mediator subunit 25. *Nat Commun* **2**: 251.

Nakayama T, Nishioka K, Dong Y-X, Shimojima T, Hirose S. 2007. Drosophila GAGA factor directs histone H3.3 replacement that prevents the heterochromatin spreading. *Genes Dev* **21**: 552–561.

Nakayama T, Shimojima T, Hirose S. 2012. The PBAP remodeling complex is required for histone H3.3 replacement at chromatin boundaries and for boundary functions. *Development* **139**: 4582–4590.

Nam Y, Sliz P, Song L, Aster JC, Blacklow SC. 2006. Structural basis for cooperativity in recruitment of MAML coactivators to Notch transcription complexes. *Cell* **124**: 973–83.

Nandagopal N, Santat LA, Lebon L, Sprinzak D, Bronner ME, Elowitz MB. 2018. Dynamic Ligand Discrimination in the Notch Signaling Pathway Article Dynamic Ligand Discrimination in the Notch Signaling Pathway. *Cell* **172**: 869–880.

Ng RK, Gurdon JB. 2008. Epigenetic memory of an active gene state depends on histone H3.3 incorporation into chromatin in the absence of transcription. *Nat Cell Biol* **10**: 102–109.

Nicolas D, Phillips NE, Naef F. 2017. What shapes eukaryotic transcriptional bursting? *Mol Biosyst* **13**: 1280–1290.

Nowling T, Bernadt C, Johnson L, Desler M, Rizzino A. 2003. The co-activator p300 associates physically with and can mediate the action of the distal enhancer of the FGF-4 gene. *J Biol Chem* **278**: 13696–705.

Oberg C, Li J, Pauley A, Wolf E, Gurney M, Lendahl U. 2001. The Notch intracellular domain is ubiquitinated and negatively regulated by the mammalian Sel-10 homolog. *J Biol Chem* **276**: 35847–53.

Orsi GA, Algazeery A, Meyer RE, Capri M, Sapey-Triomphe LM, Horard B, Gruffat H, Couble P, Aït-Ahmed O, Loppin B. 2013. Drosophila Yemanuclein and HIRA cooperate for de novo assembly of H3.3-containing nucleosomes in the male pronucleus. ed. A.C. Ferguson-Smith. *PLoS Genet* **9**: e1003285.

Oswald F, Rodriguez P, Giaimo BD, Antonello ZA, Mira L, Mittler G, Thiel VN, Collins KJ, Tabaja N, Cizelsky W, et al. 2016. A phospho-dependent mechanism involving NCoR and KMT2D controls a permissive chromatin state at Notch target genes. *Nucleic Acids Res* **44**: 4703–4720.

Oswald F, Winkler M, Cao Y, Astrahantseff K, Bourteele S, Knöchel W, Borggrefe T. 2005. RBP-Jkappa/SHARP recruits CtIP/CtBP corepressors to silence Notch target genes. *Mol Cell Biol* **25**: 10379–90.

Panne D, Maniatis T, Harrison SC. 2007. An atomic model of the interferon-beta enhanceosome. *Cell* **129**: 1111–23.

Papamichos-Chronakis M, Watanabe S, Rando OJ, Peterson CL. 2011. Global regulation of H2A.Z localization by the INO80 chromatin-remodeling enzyme is essential for genome integrity. *Cell* **144**: 200–13.

Paré A, Lemons D, Kosman D, Beaver W, Freund Y, McGinnis W. 2009. Visualization of individual Scr mRNAs during Drosophila embryogenesis yields evidence for transcriptional bursting. *Curr Biol* **19**: 2037–42.

Patel DJ, Wang Z. 2013. Readout of epigenetic modifications. *Annu Rev Biochem* **82**: 81–118.

Pengelly AR, Copur O, Jackle H, Herzig A, Muller J. 2013. A Histone Mutant Reproduces the Phenotype Caused by Loss of Histone-Modifying Factor Polycomb. *Science (80-)* **339**: 698–699.

Penton AL, Leonard LD, Spinner NB. 2012. Notch signaling in human development and disease. *Semin Cell Dev Biol* **23**: 450–457.

Perlmann T, Eriksson P, Wrange O. 1990. Quantitative analysis of the glucocorticoid receptor-DNA interaction at the mouse mammary tumor virus glucocorticoid response element. *J Biol Chem* **265**: 17222–9.

Peterlin BM, Price DH. 2006. Controlling the elongation phase of transcription with P-TEFb. *Mol Cell* **23**: 297–305.

Pierfelice T, Alberi L, Gaiano N. 2011. Notch in the vertebrate nervous system: an old dog with new tricks. *Neuron* **69**: 840–55.

Pique-Regi R, Degner JF, Pai AA, Gaffney DJ, Gilad Y, Pritchard JK. 2011. Accurate inference of transcription factor binding from DNA sequence and chromatin accessibility data. *Genome Res* **21**: 447–455.

Ponio JB-D, Wright-Crosnier C, Groyer-Picard M-T, Driancourt C, Beau I, Hadchouel M, Meunier-Rotival M. 2007. Biological function of mutant forms of JAGGED1 proteins in Alagille syndrome: inhibitory effect on Notch signaling. *Hum Mol Genet* **16**: 2683–2692.

Port F, Chen H-M, Lee T, Bullock SL. 2014. Optimized CRISPR/Cas tools for efficient germline and somatic genome engineering in Drosophila. *Proc Natl Acad Sci U S A* **111**: E2967-76.

Purvis JE, Lahav G. 2013. Encoding and decoding cellular information through signaling dynamics. *Cell* **152**: 945–56.

Rahl PB, Lin CY, Seila AC, Flynn RA, McCuine S, Burge CB, Sharp PA, Young RA. 2010. c-Myc regulates transcriptional pause release. *Cell* **141**: 432–45.

Raj A, Peskin CS, Tranchina D, Vargas DY, Tyagi S. 2006. Stochastic mRNA synthesis in mammalian cells. *PLoS Biol* **4**: e309.

Ramachandran S, Henikoff S. 2016a. Nucleosome dynamics during chromatin remodeling in vivo. *Nucleus* **7**: 20–6.

Ramachandran S, Henikoff S. 2016b. Transcriptional Regulators Compete with Nucleosomes Post-replication. *Cell* **165**: 580–92.

Rand MD, Grimm LM, Artavanis-Tsakonas S, Patriub V, Blacklow SC, Sklar J, Aster JC. 2000. Calcium depletion dissociates and activates heterodimeric notch receptors. *Mol Cell Biol* **20**: 1825–35.

Ranganathan P, Weaver KL, Capobianco AJ. 2011. Notch signalling in solid tumours: a little bit of everything but not all the time. *Nat Rev Cancer* **11**: 338–351.

Ray-Gallet D, Quivy J-P, Scamps C, Martini EM-D, Lipinski M, Almouzni G. 2002. HIRA is critical for a nucleosome assembly pathway independent of DNA synthesis. *Mol Cell* **9**: 1091–100.

Ray-Gallet D, Woolfe A, Vassias I, Pellentz C, Lacoste N, Puri A, Schultz DC, Pchelintsev NA, Adams PD, Jansen LET, et al. 2011. Dynamics of Histone H3 Deposition In Vivo Reveal a Nucleosome Gap-Filling Mechanism for H3.3 to Maintain Chromatin Integrity. *Mol Cell* **44**: 928–941.

Rebay I, Fehon RG, Artavanis-Tsakonas S. 1993. Specific truncations of Drosophila Notch define dominant activated and dominant negative forms of the receptor. *Cell* **74**: 319–29.

Rhee HS, Pugh BF. 2012. Genome-wide structure and organization of eukaryotic pre-initiation complexes. *Nature* **483**: 295–301.

Ribes V, Briscoe J. 2009. Establishing and interpreting graded Sonic Hedgehog signaling during vertebrate neural tube patterning: the role of negative feedback. *Cold Spring Harb Perspect Biol* **1**: a002014.

Roberts B, Haupt A, Tucker A, Grancharova T, Arakaki J, Fuqua MA, Nelson A, Hookway C, Ludmann SA, Mueller IA, et al. 2017. Systematic gene tagging using CRISPR/Cas9 in human stem cells to illuminate cell organization. *Mol Biol Cell* **28**: 2854–2874.

Robertson AG, Bilenky M, Tam A, Zhao Y, Zeng T, Thiessen N, Cezard T, Fejes AP, Wederell ED, Cullum R, et al. 2008. Genome-wide relationship between histone H3 lysine 4 mono- and tri-methylation and transcription factor binding. *Genome Res* **18**: 1906–17.

Rodman TC. 1967. DNA replication in salivary gland nuclei of Drosophila melanogaster at successive larval and prepupal stages. *Genetics* **55**: 375–86.

Rougvie AE, Lis JT. 1988. *The RNA Polymerase II Molecule at the 5' End of the Uninduced hspTO Gene of D. melanogaster Is Transcriptionally Engaged*.

Rowe CE, Narlikar GJ. 2010. The ATP-dependent remodeler RSC transfers histone dimers and octamers through the rapid formation of an unstable encounter intermediate. *Biochemistry* **49**: 9882–90.

Roy S, VijayRaghavan K. 1997. Homeotic genes and the regulation of myoblast migration, fusion, and fibre-specific gene expression during adult myogenesis in Drosophila. *Development* **124**: 3333–41.

Ryu H, Chung M, Dobrzyński M, Fey D, Blum Y, Lee SS, Peter M, Kholodenko BN, Jeon NL, Pertz O. 2015. Frequency modulation of ERK activation dynamics rewires cell fate. *Mol Syst Biol* **11**: 838.

Saad H, Gallardo F, Dalvai M, Tanguy-le-Gac N, Lane D, Bystricky K. 2014. DNA dynamics during early double-strand break processing revealed by non-intrusive imaging of living cells. *PLoS Genet* **10**: e1004187.

Saha A, Wittmeyer J, Cairns BR. 2005. Chromatin remodeling through directional DNA translocation from an internal nucleosomal site. *Nat Struct Mol Biol* **12**: 747–755.

Sakai A, Schwartz BE, Goldstein S, Ahmad K. 2009. Transcriptional and developmental functions of the H3.3 histone variant in Drosophila. *Curr Biol* **19**: 1816–20.

Sanchez R, Zhou M-M. 2009. The role of human bromodomains in chromatin biology and gene transcription. *Curr Opin Drug Discov Devel* **12**: 659–65.

Sancho R, Cremona CA, Behrens A. 2015. Stem cell and progenitor fate in the mammalian intestine: Notch and lateral inhibition in homeostasis and disease. *EMBO Rep* **16**: 571–81.

Sandén C, Järvstråt L, Lennartsson A, Brattås PL, Nilsson B, Gullberg U. 2014. The DEK oncoprotein binds to highly and ubiquitously expressed genes with a dual role in their transcriptional regulation. *Mol Cancer* **13**: 215.

Saunders A, Core LJ, Sutcliffe C, Lis JT, Ashe HL. 2013. Extensive polymerase pausing during Drosophila axis patterning enables high-level and pliable transcription. *Genes Dev* **27**: 1146–58.

Sawatsubashi S, Murata T, Lim J, Fujiki R, Ito S, Suzuki E, Tanabe M, Zhao Y, Kimura S, Fujiyama S, et al. 2010. A histone chaperone, DEK, transcriptionally coactivates a nuclear receptor. *Genes Dev* **24**: 159–170.

Schaaf CA, Misulovin Z, Gause M, Koenig A, Dorsett D. 2013. The Drosophila enhancer of split gene complex: architecture and coordinate regulation by notch, cohesin, and polycomb group proteins. *G3 (Bethesda)* **3**: 1785–94.

Schindelin J, Arganda-Carreras I, Frise E, Kaynig V, Longair M, Pietzsch T, Preibisch S, Rueden C, Saalfeld S, Schmid B, et al. 2012. Fiji: an open-source platform for biological-image analysis. *Nat Methods* **9**: 676–82.

Schnappauf O, Beyes S, Dertmann A, Freihen V, Frey P, Jägle S, Rose K, Michoel T, Grosschedl R, Hecht A. 2016. Enhancer decommissioning by Snail1-induced competitive displacement of TCF7L2 and down-regulation of transcriptional activators results in EPHB2 silencing. *Biochim Biophys Acta - Gene Regul Mech* **1859**: 1353–1367.

Schneiderman JI, Orsi GA, Hughes KT, Loppin B, Ahmad K. 2012. Nucleosome-depleted chromatin gaps recruit assembly factors for the H3.3 histone variant. *Proc Natl Acad Sci* **109**: 19721–19726.

Schröder S, Herker E, Itzen F, He D, Thomas S, Gilchrist DA, Kaehlcke K, Cho S, Pollard KS, Capra JA, et al. 2013. Acetylation of RNA Polymerase II Regulates Growth-Factor-Induced Gene Transcription in Mammalian Cells. *Mol Cell* **52**: 314–324.

Segal E, Fondufe-Mittendorf Y, Chen L, Thåström A, Field Y, Moore IK, Wang J-PZ, Widom J. 2006. A genomic code for nucleosome positioning. *Nature* **442**: 772–8.

Senecal A, Munsky B, Proux F, Ly N, Braye FE, Zimmer C, Mueller F, Darzacq X. 2014. Transcription factors modulate c-Fos transcriptional bursts. *Cell Rep* **8**: 75–83.

Senger K, Armstrong GW, Rowell WJ, Kwan JM, Markstein M, Levine M. 2004. Immunity regulatory DNAs share common organizational features in Drosophila. *Mol Cell* **13**: 19–32.

Shao W, Zeitlinger J. 2017. Paused RNA polymerase II inhibits new transcriptional initiation. *Nat Genet* **49**: 1045–1051.

Shi J, Zheng M, Ye Y, Li M, Chen X, Hu X, Sun J, Zhang X, Jiang C. 2014. Drosophila Brahma complex remodels nucleosome organizations in multiple aspects. *Nucleic Acids Res* **42**: 9730–9.

Shibahara K, Stillman B. 1999. Replication-dependent marking of DNA by PCNA facilitates CAF-1-coupled inheritance of chromatin. *Cell* **96**: 575–85.

Shlyueva D, Stampfel G, Stark A. 2014. Transcriptional enhancers: from properties to genome-wide predictions. *Nat Rev Genet* **15**: 272–286.

Shu W, Chen H, Bo X, Wang S. 2011. Genome-wide analysis of the relationships between DNaseI HS, histone modifications and gene expression reveals distinct modes of chromatin domains. *Nucleic Acids Res* **39**: 7428–43.

Siersbæk R, Rabiee A, Nielsen R, Sidoli S, Traynor S, Loft A, Poulsen LLC, Rogowska-Wrzesinska A, Jensen ON, Mandrup S. 2014. Transcription factor cooperativity in early adipogenic hotspots and super-enhancers. *Cell Rep* **7**: 1443–1455.

Sirinakis G, Clapier CR, Gao Y, Viswanathan R, Cairns BR, Zhang Y. 2011. The RSC chromatin remodelling ATPase translocates DNA with high force and small step size. *EMBO J* **30**: 2364–2372.

Sjöqvist M, Andersson ER. 2017. Do as I say, Not(ch) as I do: Lateral control of cell fate. *Dev Biol*.

Skalska L, Stojnic R, Li J, Fischer B, Cerda-Moya G, Sakai H, Tajbakhsh S, Russell S, Adryan B, Bray SJ. 2015. Chromatin signatures at Notch-regulated enhancers reveal large-scale changes in H3K56ac upon activation. *EMBO J* **34**: 1889–904.

Skupsky R, Burnett JC, Foley JE, Schaffer D V, Arkin AP. 2010. HIV promoter integration site primarily modulates transcriptional burst size rather than frequency. *PLoS Comput Biol* **6**.

Small S, Blair A, Levine M. 1992. Regulation of even-skipped stripe 2 in the Drosophila embryo. *EMBO J* **11**: 4047–57.

Speiser JJ, Erşahin Ç, Osipo C. 2013. The Functional Role of Notch Signaling in Triple-Negative Breast Cancer. *Vitam Horm* **93**: 277–306.

Spitz F, Furlong EEM. 2012. Transcription factors: from enhancer binding to developmental control. *Nat Rev Genet* **13**: 613–626.

Sriuranpong V, Borges MW, Strock CL, Nakakura EK, Watkins DN, Blaumueller CM, Nelkin BD, Ball DW. 2002. Notch signaling induces rapid degradation of achaete-scute homolog 1. *Mol Cell Biol* **22**: 3129–39.

St Pierre R, Kadoch C. 2017. Mammalian SWI/SNF complexes in cancer: emerging therapeutic opportunities. *Curr Opin Genet Dev* **42**: 56–67.

Stockdale C, Flaus A, Ferreira H, Owen-Hughes T. 2006. Analysis of nucleosome repositioning by yeast ISWI and Chd1 chromatin remodeling complexes. *J Biol Chem* **281**: 16279–88.

Strahl BD, Allis CD. 2000. The language of covalent histone modifications. *Nature* **403**: 41–45.

Strohner R, Wachsmuth M, Dachauer K, Mazurkiewicz J, Hochstatter J, Rippe K, Längst G. 2005. A “loop recapture” mechanism for ACF-dependent nucleosome remodeling. *Nat Struct Mol Biol* **12**: 683–690.

Struhl K, Segal E. 2013. Determinants of nucleosome positioning. *Nat Struct Mol Biol* **20**: 267–73.

Su W, Jackson S, Tjian R, Echols H. 1991. DNA looping between sites for transcriptional activation: self-association of DNA-bound Sp1. *Genes Dev* **5**: 820–6.

Subramanian V, Fields PA, Boyer LA. 2015. H2A.Z: a molecular rheostat for transcriptional control. *F1000Prime Rep* **7**: 01.

Swanson CI, Evans NC, Barolo S. 2010. Structural rules and complex regulatory circuitry constrain expression of a Notch- and EGFR-regulated eye enhancer. *Dev Cell* **18**: 359–70.

Swinstead EE, Paakinaho V, Presman DM, Hager GL. 2016. Pioneer factors and ATP-dependent chromatin remodeling factors interact dynamically: A new perspective. *BioEssays* **38**: 1150–1157.

Takahashi K, Yamanaka S. 2006. Induction of Pluripotent Stem Cells from Mouse Embryonic and Adult Fibroblast Cultures by Defined Factors. *Cell* **126**: 663–676.

Takeuchi JK, Lickert H, Bisgrove BW, Sun X, Yamamoto M, Chawengsaksophak K, Hamada H, Yost HJ, Rossant J, Bruneau BG. 2007. Baf60c is a nuclear Notch signaling component required for the establishment of left–right asymmetry. *Proc Natl Acad Sci* **104**: 846–851.

Tang Y, Zhao W, Chen Y, Zhao Y, Gu W. 2008. Acetylation is indispensable for p53 activation. *Cell* **133**: 612–26.

Taniguchi Y, Karlström H, Lundkvist J, Mizutani T, Otaka A, Vestling M, Bernstein A, Donoviel D, Lendahl U, Honjo T. 2002. Notch receptor cleavage depends on but is not directly executed by presenilins. *Proc Natl Acad Sci* **99**: 4014–4019.

Tantale K, Mueller F, Kozulic-Pirher A, Lesne A, Victor J-M, Robert M-C, Capozi S, Chouaib R, Bäcker V, Mateos-Langerak J, et al. 2016. A single-molecule view of transcription reveals convoys of RNA polymerases and multi-scale bursting. *Nat Commun* **7**: 12248.

Tay S, Hughey JJ, Lee TK, Lipniacki T, Quake SR, Covert MW. 2010. Single-cell NF-kappaB dynamics reveal digital activation and analogue information processing. *Nature* **466**: 267–71.

Taylor IC, Workman JL, Schuetz TJ, Kingston RE. 1991. Facilitated binding of GAL4 and heat shock factor to nucleosomal templates: differential function of DNA-binding domains. *Genes Dev* **5**: 1285–98.

Terriente-Félix A, de Celis JF. 2009. Osa, a subunit of the BAP chromatin-remodelling complex, participates in the regulation of gene expression in response to EGFR signalling in the Drosophila wing. *Dev Biol* **329**: 350–361.

Terriente-Felix A, Li J, Collins S, Mulligan A, Reekie I, Bernard F, Krejci A, Bray S. 2013. Notch cooperates with Lozenge/Runx to lock haemocytes into a differentiation programme. *Development* **140**: 926–937.

Teves SS, Deal RB, Henikoff S. 2012. Measuring genome-wide nucleosome turnover using CATCH-IT. *Methods Enzymol* **513**: 169–84.

Thanos D, Maniatis T. 1995. Virus induction of human IFN beta gene expression requires the assembly of an enhanceosome. *Cell* **83**: 1091–100.

Titov D V, Gilman B, He Q-L, Bhat S, Low W-K, Dang Y, Smeaton M, Demain AL, Miller PS, Kugel JF, et al. 2011. XPB, a subunit of TFIIH, is a target of the natural product triptolide. *Nat Chem Biol* **7**: 182–8.

Torres IO, Kuchenbecker KM, Nnadi CI, Fletterick RJ, Kelly MJS, Fujimori DG. 2015. Histone demethylase KDM5A is regulated by its reader domain through a positive-feedback mechanism. *Nat Commun* **6**: 6204.

Tsuda M, Takahashi S, Takahashi Y, Asahara H. 2003. Transcriptional Co-activators CREB-binding Protein and p300 Regulate Chondrocyte-specific Gene Expression via Association with Sox9. *J Biol Chem* **278**: 27224–27229.

Udugama M, M Chang FT, Chan FL, Tang MC, Pickett HA, R McGhie JD, Mayne L, Collas P, Mann JR, Wong LH. 2015. Histone variant H3.3 provides the heterochromatic H3 lysine 9 tri-methylation mark at telomeres. *Nucleic Acids Res* **43**: 10227–37.

Udugama M, Sabri A, Bartholomew B. 2011. The INO80 ATP-Dependent Chromatin Remodeling Complex Is a Nucleosome Spacing Factor. *Mol Cell Biol* **31**: 662–673.

VanderWielen BD, Yuan Z, Friedmann DR, Kovall RA. 2011. Transcriptional repression in the Notch pathway: thermodynamic characterization of CSL-MINT (Msx2-interacting nuclear target protein) complexes. *J Biol Chem* **286**: 14892–902.

Varnum-Finney B, Wu L, Yu M, Brashem-Stein C, Staats S, Flowers D, Griffin JD, Bernstein ID. 2000. Immobilization of Notch ligand, Delta-1, is required for induction of notch signaling. *J Cell Sci* **113 Pt 23**: 4313–8.

Venkatesh S, Workman JL. 2015. Histone exchange, chromatin structure and the regulation of transcription. *Nat Rev Mol Cell Biol* **16**: 178–189.

Vispe S, DeVries L, Creancier L, Besse J, Breand S, Hobson DJ, Svejstrup JQ, Annereau J-P, Cussac D, Dumontet C, et al. 2009. Triptolide is an inhibitor of RNA polymerase I and II-dependent transcription leading predominantly to down-regulation of short-lived mRNA. *Mol Cancer Ther* **8**: 2780–2790.

Voss TC, Schiltz RL, Sung M-H, Yen PM, Stamatoyannopoulos JA, Biddie SC, Johnson TA, Miranda TB, John S, Hager GL. 2011. Dynamic exchange at regulatory elements during chromatin remodeling underlies assisted loading mechanism. *Cell* **146**: 544–54.

Wallberg AE, Pedersen K, Lendahl U, Roeder RG. 2002. p300 and PCAF act cooperatively to mediate transcriptional activation from chromatin templates by notch intracellular domains in vitro. *Mol Cell Biol* **22**: 7812–9.

Wang H, Zang C, Taing L, Arnett KL, Wong YJ, Pear WS, Blacklow SC, Liu XS, Aster JC. 2014a. NOTCH1-RBPJ complexes drive target gene expression through dynamic interactions with superenhancers. *Proc Natl Acad Sci* **111**: 705–710.

Wang H, Zou J, Zhao B, Johannsen E, Ashworth T, Wong H, Pear WS, Schug J, Blacklow SC, Arnett KL, et al. 2011. Genome-wide analysis reveals conserved and divergent features of Notch1/RBPJ binding in human and murine T-lymphoblastic leukemia cells. *Proc Natl Acad Sci U S A* **108**: 14908–13.

Wang J, Scully K, Zhu X, Cai L, Zhang J, Prefontaine GG, Krones A, Ohgi KA, Zhu P, Garcia-Bassets I, et al. 2007. Opposing LSD1 complexes function in developmental gene activation and repression programmes. *Nature* **446**: 882–887.

Wang L, Du Y, Ward JM, Shimbo T, Lackford B, Zheng X, Miao Y, Zhou B, Han L, Fargo DC, et al. 2014b. INO80 Facilitates Pluripotency Gene Activation in Embryonic Stem Cell Self-Renewal, Reprogramming, and Blastocyst Development. *Cell Stem Cell* **14**: 575–591.

Wang Y, Ni T, Wang W, Liu F. 2018. Gene transcription in bursting: a unified mode for realizing accuracy and stochasticity. *Biol Rev*.

Watanabe S, Tan D, Lakshminarasimhan M, Washburn MP, Hong E-JE, Walz T, Peterson CL. 2015. Structural analyses of the chromatin remodelling enzymes INO80-C and SWR-C. *Nat Commun* **6**: 7108.

Weber CM, Ramachandran S, Henikoff S. 2014. Nucleosomes are context-specific, H2A.Z-modulated barriers to RNA polymerase. *Mol Cell* **53**: 819–30.

Wech I, Bray S, Delidakis C, Preiss A. 1999. Distinct expression patterns of different Enhancer of split bHLH genes during embryogenesis of Drosophila melanogaster. *Dev Genes Evol* **209**: 370–375.

Wehler P, Niopek D, Eils R, Di Ventura B. 2016. Optogenetic Control of Nuclear Protein Import in Living Cells Using Light-Inducible Nuclear Localization Signals (LINuS). In *Current Protocols in Chemical Biology*, Vol. 8 of, pp. 131–145, John Wiley & Sons, Inc., Hoboken, NJ, USA.

Weng L, Zhu C, Xu J, Du W. 2003. Critical role of active repression by E2F and Rb proteins in endoreplication during Drosophila development. *EMBO J* **22**: 3865–75.

West JA, Cook A, Alver BH, Stadtfeld M, Deaton AM, Hochedlinger K, Park PJ, Tolstorukov MY, Kingston RE. 2014. Nucleosomal occupancy changes locally over key regulatory regions during cell differentiation and reprogramming. *Nat Commun* **5**: 4719.

Westermark PO. 2016. Linking Core Promoter Classes to Circadian Transcription. *PLoS Genet* **12**: e1006231.

Whitehouse I, Flaus A, Cairns BR, White MF, Workman JL, Owen-Hughes T. 1999. Nucleosome mobilization catalysed by the yeast SWI/SNF complex. *Nature* **400**: 784–787.

Williamson I, Lettice LA, Hill RE, Bickmore WA. 2016. Shh and ZRS enhancer colocalisation is specific to the zone of polarising activity. *Development* **143**: 2994–3001.

Wilson JJ, Kovall RA. 2006. Crystal structure of the CSL-Notch-Mastermind ternary complex bound to DNA. *Cell* **124**: 985–96.

Wirbelauer C, Bell O, Schübeler D. 2005. Variant histone H3.3 is deposited at sites of nucleosomal displacement throughout transcribed genes while active histone modifications show a promoter-proximal bias. *Genes Dev* **19**: 1761–1766.

Wu G, Lyapina S, Das I, Li J, Gurney M, Pauley A, Chui I, Deshaies RJ, Kitajewski J. 2001. SEL-10 is an inhibitor of notch signaling that targets notch for ubiquitin-mediated protein degradation. *Mol Cell Biol* **21**: 7403–15.

Wu Q, Madany P, Akech J, Dobson JR, Douthwright S, Browne G, Colby JL, Winter GE, Bradner JE, Pratap J, et al. 2015. The SWI/SNF ATPases Are Required for Triple Negative Breast Cancer Cell Proliferation. *J Cell Physiol* **230**: 2683–94.

Xu X, Yin Z, Hudson JB, Ferguson EL, Frasch M. 1998. Smad proteins act in combination with synergistic and antagonistic regulators to target Dpp responses to the Drosophila mesoderm. *Genes Dev* **12**: 2354–70.

Yamaguchi Y, Shibata H, Handa H. 2013. Transcription elongation factors DSIF and NELF: Promoter-proximal pausing and beyond. *Biochim Biophys Acta - Gene Regul Mech* **1829**: 98–104.

Yang JG, Madrid TS, Sevastopoulos E, Narlikar GJ. 2006. The chromatin-remodeling enzyme ACF is an ATP-dependent DNA length sensor that regulates nucleosome spacing. *Nat Struct Mol Biol* **13**: 1078–1083.

Yang Z, Yik JHN, Chen R, He N, Jang MK, Ozato K, Zhou Q. 2005. Recruitment of P-TEFb for Stimulation of Transcriptional Elongation by the Bromodomain Protein Brd4. *Mol Cell* **19**: 535–545.

Yao J, Ardehali MB, Fecko CJ, Webb WW, Lis JT. 2007. Intranuclear distribution and local dynamics of RNA polymerase II during transcription activation. *Mol Cell* **28**: 978–90.

Yao J, Munson KM, Webb WW, Lis JT. 2006. Dynamics of heat shock factor association with native gene loci in living cells. *Nature* **442**: 1050–1053.

Yao J, Zobeck KL, Lis JT, Webb WW. 2008. Imaging transcription dynamics at endogenous genes in living Drosophila tissues. *Methods* **45**: 233–41.

Yatim A, Benne C, Sobhian B, Laurent-Chabalier S, Deas O, Judde J-G, Lelievre J-D, Levy Y, Benkirane M. 2012. NOTCH1 nuclear interactome reveals key regulators of its transcriptional activity and oncogenic function. *Mol Cell* **48**: 445–58.

Yildirim O, Hung J-H, Cedeno RJ, Weng Z, Lengner CJ, Rando OJ. 2014. A System for Genome-Wide Histone Variant Dynamics In ES Cells Reveals Dynamic MacroH2A2 Replacement at Promoters ed. B. Ren. *PLoS Genet* **10**: e1004515.

Yu S, Waldholm J, Böhm S, Visa N. 2014. Brahma regulates a specific trans-splicing event at the mod(mdg4) locus of Drosophila melanogaster. *RNA Biol* **11**: 134–45.

Yu Z, Wu H, Chen H, Wang R, Liang X, Liu J, Li C, Deng W-M, Jiao R. 2013. CAF-1 promotes Notch signaling through epigenetic control of target gene expression during Drosophila development. *Development* **140**: 3635–44.

Yuan X, Wu H, Xu H, Xiong H, Chu Q, Yu S, Wu GS, Wu K. 2015. Notch signaling: An emerging therapeutic target for cancer treatment. *Cancer Lett* **369**: 20–27.

Yuan Z, Praxenthaler H, Tabaja N, Torella R, Preiss A, Maier D, Kovall RA. 2016. Structure and Function of the Su(H)-Hairless Repressor Complex, the Major Antagonist of Notch Signaling in Drosophila melanogaster. *PLoS Biol* **14**: e1002509.

Zaret KS, Carroll JS. 2011. Pioneer transcription factors: establishing competence for gene expression. *Genes Dev* **25**: 2227–41.

Zaret KS, Mango SE. 2016. Pioneer transcription factors, chromatin dynamics, and cell fate control. *Curr Opin Genet Dev* **37**: 76–81.

Zeitlinger J, Stark A, Kellis M, Hong J-W, Nechaev S, Adelman K, Levine M, Young RA. 2007a. RNA polymerase stalling at developmental control genes in the Drosophila melanogaster embryo. *Nat Genet* **39**: 1512–1516.

Zeitlinger J, Zinzen RP, Stark A, Kellis M, Zhang H, Young RA, Levine M. 2007b. Whole-genome ChIP-chip analysis of Dorsal, Twist, and Snail suggests integration of diverse patterning processes in the Drosophila embryo. *Genes Dev* **21**: 385–90.

Zhang F, Wen Y, Guo X. 2014. CRISPR/Cas9 for genome editing: progress, implications and challenges. *Hum Mol Genet* **23**: R40–R46.

Zhang Y, Moqtaderi Z, Rattner BP, Euskirchen G, Snyder M, Kadonaga JT, Liu XS, Struhl K. 2009. Intrinsic histone-DNA interactions are not the major determinant of nucleosome positions in vivo. *Nat Struct Mol Biol* **16**: 847–52.

Zhang Y, Smith CL, Saha A, Grill SW, Mihardja S, Smith SB, Cairns BR, Peterson CL, Bustamante C. 2006. DNA translocation and loop formation mechanism of chromatin remodeling by SWI/SNF and RSC. *Mol Cell* **24**: 559–68.

Zhang Z, English BP, Grimm JB, Kazane SA, Hu W, Tsai A, Inouye C, You C, Piehler J, Schultz PG, et al. 2016. Rapid dynamics of general transcription factor TFIIB binding during preinitiation complex assembly revealed by single-molecule analysis. *Genes Dev* **30**: 2106–2118.

Zhu F, Farnung L, Kaasinen E, Sahu B, Yin Y, Wei B, Dodonova SO, Nitta KR, Morgunova E, Taipale M, et al. 2018. The interaction landscape between transcription factors and the nucleosome. *Nature* **562**: 76–81.

Zofall M, Persinger J, Kassabov SR, Bartholomew B. 2006. Chromatin remodeling by ISW2 and SWI/SNF requires DNA translocation inside the nucleosome. *Nat Struct Mol Biol* **13**: 339–346.

Zraly CB, Middleton FA, Dingwall AK. 2006. Hormone-response genes are direct in vivo regulatory targets of Brahma (SWI/SNF) complex function. *J Biol Chem* **281**: 35305–15.

7 APPENDICES

Appendix 1: Video information 166

Appendix 2: MATLAB scripts for cell tracking.....167

Appendix 3: R scripts for MS2 data processing.....170

APPENDIX 1: VIDEO INFORMATION

All videos show maximum projections of live GFP imaging. Time stamps shown are in minutes and second.

Video 1. Live imaging of Notch-dependent transcription. mβ MS2 cells imaged live before and after EGTA-induced Notch activation. Fluorescent foci appear rapidly in many cells, before disappearing more slowly. Time after EGTA addition is shown.

Video 2. Transcription foci do not appear under control conditions. After addition of PBS, with EGTA excluded, there is no transcriptional response comparable to that shown in Video 1 in mβ MS2 cells. Time after PBS addition is shown.

Video 3. Removal of the blasticidin cassette did not dramatically alter the Notch-dependent transcriptional response. Live imaging of "Clone cells", produced by flippase-induced recombination and cell cloning, after EGTA-induced Notch activation. Cells have a similar response to that shown in Video 1. Note that many Clone cells have two transcription foci, indicating that two copies of the edited *E(spl)mβ-HLH* gene are present. Time after EGTA addition is shown.

Video 4. MG132 perturbs the transcriptional response to EGTA. mβ MS2 cells do not show the normal transcriptional response to EGTA after treatment with MG132. Most cells do not respond, while a small proportion display a delayed response. Time after EGTA addition is shown.

Video 5. The transcriptional response to ligand-induced Notch activation. Live imaging of mβ MS2 cells co-cultured with Delta-expressing S2 cells. The mβ MS2 cells settle onto the plate at different times and form contacts with the S2 cells. Transcription foci are visible in mβ MS2 cells after they appear. (Left) MCP-GFP fluorescence from the mβ MS2 cells. (Right) Bright field imaging (greyscale) overlaid with GFP fluorescence (green). mβ MS2 cells are distinguished from the S2 cells by the presence of MCP-GFP. Time after addition of mβ MS2 cells is shown.

APPENDIX 2: MATLAB SCRIPTS FOR CELL TRACKING

In order to obtain quantitative data from the MS2 imaging experiments, the following code was used with MATLAB (MATLAB Release 2016b, The Mathworks, Inc.) to segment and track cells from maximum projection tiff files. This code was written by Julia Falo-Sanjuan, Bray laboratory, and relies on further functions available at https://github.com/juliafs93/MS2_cells/. Comments are written after the % symbol and shown here in grey.

```
%%%%%%%%%%%%%%%%%%%%%%%%%%%%%%%%%%%%%%%%%%%%%%%%%%%%%%%%%%%%%%%%%%%%%%%%
%%% CODE USED FOR EGTA-INDUCED NOTCH ACTIVATION EXPERIMENTS %%%
%%%%%%%%%%%%%%%%%%%%%%%%%%%%%%%%%%%%%%%%%%%%%%%%%%%%%%%%%%%%%%%%%%%%%%%%
% Start by running this line of code:
manual = true

%% Read in tiff tile:
if manual == true
  clear all
  [File,Path] = uigetfile('*.tif');
  Name = '_segmented/'
  mkdir([Path,File,Name])
  PathToSave = [Path,File,Name,File];
  show = 'on'
else
  show = 'off'
end

%% Setting parameters:
mkdir([Path,File,Name])

% Uses try and catch functions to import previous parameters if
they have been saved previously. Otherwise, sets new parameters.
Note that the “T0” parameter should be set to the first frame to
be analysed.
try
  Parameters = …
       readtable([Path,File,Name,File,'_parameters.txt']);
  for x = …
       [1:length(Parameters.Properties.VariableNames)]
    command = …
       strcat(char(Parameters.Properties.VariableNames(x)), …
       '=', num2str(Parameters.(x)));
    eval(command)
  end
  skip = true
catch
  disp('couldnt read parameters, set them below (press any …
 key to continue)')
  pause
  [Bits, Width,Height, Channels, SlicesO, FramesO,XRes, …
       YRes, ZRes] = readMetadata(Path, File)
  try
  XYRes=round(mean([XRes,YRes]),2);
  ZRes = round(ZRes,2);
  end
  Y0 = 1 % Y start, pixels, default 1
  Yf = Height % Y end, pixels, default Height
  X0 = 1 % X start, pixels, default 1
```

```
  Xf = Width % X end, pixels, default Width
  Z0 = 1 % Z start, pixels, default 1
  Zf = Slices0 % Z end, pixels, default Slices
  T0 = 1 % T start, frame, default 1
  Tf = Frames0-1 % T end, frame, default Frames
  Z0toSeg = 1 % Z start for segmentation, pixels, default 1
  ZftoSeg = Slices0 % Z start for segmentation, pixels, default
       Slices
  skip = false
  TimeRes=9.816; % set time resolution
End

%% Segmentation and tracking:
A = Read5d([Path,File], Channels, Slices0, Frames0);
disp('read 5d')
B = A(Y0:Yf, X0:Xf,:,Z0:Zf,T0:Tf);
Frames = size(B,5)
Slices = size(B,4)
clear A

GFP_max_proj = MAX_proj(B, 1,Frames, 1,Slices,1);

% parameters to segment and track cells:
MedianFilt = 3;
InputLow = 0;
InputHigh = 0.4;
RadiusMin = 3;
RadiusMax = 10;
Sensitivity = 0.95;
Distance = 15;
MaxN = 5;

% Filtering:
[toThresholdG] = Filter_3D(GFP_max_proj, MedianFilt, 'off');

% Increasing contrast:
[toThreshold3G] = ContrastMSD(toThresholdG, InputLow, …
       InputHigh,Bits,show);

% Segmenting cells:
[FTL_G FTL_RGB_G Stats_table_G] = SegmentNuc(toThreshold3G,…
       @FindCircles, num2cell([RadiusMin RadiusMax …
       Sensitivity]), Bits, show);

% Tracking cells:
cmap = jet(100000);
cmap_shuffled = cmap(randperm(size(cmap,1)),:);
[FTL_tracked FTL_tracked_RGB Stats_tracked] = Tracking(FTL_G,…
       Stats_table_G, cmap_shuffled, Distance,MaxN,'off',show);
[boundariesBW boundariesL boundaries_RGB] = …
       BoundariesTracked(FTL_tracked,cmap_shuffled,show);
WriteRGB(boundaries_RGB, PathToSave, …
       '_segmented_tracked_boundaries_RGB.tiff','none')
Write8b(boundariesL, PathToSave, …
       '_segmented_tracked_boundariesL.tiff')

% Measure and save F (fluorescence); save movies by F levels:
[Stats_GFP MaxF MinF] = getStatsF(FTL_tracked, GFP_max_proj);
[Stats_GFP] = printF(Stats_GFP,Path,File,Name,'on');
[FTL_tracked_meanF] = replaceLabelsbyF(FTL_tracked,…
       Stats_GFP,1,2^Bits-1,'Max');
Merged_meanF_maxGFP = (GFP_max_proj./(2.^(Bits-8)) …
       +FTL_tracked_meanF);
Write8b(Merged_meanF_maxGFP, PathToSave, '_maxF_maxGFP.tiff')
```

```
% Save all images and parameters:
Baseline=0;
parameters = table(Bits,Channels, SlicesO, FramesO,Slices…
      Frames,Width,Height,X0,Xf,Y0,Yf,Z0,Zf,T0,Tf,Z0toSeg,…
      ZftoSeg,MedianFilt,InputLow,InputHigh,RadiusMin,…
      RadiusMax,Sensitivity,Distance,MaxN,TimeRes,XYRes,ZRes);
writetable(parameters,[Path,File,Name,File,'_parameters.txt']);

Metadata = readtable(…
      '~/MATLAB_R_scripts/metadata MS2_cells_new.txt',…
      'Delimiter', '\t');
NewMetadata = cell2table({Path,File,Name,Frames,Bits,TimeRes,…
      XYRes,ZRes,Baseline},'VariableNames', {'Path','File',…
      'Name','Frames','Bits','TimeRes','XYRes','ZRes',…
      'Baseline'});
SaveMetadata = [Metadata;NewMetadata];
writetable(SaveMetadata,…
      '~/MATLAB_R_scripts/metadata MS2_cells_new.txt',…
      'Delimiter', '\t');

system('/usr/local/bin/Rscript --verbose …
      ~/MATLAB_R_scripts/RunfromMatlabZoe.R ');

FTL_tracked_meanF_maxGFP_noB_selected = …
      ~boundariesL.*Merged_meanF_maxGFP;
[FTL_tracked_meanF_maxGFP_boundaries_selected] = …
      Merge8bRGB(FTL_tracked_meanF_maxGFP_noB_selected,…
      boundaries_RGB,show);
Factor = 2;
printLabels_new(FTL_tracked_meanF_maxGFP_boundaries_selected,…
      Stats_GFP,Factor,'off', PathToSave,…
'_segmented_tracked_info.tiff','packbits')
disp('done')

%%%%%%%%%%%%%%%%%%%%%%%%%%%%%%%%%%%%%%%%%%%%%%%%%%%%%%%%%%%%%%%%%%%%%%%%%%%%%%%
%%%%%%%%%%%% CODE USED FOR CO-CULTURE EXPERIMENTS %%%%%%%%%%%%%%%%%%%%%%%%%%%%%
%%%%%%%%%%%%%%%%%%%%%%%%%%%%%%%%%%%%%%%%%%%%%%%%%%%%%%%%%%%%%%%%%%%%%%%%%%%%%%%
% Due to lower numbers of cells in the co-culture experiments,
slightly different parameters were required for the segmentation
and tracking. Therefore, the code used was the same as above,
with the following parameters substituted at the relevant
section.
  % parameters to segment and track cells:
MedianFilt = 3;
InputLow = 0.2;
InputHigh = 0.8;
RadiusMin = 7;
RadiusMax = 12;
Sensitivity = 0.94;
Distance = 15;
MaxN = 5;
```

APPENDIX 3: R SCRIPTS FOR MS2 DATA PROCESSING

The output from the MATLAB script for cell tracking is a file called "F_selected.txt", which contains maximum fluorescence values for each cell over time. The following code was used with R (R Core Team, R Foundation for Statistical Computing) to process the data as described in the Materials and methods and perform analyses. Comments are written after the # symbol and shown here in grey.

```
# Start by manually setting the working directory to the folder
containing the correct data file. Load the ggplot2 library:
library(ggplot2)

#####################################################################
#################### DATA PROCESSING ################################
#####################################################################
# Reading in data:
# Reads F_selected file and selects the columns of interest.
F_selected <- read.delim("F_selected.txt", sep="\t", header=T,
      stringsAsFactors=F)
head(F_selected)
OriginalData <- F_selected[,c(6,7,14,15)]
head(OriginalData)

# Removing short tracks:
# Uses tabulate function to get the number of occurrences of
each label, which is the number of frames each cell is present
for. Puts these numbered in a data frame, so that after short
tracks are removed, the labels remain. Finally, subsets the data
to include only those rows where the labels match the
"CutoffLabels". The "Cutoff" is the minimum number of frames to
still be included (set to 360 frames = around 1 hour).
AllOccurences <- data.frame(1:max(OriginalData$Label),
      tabulate(OriginalData$Label))
Cutoff <- 360
CutoffOccurences <- subset(AllOccurences,
      AllOccurences[,2]>=Cutoff)
CutoffLabels <- as.vector(CutoffOccurences[,1])
CutoffData <- subset(OriginalData, OriginalData$Label %in%
      CutoffLabels)

# Smoothing data:
# Aim is to calculate a moving average over 5 time points. Uses
a loop to do this for each cell. First, creates an empty data
frame "SmoothData". Then for each cell in the "CutoffData",
subsets the cell, and uses the filter function to calculate the
moving average. The sides=2 means that the average is calculated
using both the values before and after the current value. Each
cell that is processed is added to the "SmoothData" dataframe.
Important to use the "CutoffData" for this, otherwise the filter
function gets stuck on any cells where there are less than 5
time points.
SmoothData <- data.frame()
for (n in unique(CutoffData$Label)) {
  CellX <- subset(CutoffData, CutoffData$Label==n)
  CellX$MaxIntensity <- filter(CellX$MaxIntensity/5, rep(1,5),
      sides=2)
  CellX$MaxIntensity <- as.numeric(CellX$MaxIntensity)
```

```
  SmoothData <- rbind(SmoothData, CellX)
  cat("Cell number", n, "has been smoothed.", "\n")
}

# Removing background with a regression line:
# NA values are removed. Then all the values that fall within
the lower quartile are made into a subset. A regression line is
found for these values. Values are predicted from the regression
line - the whole dataset is an argument for this so that values
are predicted across the whole time, not only for those sections
of the graph below the lower quartile. The differences between
the measured and predicted values are found, and these are added
as a column in the dataset.
SignalData <- data.frame()
for (n in unique(SmoothData$Label)) {
  CellX <- subset(SmoothData, SmoothData$Label==n)
  CellX <- na.omit(CellX)
  lowerQX <- quantile(CellX$MaxIntensity, probs=0.25)
  LowValuesX <- subset(CellX, CellX$MaxIntensity<=lowerQX)
  line <- lm(MaxIntensity~Time, data=LowValuesX)
  PredictedValuesX <- predict(line, CellX)
  DifferencesX <- CellX$MaxIntensity - PredictedValuesX
  CellX <- cbind(CellX, DifferencesX)
  SignalData <- rbind(SignalData, CellX)
  cat("Background has been removed from cell number", n, ".",
      "\n")
}

# Plotting the data after background removal:
# All of the data is plotted as a PDF at this point so that it
can be analysed by eye. The height of the PDF should be adjusted
for how many graphs (individual cells) are to be plotted:
head(SignalData)
length(unique(SignalData$Label))
pdf("SignalData.pdf", width=7.5, height=200)
g <- ggplot(SignalData, aes(x=Time, y=DifferencesX,
      colour=Label)) +geom_line()
g <- g + theme(legend.position="none")
g <- g + facet_wrap(~Label, ncol=3)
g <- g + ylim(-500, 3500)
g <- g + labs(x="Time /mins", y="Fluorescence")
print(g)
dev.off()

# To save and re-open the data as a text file for later:
write.table(SignalData, file="SignalData.txt", sep="\t",
      row.names=F, col.names=T)
SignalData <- read.delim("SignalData.txt", sep="\t", header=T,
      stringsAsFactors=F)

#####################################################################
################ CATEGORISATION OF TRACKS ######################
#####################################################################
# The cells are manually divided into responding, non-responding
and problematic based on their tracks from the PDF file, and
their labels are saved in an excel csv file. This code reads
that data in, then divides the “SignalData” into the three
subsets.
CategorisedTracks <- read.csv("CategorisedTracks.csv",
      stringsAsFactors=F, header=T)
RespondingCells <- CategorisedTracks$RespondingCell
NonRespondingCells <- CategorisedTracks$NonRespondingCell
ProblematicTracks <- CategorisedTracks$ProblematicTrack
RespondingSignalData <- subset(SignalData, SignalData$Label
      %in% unique(RespondingCells))
```

```
NonRespondingSignalData <- subset(SignalData, SignalData$Label
      %in% unique(NonRespondingCells))
ProblematicSignalData <- subset(SignalData, SignalData$Label
      %in% unique(ProblematicTracks))
RespondingSignalData$Label <- as.factor(as.numeric
      (RespondingSignalData$Label))
NonRespondingSignalData$Label <- as.factor(as.numeric
      (NonRespondingSignalData$Label))
ProblematicSignalData$Label <- as.factor(as.numeric
      (ProblematicSignalData$Label))

# Counts the number of cells in each category and calculates a
percentage responding (not including the problematic tracks):
length(unique(RespondingSignalData$Label))
length(unique(NonRespondingSignalData$Label))
length(unique(ProblematicSignalData$Label))
PercentageResponding <- (length(unique(
      RespondingSignalData$Label)) /
      (length(unique(RespondingSignalData$Label)) +
      length(unique(NonRespondingSignalData$Label)))) *100
NumberRespondingStats <- data.frame(NResponding=
      length(unique(RespondingSignalData$Label)),
      NNonResponding=length(unique(
      NonRespondingSignalData$Label)),
      NProblematicTracks=length(unique(
      ProblematicSignalData$Label)),
      PercentageResponding=PercentageResponding)
write.table(NumberRespondingStats,
      file="NumberRespondingStats.txt", sep="\t",
      row.names=F, col.names=T)


#################################################################
########### FINDING MEAN AND STANDARD DEVIATION ################
#################################################################
# Finding the mean for the responding cells and saving into a
data frame (similar code was used for non-responding cells):
RespondingMeanData <- data.frame()
for (n in unique(RespondingSignalData$Frame)) {
  FrameX <- subset(RespondingSignalData,
RespondingSignalData$Frame==n)
  MeanIntensityX <- mean(FrameX$DifferencesX)
  MeanDataEntry <- data.frame(Frame=n, Time=mean(FrameX$Time),
          Mean=MeanIntensityX)
  RespondingMeanData <- rbind(RespondingMeanData,
          MeanDataEntry)
}

# Finding the standard deviation and adding to data frame of
means:
RespondingSDData <- data.frame()
for (n in unique(RespondingSignalData$Frame)) {
  FrameX <- subset(RespondingSignalData,
      RespondingSignalData$Frame==n)
  SDX <- sd(FrameX$DifferencesX)
  SDDataEntry <- data.frame(Frame=n, Time=mean(FrameX$Time),
      SD=SDX)
  RespondingSDData <- rbind(RespondingSDData, SDDataEntry)
}
SD <- RespondingSDData$SD
RespondingMeanData <- cbind(RespondingMeanData, SD)

# Plotting a graph with mean and standard deviation and saving
as EPS file:
g <- ggplot(RespondingMeanData, aes(Time))
```

```
g <- g + geom_errorbar(aes(ymax=(Mean+SD), ymin=(Mean-SD)),
      color="gray80")
g <- g + geom_line(aes(y=Mean), size=1.5, color="#05BE78")
g <- g + ylim(-100, 1300)
g <- g + scale_x_continuous(limits = c(0, 120), breaks = c(0,
      30, 60, 90, 120))
g <- g + theme_classic()
g <- g + theme(legend.position="none")
g <- g + labs(x="Time /mins", y="Mean Fluorescence Intensity")
g <- g + ggtitle("Responding Cells")
print(g)
ggsave(file="RespondingCellsMean.eps", width=10, height=7,
      units="cm")


#################################################################
############ INVESTIGATING BASELINE FLUORESCENCE ################
#################################################################
# Testing if focus intensity correlates with background MCP-GFP
fluorescence:
# Tests whether the maximum increase in fluorescence intensity
correlates with the mean background fluorescence. Uses the same
lower quartile method to find the background regression line,
then finds the mean of this line for an approximate general
background level for each cell. Writes this information into a
new data frame.
CellStats <- data.frame()
for (n in unique(RespondingSignalData$Label)) {
  CellX <- subset(RespondingSignalData,
      RespondingSignalData$Label==n)
  lowerQX <- quantile(CellX$MaxIntensity, probs=0.25)
  LowValuesX <- subset(CellX, CellX$MaxIntensity<=lowerQX)
  line <- lm(MaxIntensity~Time, data=LowValuesX)
  PredictedValuesX <- predict(line, CellX)
  IntensityX <- mean(PredictedValuesX)
  MaxX <- max(CellX$MaxIntensity)
  MaxDifferenceX <- max(CellX$DifferencesX)
  DataEntryX <- data.frame(Label=n, Background=IntensityX,
      Max=MaxX, MaxDifference=MaxDifferenceX)
  CellStats <- rbind(CellStats, DataEntryX)
}

# Plotting increased fluorescence against background:
g <- ggplot(CellStats, aes(x=Background, y=MaxDifference))
g <- g + geom_point(color="#05BE78")
g <- g + xlim(0, 2000)
g <- g + ylim(0, 4000)
g <- g + theme_classic()
g <- g + theme(legend.position="none")
g <- g + labs(x="Background fluorescence", y="Maximum
      fluorescence increase")
print(g)
ggsave(file="RespondingCellsIncreaseCorrelation.eps",
      width=10, height=7, units="cm")

# Finding correlation coefficient the graph:
str(CellStats)
cor.test(CellStats$Background, CellStats$MaxDifference,
      method="pearson")
```

```
#####################################################################
#################### ON-OFF ANALYSIS ################################
#####################################################################
# Detecting when transcription is "on":
# Code uses a for loop to run through all of the data and makes
a new column called “OnOff” which will be 1s and zeros. Uses a
moving value called “Transcription” which starts as zero but
will be changed to 1 if at least 15 frames are above the
threshold value 250, and will only be changed back to zero if at
least 15 frames are below the threshold value 250. This uses the
function all() which asks if all 15 values are above threshold
and gives the output TRUE/FALSE/NA. The if function is used to
change the value of “Transcription” depending on the output of
the all() functions.
 OnOff <- RespondingSignalData$DifferencesX
Transcription <- 0
for (n in 1:length(OnOff)) {
  A <- all(OnOff[c(n,n+(1:14))] > 250)
  B <- all(OnOff[c(n,n+(1:14))] <= 250)
  if (Transcription==0 & isTRUE(A)) {
    Transcription <- 1
  } else if (Transcription==1 & isTRUE(B)) {
    Transcription <- 0
  }
  OnOff[n] <- Transcription
}
RespondingSignalDataOnOff <- cbind(RespondingSignalData,
      OnOff)


#####################################################################
######## FINDING TRANSCRIPTION START AND END TIMES #############
#####################################################################
# Finding the time on and off:
# Uses the match function to find the first occurrence of a 1 in
the “OnOff” column of the data. Converts this from a frame to a
time. Then makes a new column in “SignalData”, “OffOn”,
reversing the order of the 1s and 0s, and finds the first (last)
occurrence of a 1. Total number of frames minus this "first"
occurrence gives the frame of the last occurrence. Converts this
to a time. Adds these data to a new data frame for the
“TimeStats”.
TimeStats <- data.frame()
for (n in unique(RespondingSignalDataOnOff$Label)) {
  CellX <- subset(RespondingSignalDataOnOff,
      RespondingSignalDataOnOff$Label==n)
  OnX <- match(1, CellX$OnOff)
  OnX <- OnX * 0.1636
  CellX$OffOn <- rev(CellX$OnOff)
  OffX <- match(1, CellX$OffOn)
  OffX <- max(CellX$Frame) - OffX
  OffX <- OffX * 0.1636
  TimeStatsEntryX <- data.frame(Label=n, TimeOn=OnX,
      TimeOff=OffX)
  TimeStats <- rbind(TimeStats, TimeStatsEntryX)
}

# Plotting “TimeOn” and “TimeOff” on a histogram:
g <- ggplot(TimeStats)
g <- g + geom_histogram(aes(TimeOff), binwidth=5,
      fill="#41F0AE")
g <- g + geom_histogram(aes(TimeOn), binwidth=5,
      fill="#099963")
g <- g + scale_x_continuous(limits = c(0, 120), breaks = c(0,
      30, 60, 90, 120))
```

```
g <- g + theme_classic()
g <- g + theme(legend.position="none")
g <- g + labs(x="Time /mins", y="Number of cells")
print(g)
ggsave(file="TimeOnOffHistogram.eps", width=10, height=7,
       units="cm")


#####################################################################
#### MANUAL TIME ADJUSTMENT FOR CO-CULTURE EXPERIMENTS #########
#####################################################################
# The following code is used to adjust the start times for co-
cultured cells, since the cells contacted the plate at different
times:
# By looking at the tiff files together with plotted tracks,
legitimate responding cells were found manually. The frame at
which the cell first appears to make contact with the plate was
recorded in an excel csv file. The following code reads that
file and subtracts the first contact frame from the data such
that time zero becomes the time each cell first contacts the
plate.
ContactFrames <- read.csv("ContactFrames.csv",
       stringsAsFactors=F, header=T)
ContactFrames <- ContactFrames[,c(1,2,3)]
ComplexData <- merge(RespondingSignalData, ContactFrames,
       by.x=2, by.y=1)
unique(ComplexData$Label)
ComplexData$RelFrame <- (ComplexData[,3]) - (ComplexData[,6])
ComplexData$RelTime <- ((ComplexData$RelFrame) * 9.816)/60
```